Title
Characterizing the function of T-box target genes in mesoderm development

Author
Maxwell, Adrienne Alecia

Publication Date
2012

Peer reviewed|Thesis/dissertation

Characterizing the function of T-box target genes in mesoderm development

By

Adrienne Alecia Maxwell

A dissertation submitted in partial satisfaction of the

requirements for the degree of

Doctor of Philosophy

in

Molecular and Cell Biology

in the

Graduate Division

of the University of California, Berkeley

Committee in charge:
Professor Sharon L. Amacher, Chair
Professor Henk Roelink
Professor Michael Levine
Professor Marvalee H. Wake

Fall 2012

Abstract

Characterizing the function of T-box target genes in mesoderm development

by

Adrienne Alecia Maxwell

Doctor of Philosophy in Molecular and Cell Biology

University of California, Berkeley

Professor Sharon L. Amacher, Chair

T-box genes encode a family of transcription factors that contain a conserved DNA-binding domain, the T-box, and have been shown to play a crucial role in various developmental processes. Two zebrafish T-box genes, *no tail (ntl)* and *spadetail (spt)*, as well as their orthologs in other vertebrates, have been shown to play important roles in the specification and patterning of posterior mesoderm. While wild-type zebrafish embryos develop ~30 somites that will later differentiate into muscle and vertebrae, *spt* mutants lack the anterior 15-17 trunk somites, and *ntl* mutants lack a notochord and the posterior 15 tail somites. Interestingly, embryos mutant for both *ntl* and *spt* lack all trunk and tail mesoderm, including tissues that form in both single mutants, indicating Ntl and Spt have overlapping functions in specifying these structures. Despite the obvious importance of T-box factors in development, relatively few of their transcriptional targets have been identified and tested to examine their role in mediating posterior mesoderm development. Recently, microarray results published by our lab and others have generated an extensive list of genes up- or down-regulated by Ntl and Spt. For my thesis I have chosen to focus on characterizing the role of several of these potential targets: *mesogenin* (*msgn1)*, which belongs to the bHLH family of transcription factors; *T-box gene 6-like* (*tbx6l*)*,* itself a T-box protein; *RNA binding motif protein 38* (*rbm38*), an RNA-binding protein; and *integrin beta 5* (*itgb5*), an adhesion and signaling molecule.

Through characterization of a null mutant, I have shown that *msgn1* functions with *spt* to promote cell migration out of the tailbud, but is not essential for zebrafish development. Additionally, I have shown that depleting *tbx6l* by morpholino oligonucleotide results in perturbation of dorsal-ventral patterning during gastrulation as well as dose-dependent loss of tail mesoderm. I have also characterized the spatial and temporal expression patterns of *rbm38* and *itgb5* and shown that both genes are expressed in the presumptive mesoderm and tailbud, where they overlap with *ntl* and *spt* expression, consistent with a role in mesodermal development. Characterizing the functions of

downstream targets will add to the gene regulatory network for specification of posterior mesoderm and help to detail the molecular mechanism of vertebrate posterior development in general.

Table of Contents

List of Figures and Tables

Chapter 1: Introduction to zebrafish development and T-box genes

Overview of development in zebrafish: gastrulation and segmentation

The normal adult body plan of animals relies on the success of earlier morphogenetic and patterning events that occur within the developing embryo. After fertilization of the fish egg, cytoplasm streams anteriorly forming a small, yolk-free domain (blastodisc) on top of, but still connected to, the yolk. The embryo then undergoes meroblastic cleavage where cell divisions occur only in the blastodisc and do not bisect the entire embryo. Several rounds of cleavage form the blastula, a ball of cells, which sit on top of the yolk (Kimmel et al., 1995). At 4 hours post fertilization (hpf) these cells initiate epiboly as they migrate vegetally along the sides of the yolk. Once cells have migrated halfway down the yolk (50% epiboly), they begin to converge dorsally, resulting in a thickening of the epiblast corresponding to the dorsal midline. This accumulation of cells will form the shield (Kimmel et al., 1995). The shield is functionally analogous to the dorsal blastopore lip of the frog and the node of the mouse, which function as the dorsal organizing centers. Transplantation of the dorsal organizer region to a host embryo induces nearby host cells to form a secondary body axis with proper dorsal-ventral and anterior-posterior patterning (Ho, 1992; Spemann and Mangold, 1924; Waddington, 1932; Storey et al., 1992; Beddington, 1994). Formation of the shield breaks the symmetry of the margin and physically marks the future dorsal side of the embryo, establishing the dorsal-ventral axis (Kimmel et al., 1995). Consequently, it also defines the midline of the embryo.

One of the first major events in the long process of achieving the specified body plan is gastrulation, during which the germ layers are specified. Gastrulation begins as cells at the margin, beginning with the shield, internalize at the leading edge at the blastoderm margin. This deep layer that forms is termed the hypoblast, which contains cells with mesodermal and endodermal character (mesendoderm). As cells enter the hypoblast they migrate anteriorly away from the margin and also converge to the dorsal side (Fig 1.1A). Gastrulation proceeds as cells internalize at the leading edge of the lateral and ventral margin even as the margin moves down the yolk due to continuing epiboly (Fig1.1A). The first mesendoderm cells to involute at the dorsal margin retain their axial position in the hypoblast and will form the prechordal plate, while dorsal axial cells which enter later will give rise to a midline rod of mesodermal cells, the notochord (Fig 1.1B,C). A portion of the dorsally converging cells in the hypoblast adjacent to the axial domain will form the paraxial mesoderm (also referred to as presomitic mesoderm or PSM) (Fig 1.1B). During this time, epiboly progresses as the epiblast layer migrates steadily down the yolk behind the margin. Once the mesendoderm has been internalized, the dorsal and ventral margins meet at the vegetal pole of the yolk to form the tailbud, ending primary gastrulation (Kimmel et al., 1995).

Following primary gastrulation, the segmentation period occurs during which the somites are formed and the body axis elongates. Somites form bilaterally along the dorsal side of the embryo as blocks of tissue separate periodically from the anterior end of the PSM (Fig1.1D). As somites are differentiating, proliferation in the tailbud provides a continual supply of mesoderm as cells exit the tailbud to enter the PSM, a process called secondary gastrulation. By 24hpf, zebrafish have formed all of their ~30 somites

(Kimmel et al., 1995). The periodic formation of somites in an anterior to posterior gradient is explained by the “clock and wavefront” model (Cooke and Zeeman, 1976; Dale and Pourquié, 2000). The “clock” is comprised of several genes with oscillating and dynamic expression in the PSM. As a result, cells in the PSM alternate between permissive and restrictive phases. The “wavefront” is established by opposing signaling gradients from the somites and the tailbud (retinoic acid (RA) and Wnt/Fibroblast growth factor (FGF) respectively) and moves caudally as newer somites are formed and the tail elongates. The wavefront primes cells in the anterior portion of the PSM (nearest the most recently formed somite) for incorporation into the next somite. Changes in the position of the wavefront affect the average size of somites, with anterior or posterior shifting of the RA/FGF interface resulting in smaller or larger somites, respectively. When the migrating wavefront reaches cells in the permissive phase of oscillations, a new somite is formed. Each oscillation cycle ends with the formation of a new somite. Although the periodicity of somite formation differs between species, a large body of literature supports the overall conservation of this mechanism of segmentation in vertebrates (reviewed by Dubrulle and Pourquié, 2004).

Gastrulation in other vertebrates

Following fertilization of the *Xenopus* egg, the 1-celled embryo undergoes several rounds of cell division to produce a blastula stage embryo. Embryonic development during this time is distinct from the zebrafish in several ways (Kimmel et al., 1995; reviewed by Gerhart and Keller, 1986). First, although the yolk is more highly concentrated in the vegetal half of the embryo, there is no separation of cytoplasm from the yolk. Second, *Xenopus* embryos undergo holoblastic cleavage, meaning the cleavage furrows extend through the whole zygote. Third, the *Xenopus* blastula forms the blastocoel, a fluid-filled space separating the vegetal cells (prospective endoderm) from the cells of the animal pole (prospective ectoderm). Gastrulation begins as a group of cells, termed the “bottle cells”, in the marginal zone (analogous to the zebrafish margin) alter their morphology and invaginate into the deeper layer of cells. Invagination begins on the dorsal side, forming the blastopore lip, which possesses dorsal organizing activity similar to the fish shield. As cells continue to traverse the dorsal lip, the blastopore lip spreads laterally and ventrally to encompass the entire margin, completing the blastopore. Internalization of mesendoderm by involution through the blastopore and blastopore closure also relies on convergent extension. Cells involuting at the dorsal lip will form foregut endoderm as well as axial and paraxial mesoderm derivatives (prechordal plate, notochord, and somites). Cells involuting at the lateral and ventral blastopore lip will form the remaining mesoderm (lateral plate and blood). During the invagination of the marginal zone, epiboly occurs as the animal pole cells intercalate and divide to fully cover the embryo (reviewed by Gerhart and Keller, 1986).

Gastrulation in the frog and fish are similar, but distinct from the process as it occurs in amniotes. In mice, the early cleavages of the embryo give rise to cells that will form the embryo as well as cells that will form the extraembryonic tissues required to nourish and protect the embryo as it develops inside the mother (reviewed by Tam and Behringer, 1987). At this stage, the inner cell mass, a group of cells that will give rise to the embryo, are surrounded by an outer ring of cells that form the trophoblast, which is the precursor to the chorion. The inner cell mass is further divided into two layers, the

epiblast and hypoblast. The epiblast will continue to divide and eventually form the mouse embryo proper while the hypoblast eventually contributes to some of the extraembryonic structures. Gastrulation begins as posterior epiblast cells delaminate and begin to migrate towards the hypoblast, occupying the space between the epiblast and hypoblast (reviewed by Tam and Behringer, 1987). The accumulation of epiblast cells at the site of invagination is the primitive streak. The primitive streak extends anteriorly during gastrulation as cells continue to ingress through it. When at its maximal extension, the anterior cells of the primitive streak form the node ("Hensen's node" in the chick), the dorsal organizing center equivalent to the zebrafish shield and *Xenopus* dorsal blastopore lip. The first cells to ingress at the streak will form the endoderm, displacing the hypoblast, and the mesoderm will ingress afterward, separating the overlying ectoderm from the endoderm. Mesodermal cells that form early will move laterally and forward to form the lateral plate mesoderm. After its formation the primitive streak regresses while the node moves posteriorly. The internalization of mesoderm and endoderm during the lateral fold is accompanied by a characteristic turning event giving rise to an embryo with the familiar curvature of the back (reviewed by Tam and Behringer, 1987). In chick, gastrulation occurs similarly through the primitive streak and ends as the ectoderm moves ventrally to cover the yolk during epiboly. Although the process of gastrulation varies between vertebrate species, the task is accomplished by analogous structures in each, engaged in similar movements, expressing similar genes. This indicates a conserved mechanism for vertebrate gastrulation.

Role of T-box genes in mesoderm development

T-box genes are a family of transcription factors characterized by a conserved T-box DNA binding domain that recognizes an 8-10 bp consensus sequence (Herrmann et al., 1990; Kispert and Herrmann, 1993; Kispert et al., 1995a). Depending on which other factors they interact with, T-box genes can function as transcriptional activators or repressors (Kispert et al., 1995a; Conlon et al., 1996; Farin et al., 2007). They have been shown to be important in germ layer formation and in several other developmental processes, including limb development, establishing left-right asymmetry, craniofacial development, heart development, and T-cell differentiation (Showell et al., 2004; Naiche et al., 2005). In this section I will discuss the T-box genes integral to mesoderm specification and patterning in vertebrate development.

T/Brachyury

T/Brachyury, the founding member of the T-box family of transcription factors, was originally identified in short-tailed mice (Herrmann et al 1990; Kispert and Herrmann, 1993). Orthologs found in vertebrates and invertebrates indicate it was present in a common ancestor (Schulte-Merker et al., 1994; Kispert et al., 1995b; Knezevic et al., 1997; Yasuo and Satoh, 1994; Marcellini et al., 2003; reviewed by Papaiannou and Silver, 1998). *Brachyury* is initially expressed in the primitive streak and later in the node and axial mesoderm derivative, the notochord (Fig 1.2 and 1.3) (Wilkinson et al., 1990). Mice heterozygous for the *Brachyury* mutation have shorter tails than their wildtype siblings, while those homozygous for *Brachyury* die during gestation, by 10 days post coitus (dpc). At this stage, *Brachyury* mutants have a

noticeable loss of notochord tissue and paraxial mesoderm posterior to the forelimb bud (Chesley, 1935).

The *Xenopus Brachyury* homolog *Xbra* shares over 90% identity with *Brachyury* in the T-box domain and is expressed in analogous tissues during development. During gastrulation, *Xbra* is expressed in cells of the presumptive mesoderm (the marginal zone in *Xenopus* as compared to the mouse primitive streak) as well as the notochord (Fig 1.2 and 1.3). *Xbra* expression is not detected in the segmental plate (Smith et al., 1991). Over-expression of full length *Xbra*, but not a truncated version, in early embryos was able to induce ectopic mesoderm as well as differentiated muscle, indicating the gene is sufficient to specify mesodermal cell fates (Cunliffe and Smith, 1992). Loss-of-function studies were performed using truncated forms of *Xbra* that removed the activation domain or chimeric forms of *Xbra* where the DNA binding domain was fused to the *Drosophila engrailed* repressor (*Xbra-En*^{R}). In those studies using *Xbra-En*^{R}, embryos injected with mRNA encoding the chimeric protein failed to gastrulate properly and resulted in tadpoles with severe truncations in the posterior body, as well as a partial or complete loss of the notochord (Conlon et al., 1996; Conlon and Smith, 1999). Nevertheless, anterior structures and muscle did form, similar to the mouse T mutant (Conlon et al., 1996; Herrmann et al., 1990). *Xbra* is required for the expression of several mesodermal markers during gastrulation, including itself, as well as markers of posterior fate (Cunliffe and Smith, 1992; Rao, 1994; Conlon et al., 1996). Interestingly, over-expression of *B304*, an *Xbra* mutant transcript that lacks the activation domain and mesoderm inducing capability, is able to induce neural genes and structures. Presumably, B304 is capable of antagonizing Xbra function through competitive binding to target gene promoters (Rao, 1994), and its effect on neuralization may be secondary, due to its inhibition of a mesodermal signal, rather than active induction of neural genes.

While *no tail* (*ntl*) was considered to be the only zebrafish ortholog of *Brachyury* (Schulte-Merker et al., 1992, 1994) for nearly 30 years, a second gene, *no tail b* (*ntlb*), was identified that is now considered to be the true ortholog of mouse *Brachyury* (Martin and Kimelman, 2008). *ntlb* is 68% identical to mouse *Brachyury*, 92% identical in the T-box domain, and shares synteny with its murine ortholog. In contrast, *ntl* only shares 60% identity with *Brachyury*, 87% identity in the T-box domain, and does not exhibit synteny (Martin and Kimelman, 2008). *ntl* is expressed in the dorsal and ventrolateral margin during gastrulation, as well as in the notochord and tailbud (Fig 1.2 and 1.3) (Schulte-Merker et al., 1992; Halpern et al., 1993). *ntlb* has a nearly identical expression domain, with its expression being initiated slightly after *ntl*. Although the genes have similar expression patterns, the *ntl* mutant phenotype displays more developmental defects than loss-of-function *of ntlb. ntl* mutants form the first 15-17 trunk somites, but have a truncated body axis that results from failure to form tail somites, and they lack a notochord (Halpern et al., 1993). This is similar to, but less severe than, the mouse *Brachyury* mutant phenotype. In contrast, depletion of *ntlb* function using antisense morpholino oligonucleotides (MOs) had no discernible morphological defects (Martin and Kimelman, 2008). However, loss of both *ntl* and *ntlb* together results in the loss of nearly all somites and notochord, recapitulating the mouse mutant phenotype (Martin and Kimelman, 2008; Chesley, 1935). Together with the identical expression patterns of *ntl* and *ntlb*, this demonstrates that although not required for zebrafish development, Ntlb function overlaps with Ntl in forming the posterior mesoderm.

In addition to conserved expression and function, *Brachyury* orthologs are regulated by similar signaling mechanisms. *Brachyury, Xbra* and *ntl* have been shown to function downstream of several mesoderm inducing factors, most notably FGF and activin. (Smith et al., 1991; Isaacs et al., 1994; Schulte-Merker and Smith, 1995; Griffin et al., 1995; Latinkić et al., 1997). Studies in zebrafish and *Xenopus* also revealed that FGF is regulated by *ntl* and *Xbra*, respectively. *ntl* mutants exposed to low doses of SU5402, a pharmacological inhibitor of FGF signaling, showed a complete absence of trunk muscle, whereas $ntl^{+/+}$ and $ntl^{+/-}$ embryos exposed to the same SU5402 dose exhibited wildtype muscle staining (Griffin and Kimelman, 2003), indicating decreased FGF activity in *ntl* mutants. In *Xenopus*, inhibiting FGF signaling with a dominant negative FGF receptor blocked *Xbra* induction of ventral mesoderm in animal cap assays (Schulte-Merker and Smith, 1995). Thus, *Xenopus* and zebrafish *Brachyury* orthologs form a positive regulatory feedback loop with members of the FGF signaling pathway which is required for specification and formation of the posterior mesoderm.

In summary, the spatiotemporal and functional role of *Brachyury* is conserved in vertebrates, most notably its requirement for the specification of axial mesoderm as well as development of posterior mesoderm derivatives. *Brachyury* homologs have also been identified in nonvertebrates. While the development of mesodermal lineages is not conserved between vertebrates and invertebrates, the expression of *Brachyury* orthologs in these organisms is observed in notochord precursors and other mesodermal tissues, as well as in ectoderm and endoderm derivatives (Kispert et al., 1995; Harada et al., 1995; Corbo et al., 1997; reviewed by Papaioannou and Silver, 1998). Despite this divergent expression of *Brachyury*, invertebrate orthologs are capable of inducing mesoderm in *Xenopus* animal cap explants as efficiently as their vertebrate counterparts (Marcellini et al., 2003), highlighting the evolutionarily conserved role for *Brachyury* in mesoderm development.

VegT/spt

Xenopus VegT was reported near simultaneously by four different groups (King and Zhang, 1996; Lustig et al., 1996; Stennard et al., 1996; Horb and Thomsen, 1997). *In situ* and RT-PCR analysis revealed that *VegT* is maternal, the RNA being ubiquitously deposited in the oocyte before the transcript is localized to the vegetal hemisphere. After fertilization and during the blastula stage, the maternal transcript remains localized to the vegetal pole of the embryo. Zygotic expression of *VegT* is initiated at the dorsal margin prior to gastrulation and subsequently spreads ventrally to encompass the entire margin before the transcript is cleared from the dorsal midline region of the margin (Fig 1.2). Later expression is detected in the posterior paraxial mesoderm as well as in neurons flanking the spinal cord along the body (Fig 1.3) (King and Zhang, 1996; Lustig et al., 1996; Stennard et al., 1996; Horb and Thomsen, 1997). Based on these reports, *VegT* overlaps with *Xbra* in the presumptive mesoderm of the margin but the two have distinctly different expression patterns in the axial mesoderm.

Over-expression of *VegT*, as well as disruption of its function, has demonstrated its important role in both germ layer formation and patterning. Injection of *VegT* mRNA into early 2 to 8-cell embryos causes several patterning defects including the induction of a second blastopore lip and a failure to gastrulate properly (Lustig et al., 1996; Stennard et al., 1996; Zhang and King et al., 1996). Injection of *VegT* into the vegetal

cells is able to induce a secondary axis in 17% - 56% of embryos in a dose-dependent manner. The secondary axes formed tail mesoderm but lacked more anterior head structures. Conversely, injection in the animal pole cells inhibits head formation but does not result in secondary tails (Zhang and King, 1996), indicating other vegetally-localized determinants are necessary for induction of a secondary axis. *VegT* is also capable of inducing an array of ventral, dorsal and posterior mesoderm markers. At low doses, *VegT* induces ventral and posterior genes such as *Xbra*, *Xwnt8*, and muscle differentiation marker *XmyoD* (King and Zhang, 1996; Lustig et al., 1996; Stennard et al., 1996; Horb and Thomsen, 1997). At higher doses, *VegT* induces dorsal mesoderm markers *goosecoid* (*gsc*) (Cho et al., 1991; Stachel et al., 1993) and *chordin* (Sasai et al., 1994), both of which are expressed in the organizer and capable of inducing secondary axes, as well as *muscle actin*, a marker of differentiated somitic muscle (King and Zhang, 1996; Lustig et al., 1996; Stennard et al., 1996; Horb and Thomsen, 1997). The dose-dependent effect of *VegT* on gene expression in animal caps mimics the exposure of dorsal and ventral regions to *VegT* in the context of the whole embryo. *VegT* expression is initiated on the dorsal side and continues to be expressed there as expression initiates in the lateral and ventral margin, respectively. Additionally, *VegT* expression in the dorsal margin is more abundant than in the ventral margin (Horb and Thomsen, 1997). As a result, dorsal genes presumably have more exposure to VegT, explaining their induction at higher *VegT* doses. In addition to inducing transcriptional responses associated with mesoderm identity, low doses of *VegT* can induce injected animal caps to form vesicles and mesenchyme as opposed to dense aggregates of epidermis formed in uninjected animal caps (Stennard et al., 1996; Zhang and King, 1996; Horb and Thomsen, 1997). This is a typical morphological response to ventral mesoderm activators. At high doses, *VegT* can induce animal caps to elongate, with 30% showing differentiation of muscle, but not notochord differentiation (Horb and Thomsen, 1997).

When a dominant negative form of *VegT*, *VegT-En*^{R}, is injected into the marginal zone of 2-cell embryos, the blastopore lip fails to invaginate and expression of dorsal genes *Xbra* and *gsc* are lost. *VegT-En*^{R} injected embryos that are raised to tadpole stage show different patterning defects reflecting the role of *VegT* in development. Dorsally injected embryos fail to gastrulate properly and do not form anterior head structures, while ventrally injected embryos form head structures, but have severely truncated body axes resulting from the absence of the posterior body. This phenotype can be rescued specifically by co-injection of *VegT* mRNA (Horb and Thomsen, 1997). Depletion of the maternal *VegT* transcript with antisense MOs reveals that *VegT* has an earlier role in patterning the ectoderm and endoderm as well as inducing mesoderm in the early embryo (Zhang et al., 1998).

VegT orthologs have been identified in several vertebrates including zebrafish, chick, and axolotl (Knezevic et al., 1997; Ruvinsky et al., 1998; Griffin et al., 1998; Nath and Elison, 2006) with conservation of T-box domain sequence and embryonic expression patterns. The zebrafish ortholog of *VegT*, *spadetail*/*tbx16* (*spt*), was identified and cloned independently by two groups (Griffin et al., 1998; Ruvinsky et al., 1998). *spt* differs from *VegT* in that it is not maternally expressed and does not participate in the specification of the endoderm (Ruvinsky et al., 1998; Griffin et al.,

1998), the latter of which is the function of another zebrafish T-box gene, *eomesodermin* (Bjornson et al., 2005; Du et al., 2012).

spt is first expressed in the blastula, being restricted to the margin prior to the onset of epiboly. During gastrulation, the dorsal midline margin cells expressing *spt* involute and migrate anteriorly, where they will form the prechordal plate. Consequently, expression is absent from the dorsal notochord precursor cells (Fig 1.2). From gastrulation through segmentation, *spt* expression is practically identical to that of *VegT*, being expressed in the paraxial mesoderm and tailbud, and later in spinal cord neurons along the body (Fig 1.3) (Lustig et al., 1996; Ruvinsky et al., 1998; Griffin et al., 1998). Zebrafish mutants homozygous for the *b104 spt* allele, which deletes the activation domain, have a severe deficiency of trunk paraxial mesoderm and patterning defects in lateral mesoderm derivatives (Kimmel et al., 1989; Griffin et al., 1998). Unlike *VegT*-depleted embryos, *spt* mutants gastrulate properly, but further analysis revealed *spt* is required cell-autonomously in precursors of trunk paraxial mesoderm for the convergent extension movements required to form trunk mesoderm. Instead of converging dorsally, *spt* mutant cells accumulate in the tailbud, giving *spt* mutants a noticeably larger, spade-shaped tail (Kimmel et al., 1989; Ho and Kane, 1990; Griffin et al., 1998). Considering the conservation of expression and orthologous relationship between *VegT* and *spt*, it is interesting that the roles of Spt and VegT in mesoderm development are not conserved. Instead, the *spt* mutant in zebrafish is very similar to the mutant phenotype for the murine T-box gene *Tbx6,* discussed below (Chapman et al., 1998), indicating different T-box genes have evolved to perform similar roles in vertebrate development.

Tbx6

Mouse *Tbx6* was originally identified in a search for additional T-box genes involved in development. During gastrulation, *Tbx6* is expressed in the primitive streak, paraxial mesoderm, and later the tailbud, but does not overlap with *Brachyury* expression in the node or axial mesoderm (Fig 1.2 and 1.3) (Chapman et al., 1996). Loss-of-function studies revealed that Tbx6 is required for specification and later patterning of paraxial mesoderm, in addition to inhibiting neural identity. The mouse *Tbx6* null mutant forms two ectopic neural tubes in the place of somites and exhibits an enlarged tailbud resulting from cells that are retained in the tailbud (Chapman et al., 1998). However, *in vitro* assays showed that, upon treatment with retinoic acid, $Tbx6^{-/-}$ embryonic stem cells are capable of muscle differentiation (Chapman et al., 2003), demonstrating that Tbx6 is not absolutely required for this process. In mice homozygous for a hypomorphic allele of *Tbx6* ($Tbx6^{rv}$), paraxial mesoderm is specified but improperly patterned, resulting in vertebral fusions along the body axis. As a result, they exhibit less severe tail enlargements, and ectopic neural tube formation is confined to the tail (Theiler and Varnum, 1985; Watabe-Rudolph et al., 2002; White et al., 2003). A single ectopic neural tube forms ventral to the endogenous structure in mouse *Wnt3a* mutants, presumably due to loss of *Tbx6* expression in *Wnt3a* mutants. (Takada et al., 1994; Yoshikawa et al., 1997; Nowotschin et al., 2012). Furthermore, Tbx6 repression of *Sox2* is required for specifying paraxial mesoderm as opposed to neural fate, and inhibiting expression of *Sox2* in a $Tbx6^{-/-}$ background prevents formation of the ectopic neural tubes (Takemoto et al., 2011; Nowotschin et al., 2012).

Xenopus Xtbx6 is ~70% identical to mouse and human *Tbx6* in the T-box domain and its expression domain overlaps largely with that of *VegT*. *Xtbx6* is expressed in the ventrolateral mesoderm of gastrulating embryos and is detected in the tailbud and paraxial mesoderm as the trunk and posterior body are formed (Fig 1.2 and 1.3). The mesoderm-inducing factors Activin and bFGF can induce *Xtbx6,* and it positively regulates its own expression (Uchiyama et al., 2001). Over-expression of X*tbx6* induces mesoderm markers such as *Xwnt8* and *Xmyod* as well as the endoderm marker *sox17a*, while inhibiting the induction of neural/ectoderm markers. Blocking X*tbx6* function by expressing *Xtbx6-En*^{R}, a repressor form of the transcription factor, causes increased expression of the neural markers *Otx2* and *N-cam* while decreasing the expression of mesodermal markers (Uchiyama et al., 2001; Li et al., 2006). This demonstrates that *Xtbx6* and mouse *Tbx6* have a conserved function in simultaneously promoting mesoderm identity and inhibiting neural fate. In animal cap explants, X*tbx6* can induce elongation and extensions typical of convergent extension behaviors observed in mesoderm (Uchiyama et al., 2001; Li et al., 2006). Knockdown of X*tbx6* function causes a disruption of somite boundaries (Tazumi et al., 2008). Although cells are able to migrate out of the tailbud, they exhibit uniform expression of *myoD*, a marker of somite AP patterning normally confined to the caudal somite compartment. Embryos lacking *Xtbx6* function also show a complete loss of ventral body wall muscle (Tazumi et al., 2008). These studies demonstrate that similar to mouse *Tbx6*, *Xtbx6* is also involved in establishing the proper patterning of the paraxial mesoderm as well as later muscle differentiation.

tbx6l (previously *tbx6*) was originally designated the zebrafish *Tbx6* ortholog because of its conserved expression pattern and protein sequence. Like the other vertebrate *Tbx6* genes, *tbx6l* expression overlaps with *spt* and *ntl/ntlb* in the ventrolateral margin, paraxial mesoderm and later tailbud, but does not overlap with *ntl/ntlb* expression in the dorsal midline or axial mesoderm (Fig 1.2 and 1.3) (Hug et al., 1997). In 2003, Goering et al. reported as “data not shown” that a targeted knockdown of *tbx6l* using antisense morpholino oligonucleotides resulted in mild axial defects, while over-expression of either full-length *tbx6l* or the *tbx6l* T-box domain alone were sufficient to phenocopy loss of Ntl activity. Thus, Tbx6l may inhibit axial mesoderm fates by antagonizing Ntl function. In contrast, the expression of another mesodermally expressed zebrafish*Tbx6* paralog, *tbx6* (previously *tbx24*) (Nikaido et al., 2002), is initiated later during development and overlaps with other T-box gene members in a portion of the paraxial mesoderm (Fig 1.2). *tbx6* is later confined to the anterior PSM, terminating as somites are formed (Fig 1.3) (Nikaido et al., 2002). *tbx6* is slightly more similar to *Tbx6* orthologs in the sequence of its T-domain (60-62% identity compared to 56-57% identity for *tbx6l*) and also has conserved function with other *Tbx6* genes. *tbx6* and *Tbx6* paralogs in frog and mouse form a complex with members of the Mesp family of basic-helix-loop-helix transcription factors and the Ripply family of transcriptional co-repressors to establish somite boundaries and inhibit expression of PSM genes (Kawamura et al., 2008; Hitachi et al., 2008; Oginuma et al., 2008; Takahashi et al., 2010). Additionally, zebrafish *tbx6* is required for patterning of specified paraxial mesoderm. In *fused somite* mutants, which lack *tbx6*, somites become fused and morphological boundaries are absent. At the molecular level, somites lose their distinct rostral-caudal expression patterns, instead expressing caudal markers in both the

rostral and caudal somite compartments (Nikaido et al., 2002). This caudalization of paraxial mesoderm also occurs as a result of knocking down *Xtbx6* (Tazumi et al., 2008). Thus, the zebrafish genome contains two *Tbx6* paralogs; *tbx6l* has conserved expression with vertebrate *Tbx6* genes and unknown function, while *tbx6* has conserved function with vertebrate *Tbx6* genes but only a slight overlap of expression in the paraxial mesoderm.

T-box gene interactions in zebrafish development

In *ntl* mutants, *tbx6l* is expressed prior to gastrulation and throughout trunk somitogenesis, becoming severely decreased as tail somites enter the PSM (Hug et al., 1997). Conversely, expression of *tbx6l* is down-regulated in *spt* mutants during gastrulation, but recovers during segmentation as tail mesoderm progenitors begin to populate the tailbud (Griffin et al., 1998). This later expression of *tbx6l* is most likely regulated by *ntl* (Griffin et al., 1998). In *spt*;*ntl* double mutants expression of *tbx6l* is completely lost during gastrulation and segmentation stages (Griffin et al., 1998). Similarly, the significant reduction in *spt* expression observed in *spt*;*ntl* double mutants, compared to its expression in *spt* single mutants, reveals that *spt* is also regulated by itself and *ntl* (Griffin et al. 1998; Ruvinsky et al., 1998). To date, there has been no evidence to support *tbx6* regulation by or of T-box gene family members *ntl*, *spt,* or *tbx6l*.

With the exception of *tbx6*, zebrafish T-box genes involved in mesoderm development share a large region of expression overlap in the mesoderm. *ntl* and *spt* expression in the presumptive mesoderm and precursors of somitic mesoderm overlap in the margin and tailbud of the developing embryo, but single mutant studies have shown that each gene regulates a distinct region of posterior mesoderm (Kimmel et al., 1989; Halpern et al., 1993). *spt* is required for formation of the trunk mesoderm while *ntl*, in addition to specifying the notochord, is required for formation of the tail mesoderm posterior to the anus. When *ntl* and *spt* function are lost in *spt;ntl* double mutants, trunk and tail mesoderm are absent; additionally the pronephros and medial floor plate, structures which are formed in both single mutants, are also lacking (Amacher et al. 2002), indicating that the two T-box proteins function together for specifying lateral plate mesoderm derivatives and patterning the neural tube. The overlapping functions of Spt and Ntl are further demonstrated by the synergistic phenotype observed in a *spt*-enhanced ($spt^{-/-}$; $ntl^{+/-}$) mutant. *spt*-enhanced mutants still exhibit the enlarged tailbud and have reduced trunk mesoderm, but they also fail to form tail mesoderm and have a deficit of axial mesoderm (Goering et al., 2003).

Tbx6l has been shown to antagonize Ntl function. Ectopic expression of mRNA encoding Tbx6l or the Tbx6l DNA binding domain mimics the activity of Ntl-En^{R}, a transcriptional repressor form of Ntl. This inhibition of Ntl function is most likely through competitive binding of T-box binding sites and not regulation of *ntl* expression itself (Goering et al., 2003). Due to the largely overlapping expression domains and phylogenetic grouping of Tbx6l and Spt, in addition to the temporal regulation of *tbx6l* by Ntl and Spt, it has been proposed that *spt* and *tbx6l* perform similar functions in the trunk and tail mesoderm, respectively (Griffin et al., 1998; Amacher et al., 2002).

Identification of Bra/Ntl and VegT/Spt targets

While Brachyury, VegT, Tbx6 and their metazoan orthologs had all been shown to be capable of inducing markers and characteristics of mesoderm, few direct targets were known. Through candidate gene approach, subtractive hybridization screens, and functional analysis of T-box proteins, several downstream targets of the mesoderm-inducing T-box transcription factors were identified. Some of the earlier targets identified include transcription factors belonging to the *Bix* (*Brachyury inducible homeobox*) family of homeobox genes (Tada et al., 1998; Casey et al., 1999), the *papc* gene encoding a cell adhesion molecule (Yamamoto et al., 1998), and signaling ligand gene *Xwnt11* (Tada and Smith, 2000; Saka et al., 2000). More recently, large-scale efforts employing the use of chromatin immunoprecipitation, cell sorting, and microarrays have generated an extensive list of potential T-box targets regulated during mesoderm development (Takahashi et al., 1999; Hotta et al., 2000; Taverner et al., 2005; Garnett et al., 2009; Morley et al., 2009; Shestopalov et al., 2012). These targets include genes that encode transcription factors, components of cell signaling pathways, cell-cell adhesion molecules, and extracellular matrix proteins.

T-box transcription factors primarily act on their targets through binding to the conserved consensus T-box binding site motif TCACACCT (Kispert and Herrmann, 1993; Kispert et al., 1995b; reviewed by Naiche et al., 2005; Garnett et al., 2009;). All T-box genes identified to date encode proteins that are capable of binding the core consensus sequence *in vitro* (reviewed by Naiche et al., 2005). Because T-box factors are capable of inducing overlapping as well as distinct sets of target genes and have largely overlapping expression profiles themselves, one important question is how target specificity of each T-box protein is achieved *in vivo*. Comparing the binding affinities of mesodermal T-box genes (Xbra, VegT and Eomes in *Xenopus*; Ntl, Spt, and Tbx6l in zebrafish) to different nucleotide sequences confirmed that these transcription factors recognize very similar binding motifs (Conlon et al., 2001; Garnett et al., 2009). The C-terminal portion in Brachyury contains several activator and repressor domains, and this domain has a significant role in regulation of target genes of other T-box proteins. In *Xenopus*, chimeric constructs containing the N-terminus of VegT or Eomes fused to the C-terminus of Xbra proved sufficient to inhibit induction of VegT and Eomes targets (Conlon et al., 2001). In addition to the activation domain, this regulatory region may contain inhibitory sequences or dictate interactions with co-regulators of gene transcription. T-box genes also differ in their preferential binding to regions consisting of a particular orientation and spacing of T-box sites (Kispert and Hermann 1993; Kispert et al., 1995b; Conlon et al., 2001).

Determining the function of Ntl and Spt targets in mesoderm development

The Amacher lab performed a microarray analysis to identify genes regulated by Ntl and Spt during early development. The results identified more than 40 potential targets falling into four classes. Class I genes (Spt-regulated) exhibited a down-regulation of two-fold or greater in Spt-depleted embryos and Spt;Ntl-depleted embryos, class II genes (Ntl-regulated) exhibited a down-regulation of two-fold or greater in Ntl-depleted embryos and Spt;Ntl-depleted embryos, class III ("redundant") genes exhibited a down-regulation of two-fold or greater *only* in Spt;Ntl-depleted embryos but not in single mutants, and class IV ("co-regulated") genes exhibited a down-regulation of two-fold or greater in Spt-, Ntl-, and Spt;Ntl-depleted embryos (Garnett et al., 2009). Single

mutant phenotypes demonstrate that Spt and Ntl clearly have distinct targets through which they control different developmental aspects. However, the *spt*-enhanced mutant phenotype, in addition to the co-expression of Spt and Ntl in cells as they internalize at the margin, demonstrate that the two transcription factors also work together in paraxial mesoderm development, possibly by regulating common targets. To identify the genes that could be required for both trunk and tail mesoderm, I focused on genes from the microarray which were "synergistically" down-regulated in *spt*;*ntl* double mutants when compared to single mutants (i.e., class III and class IV targets), indicating they were targets of both Spt and Ntl. The top two most down-regulated transcripts in the double mutants are *msgn1* (30 fold down-regulated) and *tbx6l* (25 fold down-regulated), while *rbm38* and *itgb5* represented genes with undefined roles in mesoderm development (Garnett et al., 2009).

In this dissertation I report the developmental role of transcription factors and T-box protein targets, Msgn1 and Tbx6l, as determined by loss-of-function studies. I have shown that Msgn1 exhibits functional overlap with Spt, while the T-box transcription factor Tbx6l is likely required for tail formation. Additionally, I have demonstrated that *rbm38* and *itgb5* expression coincide with regions of overlapping *ntl* and *spt* expression in mesodermal tissues, supporting a role for these targets in mesoderm development.

Figure 1.1

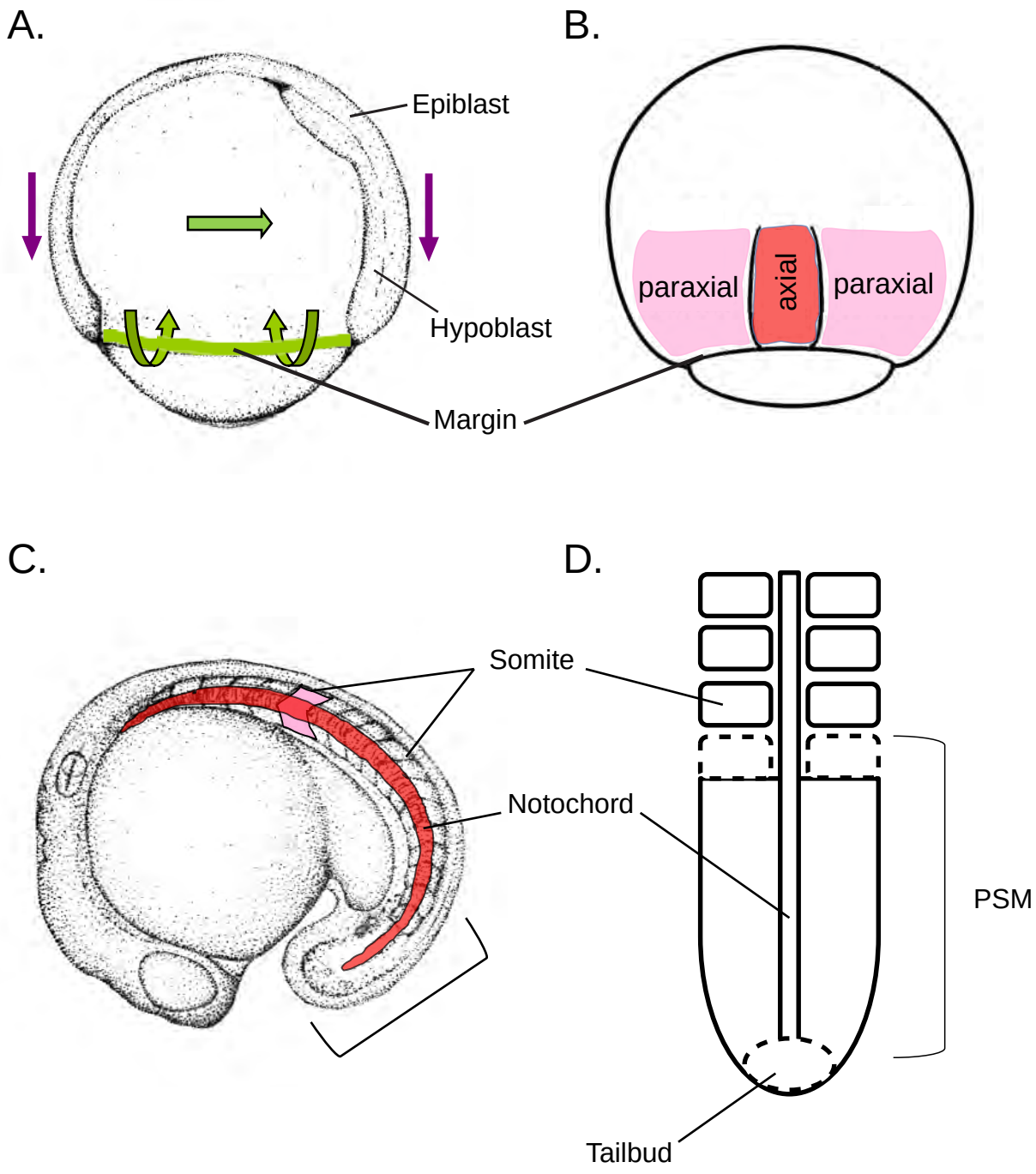
A.
Epiblast
Hypoblast
Margin
B.
paraxial
axial
paraxial
C.
Somite
Notochord
D.
PSM
Tailbud

Figure 1.1 **Gastrulation and segmentation in zebrafish development**

(A) Lateral view of a gastrula stage embryo at 70% epiboly. Dorsal is to the right and anterior is to the top. The margin is highlighted in green. The arrows represent the cell movements occurring during gastrulation. Green arrows represent the involution at the margin and dorsal convergence of hypoblast cells. The purple arrows represent the downward migration of the overlying epiblast during epiboly (B) A dorsal view of the embryo in (A) showing the hypoblast. Cells migrating at the midline of the dorsal margin become part of the axial mesoderm (red). Paraxial mesoderm (pink) lies adjacent to the axial mesoderm. (C) Lateral view of a segmentation stage embryo at ~18 somites. Dorsal is to the top and anterior is to the left. The axial mesoderm will give rise to the notochord (red) and the paraxial mesoderm will give rise to somites (pink). (D) A dorsal view of the bracketed tail region in the embryo in (C). Anterior is to the top. Somites form as they pinch off from the anterior end of the PSM. The dotted lines represent the next somite to form.

Figure 1.2

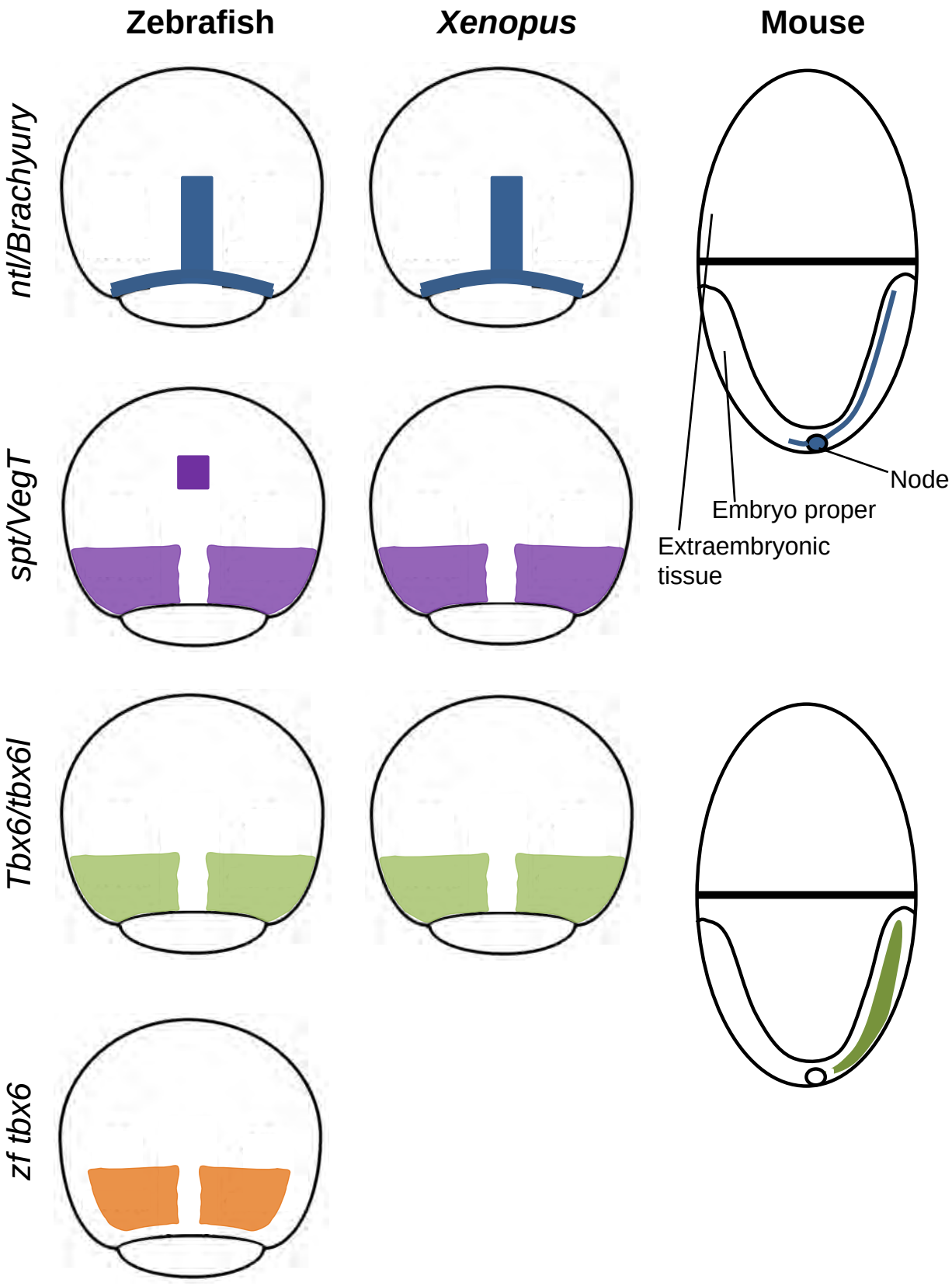
Zebrafish
Xenopus
Mouse
ntl/Brachyury
spt/VegT
Tbx6/tbx6l
zf tbx6
Node
Embryo proper
Extraembryonic tissue

Figure 1.2 **T-box gene expression in gastrula stage embryos**

Brachyury/*ntl* (blue), *VegT/spt* (purple), *Tbx6/tbx6l* (green), and *tbx6* (orange) expression in zebrafish, *Xenopus*, and mouse embryos during gastrulation. The presumptive mesoderm of the margin in zebrafish and *Xenopus* is analogous to the primitive streak in mouse. *Brachyury* orthologs overlap with expression of *VegT*/*spt* and *Tbx6* paraglogs in the presumptive mesoderm, but are the only T-box gene expressed in the notochord precursor cells in the axial mesoderm. Zebrafish *ntlb* expression is identical to *ntl* expression at this time. At this stage, *spt* is expressed in the prechordal plate in the axial domain whereas *VegT* is not. Mouse lacks a *VegT* ortholog. *Tbx6* paralogs in vertebrates are expressed in the presumptive mesoderm and paraxial mesoderm with the exception of zebrafish *tbx6* which is only expressed in the paraxial mesoderm.

Figure 1.3

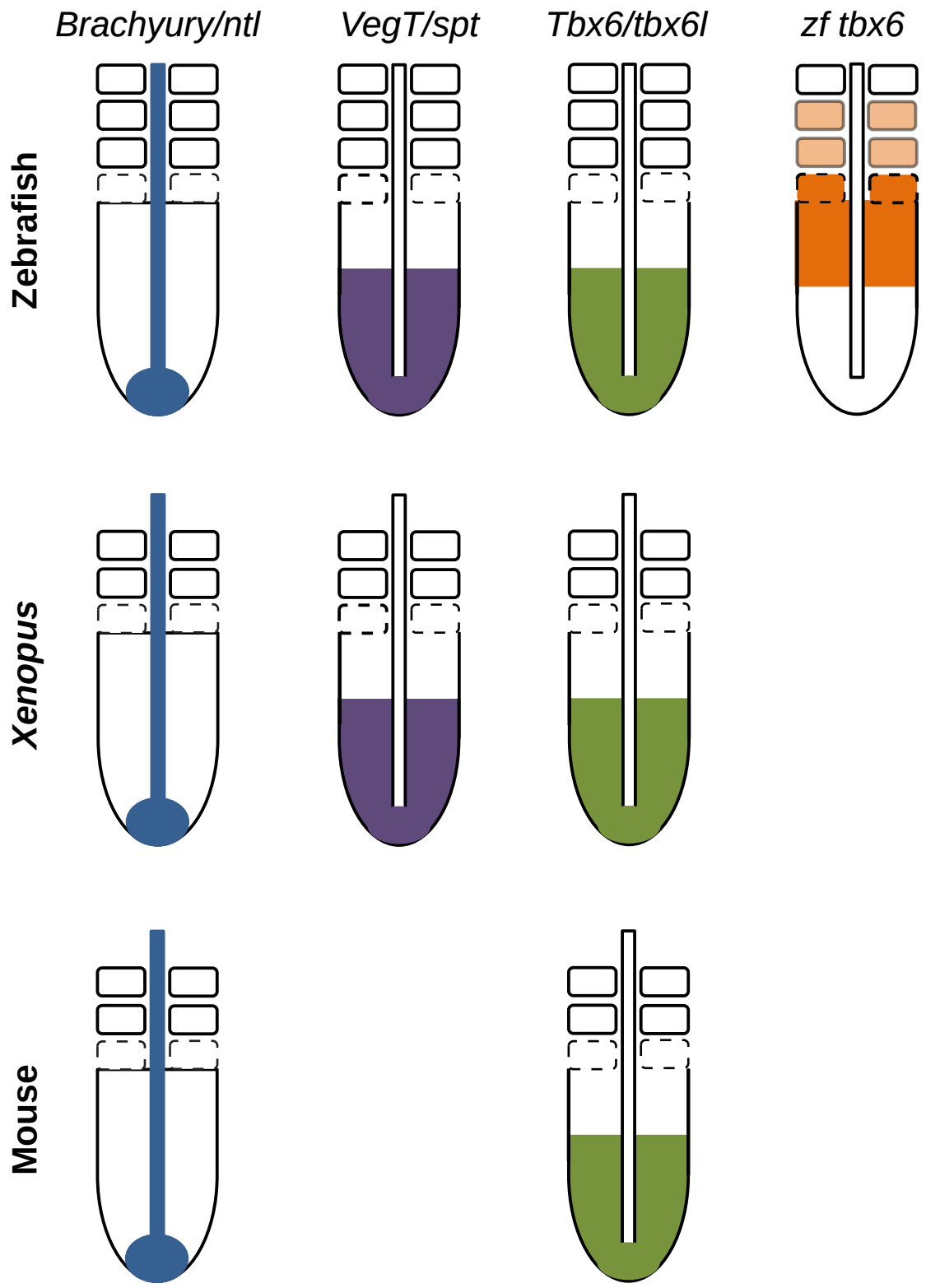
Brachyury/ntl
VegT/spt
Tbx6/tbx6l
zf tbx6
Zebrafish
Xenopus
Mouse

Figure 1.3 **T-box gene expression during somitogenesis**

Brachyury/*ntl* (blue), *VegT/spt* (purple), *Tbx6/tbx6l* (green), and *tbx6* (orange) expression in zebrafish, *Xenopus*, and mouse embryos during segmentation. Refer to Figure 1.1D for a diagram of the tail during segmentation. *Brachyury* orthologs are expressed in the tailbud and notochord. *VegT*/*spt* expression overlaps with *Brachyury* in the tailbud and is also present in the posterior PSM. *Tbx6* paralogs share the same expression profile as *VegT*/*spt* with the exception of zebrafish *tbx6,* which is expressed in the intermediate and anterior PSM. *tbx6* expression is also seen in the two most recently formed somites.

Chapter 2: Phenotypic and functional analysis of *msgn1*

Background

Mespo/Msgn1 is a transcriptional activator belonging to the Mesp family of basic helix-loop-helix (bHLH) transcription factors (Joseph and Casetta, 1999). Originally identified in *Xenopus* (as *Mespo)*, *Msgn1* orthologs are present in other vertebrates including chick, mouse and zebrafish (Buchberger et al., 2000; Yoon et al., 2000; Yoo et al., 2003). *Xenopus Mespo* expression is first detected during gastrulation where it is expressed in the ventrolateral mesoderm of the closing blastoderm, where it overlaps with *Xbra* and *VegT* expression, but not in the dorsal mesoderm. As the blastopore closes and somitogenesis proceeds, *Mespo* is expressed in the paraxial mesoderm and tailbud (Joseph and Casetta, 1999). Similarly, in mouse, *Msgn1* is initially expressed in the mesoderm of the primitive streak, becoming restricted to the posterior PSM and tailbud after the primitive streak regresses, where it overlaps with *Tbx6* expression (Yoon et al., 2000).

Over-expression of either murine *Msgn1* or *Xenopus Mespo* in *Xenopus* animal cap assays induced the expression of several genes indicative of ventrolateral mesoderm identity, including the *Xenopus* orthologs of B*rachyury*, *Wnt8*, and *MyoD*, but were unable to induce dorsal mesodermal markers *gsc* and *chordin* (Yoon et al., 2000; Tazumi et al., 2008). Loss-of-function studies indicate that *Msgn1* is required for proper differentiation and patterning of posterior mesoderm. Mice *Msgn1* null mutants fail to form somites or even generate paraxial mesoderm posterior to the forelimb, instead exhibiting grossly enlarged tailbuds due to unspecified cells which fail to migrate from the tailbud (Yoon and Wold, 2000). In *Xenopus*, loss-of-function studies were performed using a translation blocking MO to deplete *Mespo* function. *Mespo* morphants were able to form paraxial mesoderm, as indicated by their expression of somite and PSM markers *Paraxis* and *Papc*, but had disrupted somite boundaries. Additionally, the rostral-caudal patterning within somite compartments was lost (Wang et al., 2007). Thus it would appear that while the importance of *Msgn1* in mesoderm development is maintained, its biological function and mechanism are not.

The zebrafish *msgn1* ortholog is 75-80% identical to the mouse and *Xenopus* orthologs in the bHLH domain and shows a similar spatiotemporal expression pattern during development (Yoo et al., 2003). During gastrulation *msgn1* is expressed only in the ventrolateral margin and during segmentation expression is localized to the posterior PSM and tailbud (Yoo et al., 2003). *msgn1* expression is downstream of T-box proteins Ntl and Spt in zebrafish (Goering et al., 2003; Garnett et al., 2009), though its expression is regulated by the Tbx6 T-box transcription factor in *Xenopus* (Yoon et al., 2000; Wittler et al., 2007). Currently, it is not known whether zebrafish *msgn1* also regulates the expression of mesodermal T-box genes in the same manner as its orthologs in other species (Yoon et al., 2000). I obtained a line carrying a null *msgn1* allele from the zebrafish TILLING consortium and have used it to characterize the role of Msgn1 during mesoderm development in zebrafish.

Materials and Methods

Zebrafish stocks and husbandry

Wildtype embryos used were from the AB genetic background. The *msgn1*^{fh273} mutant was obtained from a TILLING screen of ENU mutagenized F1 fish (Draper, 2004). The fh273 allele introduces a nonsense mutation encoding an early stop codon near the beginning of the bHLH domain of the protein, Q92*. To identify the *msgn1* phenotype, fish were sorted by sex and set up in pairwise crosses. Otherwise, embryos were collected periodically from collecting cages made from pyrex dishes with mesh lids left in the fish tanks. Single and double mutant analyses with *spt* were done using the previously reported *spt*^{b104} allele (Griffin et al., 1998). Single and double mutant analyses with *ntl* were done using the previously reported *ntl*^{b195} allele (Schulte-Merker et al., 1994). Embryos were raised at 28.5°C unless otherwise noted. Lines for the following transgenes were obtained from the lab of David Kimelman: *hs:ntl (w73)*, *hs:spt (w72)*, *hs:TCFΔC (w74)*, and *hs:CA-ßcat (w75)* (Martin and Kimelman, 2010; Row et al., 2011; Martin and Kimelman, 2012). The *hs:dkk1-GFP (w32)* embryos were described in Stoick-Cooper et al., 2007.

Genotyping and PCR analysis

To collect genomic DNA, embryos from *msgn1*$^{+/-}$ intercrosses were anesthetized with tricaine. For a working dilution of tricaine, 4.2mL of a stock solution (0.4 g 3-amino benzoic acid ethylester (Sigma), 0.8 g Na_2HPO_4 (anhydrous) dissolved in 100 mL RO water) was diluted in 100mL of system water. Fish were immobilized in tricaine and briefly rinsed in system water. Their caudal fins were then cut with surgical scissors and placed in 0.6ul tubes containing 50ul of 1x ThermoPol Buffer (New England BioLabs). Using a thermocycler, the tissue was heated to 98°C for 10 minutes and cooled to 55°C. After 5 minutes at 55°C, 5 ul of 10mg/mL Proteinase K (NEB) was added to each tube. The tubes were incubated at 55°C for 1 hour before the enzyme was inactivated by heating to 98°C for 10 minutes. The samples were cooled to 4°C, then spun down in a tabletop centrifuge at 4°C for 10 minutes. The DNA-containing supernatant was transferred to new tubes and used for subsequent genotyping PCR. The primers used for genotyping *msgn*1 wildtype, and mutant alleles are: GT84 (-AGCAGAAGCCGAAAG TGAAG-3') and GT85 (5'-TGGTGTATTTGAGCGTCTGG-3'). The thermocycler program used is:

1) 95°C 2:00
2) 95°C 0:30
3) 64°C 0:30
4) 72°C 2:00
5) Repeat steps 2-4 for 40-42 cycles
6) 72°C 10:00
7) 4°C

5-10ul of the PCR product were digested with PvuII (Roche or Promega) overnight at 37°C. The digestion reaction was run on a 1.5% Agarose gel in 1x TBE buffer. The gel was then stained in 1xTBE containing 0.5ug/mL ethidium bromide.

Probe Synthesis

To generate linear templates for antisense probes against *ntl, myoD, tbx6 and msgn1* the following digests were performed: *ntl*, XhoI; *myoD*, XbaI (Allende et al., 1996); *tbx6*, SalI (Nikaido et al,. 2002); *msgn1*, BamHI (Goering et al., 2003). The digests were phenol-chloroform extracted and the DNA was precipitated with 3M sodium acetate and ethanol. The resulting pellets were suspended in 20ul of nuclease free molecular grade water and used in the following transcription reaction:

1 ug	DNA template
2 ul	10x transcription buffer
2 ul	10x labeling mix (digoxigenin- or fluorescein-labeled UTP)
1 ul	T7 or T3 RNA polymerase
1 ul	RNAse inhibitor
X ul	nuclease free water to 20 ul

T7 RNA polymerase was used in reactions for the *ntl, myoD,* and *msgn1* antisense probe. T3 RNA polymerase was used in the reaction for the *tbx6* antisense probe. Each 20 ul transcription reaction was incubated at 37°C for 2 hours and stopped with the addition of 2 ul 0.2M EDTA (pH 8). The RNA probe was precipitated by adding 2 ul 5M LiCl and 75 ul cold ethanol and storing at -70°C for 1 hour. The probe was pelleted by centrifugation at 13000rpm for 30 minutes, washed with 70% ethanol, and air-dried for 5 minutes. Each pellet was suspended in 100 ul nuclease free water. Probes were diluted 1:200 in pre-hybridization buffer for *in situ* hybridizations.

***In situ* hybridization and imaging**

To visualize mRNA transcripts, I used an *in situ* protocol based on that described in Thisse et al. (1993). Embryos were fixed in 4% paraformaldehyde at 4°C overnight. Embryos were rinsed twice with PBST (1XPBS, 0.1% Tween-20) to remove the fixative. Embryos younger than 20 somites were then dechorionated in petri dishes containing PBST. Those older than 20 somites were dechorionated prior to fixation. Following the quick rinses and dechorionation, embryos were washed 5 times for 5 minutes in PBST. Somite stage embryos were treated with Proteinase K (0.01ug/ul diluted in PBST), fixed for 20 minutes in 4% PFA at room temperature, and the PBST washes were repeated. Embryos were then incubated in 500ul of hybridization buffer (50% formamide, 5X SSC, 50ug/mL heparin, 500ug/mL yeast tRNA, 0.1% Tween-20, and 9.2uM citric acid to bring to pH ~6) at 65°C for 2-4 hours. The hybridization buffer was removed and replaced with hybridization solution containing digoxigenin- or fluorescein-labeled probe (1:200 dilution in hybridization buffer). Embryos were incubated in the probe at 65°C overnight. The following washes were done at 65°C: (1) 5 minutes in 2:1 hybridization buffer:2X SSC (2) 5 minutes in 1:2 hybridization buffer:2X SSC (3) 5 minutes in 2X SSC (0.1% Tween-20) (4) 20 minutes in 0.2X SSC (0.1% Tween-20) (5) Two 20 minute washes in 0.1XSSC (0.1% Tween-20). The remaining steps were carried out at room temperature: (6) 5 minutes in 2:1 0.1XSSC:PBST (7) 5 minutes in 1:2 0.1XSSC:PBST (8) 5 minutes in PBST. Embryos were blocked for 1 hour (0.05g/mL BSA, 2% sheep serum in PBST). The embryos were then incubated for 2 hours in a 1:5,000 dilution (anti-digoxigenin) or 1:10,000 dilution (anti-fluorescein) of the corresponding antibody conjugated to alkaline phosphatase. Embryos were washed 8 times for 15 minutes in PBST, followed by three

5-minute washes in alkaline phosphatase buffer (100mM Tris-HCl, 50mM MgCl2, 100mM NaCl, 0.1% Tween-20). Transcripts were visualized by transferring embryos into 500ul of coloration solution (4.5ul/mL NBT, 3.5ul/mL BCIP in alkaline phosphatase buffer) and viewed periodically to check for developing signal. The coloration reaction was stopped by washing 3 times with water, fixing 20-30 minutes in 4% PFA, and washing 5 times for 5 minutes with PBST. Fixed embryos stained by *in situ* hybridization were mounted in two ways. Wholemount embryos were dehydrated through washes in 1:1 1X PBST:methanol and 100% methanol, rehydrated and cleared in 1:1 Benzyl benzoate: Benzyl alcohol, and mounted in Permount (Fisher Scientific) on bridged slides to be photographed. Flat mount embryos were deyolked in 1X PBST, processed through a series of 5-10 minute glycerol washes (30% glycerol in PBST, 50% glycerol in PBST, and 70% glycerol in PBST), and mounted in 70% glycerol on a glass slide between vacuum grease posts for photographing. Live embryos were placed in 2:1 1.2% low melt agarose (Genesee Scientific):10x tricaine (final concentration of ~3x tricaine) and mounted between two coverslips to be photographed.

Microinjection

To make microinjection needles, borosilicate capillary tubes with filament (O.D. 1.2 mm, I.D. 0.94 mm; 10cm length, Sutter Instruments) were pulled using a micropipette puller (Sutter Instrument Co. Flaming/Brown Micropipette Puller, Model P-87). Needles were loaded with the injection solution and inserted into a pressure injector (Applied Scientific Instrumentation, #MMPI-3). Embryos were injected at the 1-2 cell stage with ~1-5 nL.

Morpholinos

The *mespa* morpholino (MO) sequence was previously published (Hart et al., 2007). The *mespa* MO was diluted to a concentration of 5ng/nL in a 0.2M KCl, 0.1% phenol red carrier solution. *mespa* MO or the carrier (control) solution were injected into embryos from a wildtype cross or embryos from a *msgn1* heterozygous intercross at the 1-cell stage. Siblings were raised to the 20 somite stage, scored for the *msgn1* mutant or *mespa* morphant phenotype and genotyped for the *msgn1*^{fh273} allele. The *spt* MO cocktail is a combination of two translation-blocking morpholinos (*spt-b* MO *and spt-c* MO) published previously (Garnett et al., 2009).

Heat-shock experiments

For experiments utilizing the *hs:dkk1-GFP* transgene (Stoick-Cooper et al., 2007), embryos were raised to the 5-somite or 13-somite stage at 28.5°C, shifted to 42°C fish water and incubated at 37°C for 1 hour. Embryos were then transferred to 25°C to recover for 4 or 7 hours before fixation in 4% PFA and *in situ* hybridization. For experiments using the *hs:TCFΔC*, *hs:spt*, *hs:ntl*, and *hs:CA-Bcat* transgenes, embryos were raised to the 13 somite stage at 25°C, shifted to 40°C, 40.5°C, or 41°C as indicated and incubated for 30 minutes, followed by a 3 hour recovery at 25°C. Embryos were then fixed and assayed for expression of *tbx6* or *msgn1* by *in situ* hybridization.

Nomenclature History

Zebrafish genes *tbx6* and *tbx24* were renamed in October 2011 in order to reflect the true orthologous relationship to human *Tbx6*. *tbx24* (Nikaido et al., 2002), which is considered to be the true human *tbx6* ortholog, was renamed *tbx6.* The previous *tbx6* gene (Hug et al., 1997) was renamed as *tbx6l* (*T-box gene 6-like)* to reflect its homology to human *Tbx6*.

Results

Loss of Msgn1 function results in a transiently enlargement of the tailbud and an increased number of somites at the end of segmentation

We received adult fish that were heterozygous for the *fh273 msgn1* allele. *msgn1*^{fh273} is a nonsense mutation at residue 92 that encodes a stop codon instead of glutamine (Q92*) (Fig 2.1 A). The resulting truncation occurs in the middle of the first helix in the bHLH motif (Sawada et al., 2000), such that the resulting protein product is likely unable to dimerize and bind to DNA. In order to identify the phenotype of *msgn1* mutants, I set up pairwise crosses of heterozygous fish and scored their progeny at 24 hpf based on morphology. While there were several defects observed at low percentages in some of the crosses, there was a slight enlargement of the tailbud that occurred in roughly a quarter of the progeny of all pairwise crosses (Fig 2.1 B,C). Embryos with an enlarged tailbud were genotyped and were found to be homozygous for the *fh273* allele. Thus, *msgn1* mutants develop a slightly enlarged tailbud that is readily detected by the 20-somite stage. This is reminiscent of the enlarged tailbud characteristic of the *spt* mutant phenotype. In *spt* mutants, the dramatic enlargement of the tailbud is caused by trunk mesoderm progenitors that fail to migrate out of the tailbud (Kimmel et al., 1989; Ho and Kane, 1990). In both *spt* and *msgn1* mutants the ball of cells in the tailbud continues to express *ntl,* a marker of progenitor mesoderm identity (Fig 2.6 C,E). Unlike *spt* mutants, in which the enlarged tailbud persists, the tailbud of *msgn1* mutants diminishes in size as somitogenesis progresses and by 48 hpf the mutants are indistinguishable from their wild-type siblings (Fig 2.1 D,E). *msgn1* mutants raised to adulthood are viable and fertile.

While the *msgn1* mutant phenotype is transient, I reasoned that if the slightly enlarged tailbud was truly reminiscent of the *spt* phenotype, *msgn1* mutants may generate fewer somites than their wildtype siblings. To score the number of somites, I fixed embryos at 36 hpf to ensure that all tail boundaries had formed and performed *in situ* hybridization (ISH) for the somite boundary marker *cb1045* (Fig 2.3 A,B). Embryos were scored for somite number based on somite boundary staining of *cb1045* and subsequently genotyped for the *msgn1*^{fh273} allele. Surprisingly, *msgn1* mutants formed an average of 1.6 more somites than their wildtype siblings (msgn1$^{-/-}$ avg = 33.1 somites; wildtype avg = 31.5 somites; p=0.002) (Fig 2.4), indicating that, unlike *spt, msgn1* is not required for the migration of cells from the tailbud. The cause of the extra somites generated in *msgn1* mutants is addressed in the discussion below.

Neither a second copy of *msgn1* nor maternally provided product is masking the defects of a zygotic *msgn1* mutant

The subtlety of the *msgn1* mutant phenotype in zebrafish, especially when compared to that reported for mouse and *Xenopus*, could be due to several reasons: (1) the mutation is not a null, (2) there is a second copy of the *msgn1* gene in the zebrafish genome, (3) *msgn1* is acting early in development and the presence of maternal product, either as mRNA or protein, is sufficient to aid the embryo through development, or (4) there is another gene acting in parallel with *msgn1*, such that the loss of *msgn1* has a minor effect on development. I address these possibilities in order below. First, the nature of the *fh273* point mutation should block dimerization and subsequent DNA binding (Maroto et al., 2009) of *msgn1* to gene targets, predicting a functional null. Second, using BLAST, the Ensembl Genome Browser, and ZFIN (The Zebrafish Model Organism Database), we were unable to identify a second copy of the *msgn1* gene in the current genomic assembly. Third, to test for maternal mRNA contribution I collected 2- to 4-cell stage embryos from a cross of wild-type fish. Some of these embryos were fixed to assay for *msgn1* mRNA by *in situ* hybridization, and RNA was extracted from the remaining embryos for RT-PCR analysis. The ISH results indicated no presence of maternal transcript. The RT-PCR analysis of maternal *msgn1* expression yielded contradictory results. Unfortunately, the *msgn1* gene does not contain an intron and I was therefore unable to definitively attribute amplification of a *msgn1* band to maternal expression or genomic contamination (Fig 2.2 A,B, data not shown). In order to definitively address whether there was maternal contribution potentially masking zygotic loss-of-function defects, I set up two pairwise crosses of *msgn1* mutant females to *msgn1* heterozygous males. The mutant phenotype segregated with Mendelian ratios, with roughly 50% of the progeny from each pairwise cross displaying the slightly enlarged tailbud characteristic of *msgn1* mutants (Fig 2.2, C). The enlargement observed in the maternal-zygotic *msgn1* mutants was no more severe, either in size or perdurance of the enlarged tailbud, than that observed in the zygotic *msgn1* mutants. The maternal-zygotic embryos were not raised to assay viability and fertility compared to the zygotic mutants. At the same time, two pairwise crosses between *msgn1* heterozygous females and *msgn1* homozygous males were set up, and their progeny was scored. Similarly, nearly 50% of the progeny displayed the *msgn1* phenotype (Fig 2.2, D). There was also no difference in the severity of the phenotypes when comparing mutants from the *msgn1*$^{-/-}$ mother to mutants from the *msgn1*$^{+/-}$ mother. Thus, I conclude that maternal contribution is not compensating for the loss of zygotic *msgn1*.

***mespa* does not have an overlapping role with *msgn1* in the developing embryo**

Another possible explanation for the subtle phenotype observed when knocking down *msgn1* is a different gene with overlapping function. Initially, we hypothesized the subtle *msgn1* loss of function phenotype may be due to functional redundancy with another Mesp family gene, and chose to examine the genetic interaction between *msgn1* and *mesoderm posterior aa* (*mespaa*). Like *msgn1*, *mespaa* was identified as a potential downstream target of mesoderm transcription factors Ntl and Spt (Garnett et al., 2009; Morley et al., 2009). *mespaa* also has a spatiotemporal expression pattern very similar to that of *msgn1* during gastrulation (Sawada et al., 2000). I used a previously published *mespaa* morpholino (MO) to deplete *mespaa* function in *msgn1*

mutants. I tested a range of *mespaa* MO doses in wildtype embryos to identify a suboptimal dose that would decrease *mespaa* expression without yielding an obvious phenotype, as well as a second dose that mimicked the *mespaa* MO phenotype reported previously (Hart et al., 2007). Injection doses between 12-25 ng were toxic, doses of 6-8 ng gave body axis truncations and tail defects similar to those published by Hart et al. (2007), and doses of 1-2 ng were suboptimal. I injected the progeny of a *msgn1*$^{+/-}$ intercross with the suboptimal dose and the 6-8ng dose of *mespaa* MO. If there were a genetic interaction or functional redundancy between *msgn1* and *mespaa*, I expected to see increased severity of the *msgn1* phenotype with either complete or partial loss of *mespaa* function. Instead, I observed no phenotypic indication of a *msgn1*/*mespaa* genetic interaction (data not shown).

msgn1 and *spt* function together in zebrafish mesoderm development

Because *msgn1* is a known target of Spt, and its loss-of-function phenotype resembles a less severe version of the *spt* loss-of-function phenotype, I hypothesized that the two genes may have overlapping roles during development. To test this hypothesis, I made a *spt*$^{+/-}$*;msgn1*$^{+/-}$ line to determine the effects, if any, of depleting *msgn1* in a *spt* mutant background. *spt*$^{+/-}$*;msgn1*$^{+/-}$ fish were crossed and their progeny were scored based on morphology and then genotyped. Whereas somites form in *msgn1* (trunk and tail, Fig 2.5 B) and *spt* single mutants (trunk only, Fig 2.5 D), *spt*;*msgn1* double mutants lack both tail and trunk somites (Fig 2.5E), recapitulating the mouse *Msgn1* mutant phenotype (Yoon and Wold, 2000). *spt*;*msgn1* double mutants also have a more severe enlargement of the tailbud than that exhibited in either *msgn1* or *spt* single mutants (Fig 2.5 B,D,E). The cells accumulating in the tailbud express the progenitor marker *ntl* (Fig 2.6F), suggesting that the accumulating cells are progenitors that failed to exit the tailbud and differentiate. Further evidence for the genetic interaction between *msgn1* and *spt* is demonstrated by the *msgn1*$^{-/-}$*;spt*$^{+/-}$ mutants. Removing one functional copy of *spt* in a *msgn1*$^{-/-}$ background enhances the severity of the tailbud enlargement observed in *msgn1* single mutants (Fig 2.5C). However, these *msgn1*-enhanced mutants form the same number of somites as *msgn1* single mutants (Figure 2.4), although the most posterior somites have slightly perturbed boundaries (Fig 2.3, C).

Mesoderm progenitors fail to differentiate in *spt*;*msgn1* double mutants

Mesoderm differentiation progresses as cells move ventrally from the tailbud epiblast into the underlying hypoblast. This region is subdivided into three main regions, each with its own distinct expression of mesoderm markers. As the cell enters the hypoblast it becomes part of the posterior body wall, which expresses *ntl* and *wnt8a* (Griffin and Kimelman, 2002). *ntl* and *wnt8*a function in a positive feedback loop to inhibit differentiation of cells in the posterior body wall, which serves to maintain a population of mesodermal progenitor cells (Griffin and Kimelman, 2002; Martin and Kimelman, 2008; Martin and Kimelman, 2010). The progenitor cells then exit the posterior body wall and enter the maturation zone. In this transitional zone, cells express mesodermal transcription factors, *spt, tbx6l* and *msgn1,* in addition to *ntl* and *wnt8a* (Griffin and Kimelman, 2002). Finally, cells migrate from the maturation zone into the posterior PSM where they continue to express *spt, tbx6l* and *msgn1* but down-

regulate the progenitor markers *ntl* and *wnt8a* (Griffin and Kimelman, 2002). As cells are displaced more anteriorly within the PSM and differentiate further, they begin to express *tbx6*. Finally, once cells have passed through the anterior PSM and have been incorporated into somites, the caudal half of the somite expresses *myoD,* a marker of later muscle differentiation (Weinberg et al., 1996; Rudnicki et al., 1993; Hinits et al., 2011) (Fig 2.6, A).

As mentioned previously, *msgn1* and *msgn1*-enhanced mutants complete somitogenesis, indicating mesoderm differentiation is largely unaffected. This is further demonstrated at the molecular level as *ntl, tbx6,* and *myoD* expression in the *msgn1* and *msgn1*-enhanced mutants are relatively unchanged compared to wildtypes (Fig 2.6, B-D, G-I, L-N). *spt* mutant somitic precursors fail to progress from the tailbud to trunk, which accounts for the accumulation of progenitor cells in the tailbud, but are able to form somites in the tail (Kimmel et al., 1989; Ho and Kane, 1990). In *spt* mutants, *tbx6* and *myoD* expression recover in the PSM as progenitors that will contribute to the tail paraxial mesoderm migrate out of the tailbud (Fig 2.6, J,O). In contrast, *tbx6* and *myoD* expression are completely absent in *spt*;*msgn1* double mutants. In addition, an even larger ball of *ntl*-expressing progenitor cells accumulates in the double mutant tailbud (Fig 2.6 F).

Expression of *msgn1* is required, in addition to the absence of progenitor genes *ntl* and *wnt8a,* for the induction of anterior PSM gebe *tbx6*

A one hour pulse of *msgn1* at the 13-somite stage causes ectopic expression of *tbx6* in the somites 2 hours post-heat-shock (hpHS) and down-regulation of progenitor markers *ntl* and *wnt8a* in the tailbud at 7 hpHS (Rita Fior, personal communication). Ectopic *tbx6* expression is observed in the tailbud after 7 hpHS, once *ntl* and *wnt8a* tailbud expression are absent (Rita Fior, personal communication). This suggests that *tbx6* expression is positively regulated by *msgn1*, but only outside of the *ntl/wnt*-expressing tailbud domain. To test this possibility we used a transgenic line, *hs:dkk1-GFP* (Stoick-Cooper et al., 2007), to inhibit Wnt signaling by expressing the extracellular Wnt antagonist gene *dickkopf* (*dkk1*) under heat-shock control. Loss of Wnt signaling abolishes the *ntl*/*wnt* positive feedback loop in the tailbud and thus results in the loss of both *ntl* and *wnt8a* expression in the tailbud (Martin and Kimelman, 2008). *hs:dkk1-GFP* progeny were injected at the 1-cell stage with either a control carrier solution or *spt* MO. The purpose of injecting the *spt* MO was to increase the size of the tissue being scored. Embryos were raised to either the 5- or 13-somite stage (to assess the effect on trunk and tail mesoderm development, respectively), heat-shocked for 1 hour at 37°C, and allowed to recover for 4 or 7 hours (Table 2.1).

Embryos were sorted as having strong (GFP+), weak (GFP+/-), or no fluorescence (GFP-), and assessed for *tbx6* expression (Fig 2.7). Embryos that were not subjected to heat-shock did not express GFP (n=74). GFP+ embryos injected with the control solution did not show ectopic *tbx6* expression (Fig 2.8 A,B; Table 2.1). Surprisingly, ectopic induction of *tbx6* was only observed in the tailbuds of GFP+ embryos that were depleted of *spt* function (Table 2.1). In embryos heat-shocked at 5-somites, the ectopic *tbx6* expression was primarily present in the cells of the dorsal midline, with a few cells expressing *tbx6* in the tailbud (Fig 2.8 C-E). Embryos that were heat-shocked at 13-somites showed more tailbud *tbx6* expression (Fig 2.8 F-J). Based

on these results, it appears that *spt* also plays a role in inhibiting the differentiation of mesoderm cells as determined by expression of the PSM marker *tbx6*. These results show that loss of *ntl/wnt* expression in progenitor cells is not sufficient for *tbx6* to be activated by *msgn1* in the tailbud. However, they do not address whether *msgn1* is ectopically expressed when progenitor identity is lost, but at insufficient levels to induce *tbx6*. To address this possibility, I used a stable line to induce expression of a dominant negative form of TCF (*hs:TCFΔC*) which lacks the DNA binding domain and inhibits the transcriptional response to Wnt signaling (Martin and Kimelman, 2012). In this construct, the truncated TCF is fused to GFP. Embryos were raised to the shield stage, heat-shocked for 30 minutes at 41°C, and allowed to recover for 3 hours. Embryos were sorted based on GFP expression and hybridized with a probe against *msgn1*. There was no *msgn1* expression outside of the endogenous expression domain observed in GFP positive (n=33), GFP negative (n=17) or no heat-shock controls (n=43) (data not shown). I conclude from the data that while inhibiting progenitor identity of cells by knocking down the Ntl/Wnt regulatory loop is required to alleviate the repression of differentiation in the tail, it is not sufficient to induce expression of later differentiation genes, *msgn1* and *tbx6*.

msgn1 does not have an overt genetic interaction with *ntl*

In addition to being regulated by Spt, *msgn1* is also regulated by Ntl during mesoderm development (Goering et al., 2003; Garnett et al., 2009; Morley et al., 2009). To investigate whether *msgn1* interacts with *ntl* in a similar manner to interact its interaction with *spt*, I set up an intercross between $ntl^{+/-};msgn1^{+/-}$ fish. The progeny were scored, and based on their morphology, were classified as *ntl* mutants, *msgn1* mutants, or wildtype embryos (Fig 2.9). *ntl* mutants were genotyped for both the *ntl* and *msgn1* mutant alleles and *ntl;msgn1* double mutants were found to segregate with and were indistinguishable from the *ntl* single mutants. Additionally, loss of a functional copy of *ntl* in a $msgn1^{-/-}$ background did not enhance the *msgn1* phenotype. Thus, I conclude that *msgn1* and *ntl* do not interact genetically.

Discussion

msgn1 is not required for zebrafish development

I have shown that zebrafish *msgn1* mutants display an enlarged tailbud during segmentation as compared to wildtype embryos. Like *spt* mutants, this enlargement appears to be caused by the accumulation of progenitor cells in the tailbud. Unlike the *spt* mutant, these cells do not eventually undergo cell death. Instead, our work suggests cells accumulating in the tailbud of *msgn1* mutants do eventually exit from the tailbud and incorporate into somitic mesoderm. This delayed migration might be the reason why *msgn1* mutants form more somites than wildtype counterparts (Fig 2.4). The generation of extra somites in *msgn1* mutants could also be the result of an increase in the frequency of the molecular oscillations that make up the “clock” regulating somitogenesis. The increased frequency of the oscillations would increase the number of somites . In mouse, *msgn1* has been shown to regulate the expression of several “clock” genes (Yoon and Wold, 2000; Chalamalasetty et al., 2011). However, I favor the former explanation since cell tracking experiments performed by our collaborators, Rita

Fior and Leonor Saude, in addition to the wild-type expression of PSM and somite markers in *msgn1* and *msgn1*-enhanced mutants, show that *msgn1* mutant cells exit the tailbud, but are slower to do so than wildtype cells (Fig 2.5; Rita Fior, personal communication). The subtle phenotype of *msgn1* mutants, in addition to their viability and fertility as adults, indicates that *msgn1* is not required for the specification or subsequent patterning of paraxial mesoderm in zebrafish, in sharp contrast to the role of *msgn1* orthologs in other vertebrates (Yoon and Wold, 2000; Yoon et al., 2000; Wang et al., 2007).

Genetic interaction of *msgn1* and *spt* in the paraxial mesoderm

The similarity between *msgn1* mutants and *spt* mutants led me to investigate a genetic interaction between the two, and I showed that *msgn1* and *spt* function together in the tailbud to promote the transition of cells from the tailbud to the PSM. The *spt*;*msgn1* double mutant phenotype is nearly identical to that of the mouse *Msgn1* mutant, indicating that the role of *Msgn1* in mice is predominantly carried out by *spt* in zebrafish, with assistance from *msgn1*. Having one or more transcriptional targets shared by Spt and Msgn1 would explain why the loss of *msgn1* in a *spt* mutant may compound the effects exhibited by either single mutant. Recently, Row et al. (2011) reported that *spt* mutant cells stall in their epithelial to mesenchymal transition, failing to down-regulate cell protrusions and cell-cell contacts at the time wild-type cells do. The argument for *spt* as the main mediator of this transition is also supported by the fact that mesoderm development in the *msgn1*-enhanced mutants is no more affected than in *msgn1* single mutants, despite only having one functional copy of the wild-type *spt* allele.

There is strong support for distinct pathways regulating the formation of anterior versus posterior somites (Griffin et al., 1995; Kanki and Ho, 1997; Griffin et al., 1998; Julich et al., 2005; reviewed by Holley, 2007). Given that tail somites form in *spt* mutants, it is also possible that a third gene, in addition to *msgn1* and *spt*, regulates the tailbud to PSM transition in a regulatory network governing tail mesoderm formation. One obvious candidate would be *ntl.* Ntl is required for tail formation in zebrafish and is also upstream of *msgn1* during tail somitogenesis. Moreover, the *spt*-enhanced mutant reported by Goering et al. (2003), in which the *spt* mutant also lacks one functional copy of the *ntl* gene, displays a severe loss of trunk *and* tail mesoderm. However, based on the absence of a synergistic *ntl*;*msgn1* double mutant phenotype, it is unlikely that *ntl* functions similarly to *spt* and *msgn1* in mediating migration of cells out of the tailbud. *one-eyed pinhead* (*oep*), which encodes a co-receptor required for Nodal signaling (Gritsman et al., 1999), is also a good candidate for a gene sharing functional redundancy with *spt* in the tail segmentation program. Maternal-zygotic *oep* (*MZoep*) mutants fail to form trunk paraxial mesoderm and axial mesoderm derivatives but do generate tail somites (Gritsman et al., 1999). Szeto and Kimelman (2006) demonstrated that the body axis is divided into different regions and that exposure to signals from the Bmp and Nodal signaling families dictate the time and position along the body axis that cells exit the tailbud to be incorporated into somites of each region. In contrast to Nodal signaling mutants, BMP signaling mutants are severely dorsalized, exhibiting posterior truncations and an absence of ventrally-derived tail structures (Mullins et al., 1996; Kishimoto et al., 1997; Feldman et al., 1998; Gritsman et al., 1999; Schmid et al., 2000;

Pyati et al., 2005). In accordance with these results, constitutive activation of nodal signaling in *MZoep* mutants rescued formation of the anterior trunk somites while over-expression of *bmp2b* in *MZoep* mutants resulted in somites with more posterior tail positions (Szeto and Kimelman, 2006). *oep*;*spt* mutants are similar to *spt*;*msgn1* double mutants, exhibiting a complete loss of trunk and paraxial mesoderm and an accumulation of *ntl*-staining cells in the tailbud (Griffin and Kimelman, 2002). Interestingly, *msgn1* expression is not decreased in the *oep*;*spt* double mutant indicating that the *oep;spt* and the *spt*;*msgn1* pathways may converge on similar targets, which in turn mediate the migration of mesodermal cells out of the tailbud. Another possibility that has not been tested is that *spt*;*msgn1* double mutants may exhibit decreased Nodal signaling, which would be another way to explain the nearly identical *oep;spt* and *spt*;*msgn1* posterior mesoderm mutant phenotypes.

Finally, despite the fact that mouse Msgn1 and *Xenopus* Mespo are highly conserved and exhibit the same mesoderm-inducing effects in *Xenopus* animal cap assays (Yoon et al., 2000; Tazumi et al., 2008), the loss-of-function phenotype in *Xenopus* suggests that function may not be entirely conserved between the two vertebrate species. In *Xenopus*, Mespo-depleted cells exit the tailbud but are not properly patterned, resulting in undifferentiated paraxial mesoderm, but no accumulation of cells in the tail (Wang et al., 2007). In fact, to date, there is no gene whose deficiency results in the accumulation of mesodermal cells in the tailbud of *Xenopus* embryos. Thus, it is entirely possible that the migration of cells from the tailbud to the PSM in *Xenopus* is governed by an as yet unknown gene.

Loss of progenitor identity is not sufficient to induce differentiation of mesoderm in the tailbud

Data collected by our collaborators (Rita Fior and Leonor Saude) indicated that global over-expression of *msgn1* results in body truncations at the trunk level and loss of notochord. Additionally, following a pulse of *msgn1* over-expression from a heat-shock promoter, they saw ectopic *tbx6* expression in the somites by 2 hpHS but only detected ectopic *tbx6* expression in the tailbud correlating with the loss of *ntl* and *wnt8a* expression (Rita Fior, personal communication). This is similar to the defects caused by *Mespo* over-expression in *Xenopus*. Injection of *Mespo* transcripts into the dorsal marginal zone of *Xenopus* embryos inhibits the expression of the dorsal marker *chordin* and at the tailbud stage many yield truncated axes and notochord defects (Yoon et al., 2000). Thus, one conserved function of Msgn1 may be to inhibit dorsal mesoderm fates. Mouse *Msgn1* and *Xenopus Mespo* are also capable of inducing ventrolateral markers and behaviors (Yoon et al., 2000). Whether *msgn1* has the potential to induce markers of panmesodermal and ventral mesoderm identity in the same manner as its vertebrate orthologs was not tested, but the downregulation of *ntl*, *wnt8a, and wnt3a* transcripts in response to global *msgn1* expression indicates a potential negative feedback loop. Similarly, in mouse *Msgn1* null mutants, expression of *Wnt3a* is upregulated, indicating conservation of the Wnt/Msgn1 negative feedback loop in vertebrate posterior development (Nowotschin et al., 2012). In zebrafish, *ntl* and *wnt8a/wnt3a* form a positive feedback loop that serves to maintain a stem-cell like population of progenitors in the tailbud (Martin and Kimelman, 2008, 2010). This mechanism is also conserved in mouse; *Wnt3a* null mice exhibit reduced *Brachyury* expression, an absence of somites

posterior to the forelimb, and posterior truncations, while *Brachyury* mutants have reduced *Wnt3a* expression (Takada et al., 1994; Yamaguchi et al., 1999). Although its expression is initiated in the tailbud, Msgn1 acts to repress progenitor cell identity and behavior, promoting movement of cells into the PSM where they are able to differentiate outside of the influence of pro-proliferation signals of the tailbud.

We hypothesized that in the negative feedback loop, *msgn1* expression is activated by Ntl and Wnt signaling in progenitor cells as they enter the maturation zone. Msgn1 then down-regulates *ntl*, *wnt8a*, and *wnt3a* expression, which is required for cells to enter the PSM and for the expression of later differentiation markers such as *tbx6*. If the proposed network is correct, we expected that inhibiting the Ntl/Wnt loop would be sufficient to induce ectopic expression of *tbx6*. We expressed inhibitors of Wnt signaling, which also result in the loss of *ntl* in the tailbud, but did not detect ectopic expression of *tbx6* in the tailbud. It could be argued that because *msgn1* is a target of *ntl*, a decrease in *ntl* expression would result in a loss of *msgn1* expression and thus no induction of *tbx6*. However, downregulation of *spt,* of which *msgn1* is also a target, in addition to knocking down *ntl* and *wnt* expression esulted in ectopic *tbx6* expression in both the progenitor zone and dorsal midline. Even though *spt* expression does not appear to be negatively regulated by over-expression of *msgn1* (Rita Fior, peronsal communication), neither *spt*, *ntl*, nor *wnt8a* expression overlap with *tbx6* expression, leaving the possibility that their activity in the tailbud and paraxial mesoderm serve to inhibit *tbx6* expression and intermediate mesoderm identity until cells have shifted into the anterior PSM. Based on the above results, *msgn1* may have two roles in the tailbud. The first is to promote a permissive environment for differentiation by turning off the progenitor identity of cells through its negative regulation of *ntl, wnt8a, and wnt3a* expression. The second may be to induce *tbx6* expression directly or indirectly for later differentiation.

Figure 2.1

A.

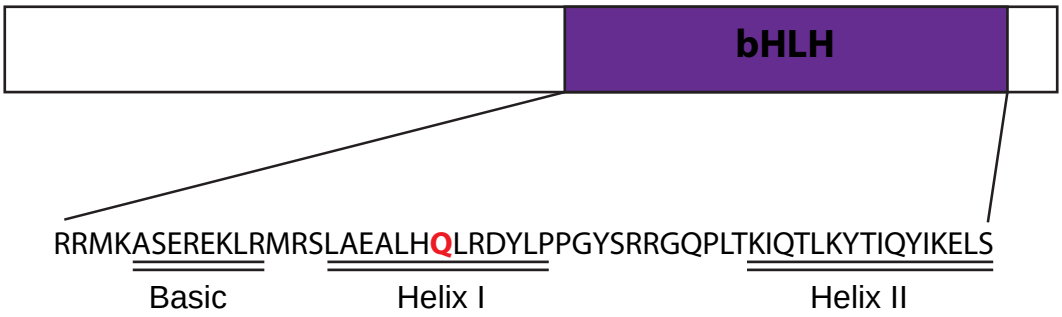
bHLH
RRMKASEREKLRMRSLAEALHQLRDYLPPGYSRRGQPLTKIQTLKYTIQYIKELS
Basic
Helix I
Helix II

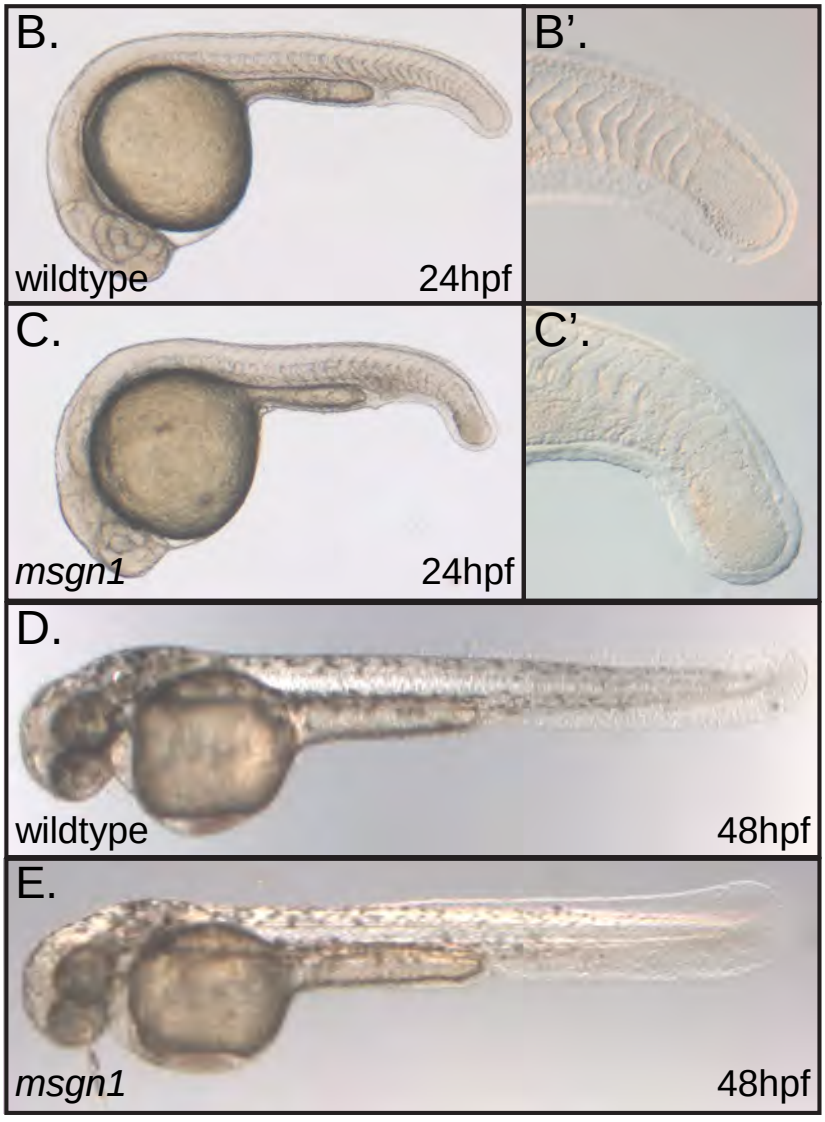
B.
wildtype
24hpf
B'.
C.
msgn1
24hpf
C'.
D.
wildtype
48hpf
E.
msgn1
48hpf

Figure 2.1. **The null *msgn1* mutant phenotype is subtle**

(A) A diagram of the *msgn1* coding sequence is shown with the bHLH binding domain in purple. Underneath, the amino acid sequence of the bHLH domain is shown with the basic domain and helices double-underlined. The red residue indicates the glutamine which is mutated to a stop codon in the *fh273* allele. Wildtype embryos (B) or *msgn1* $^{-/-}$ mutants (C) at 24hpf. (B') and (C') are magnifications of the tails of the embryos to the left. Wildtype embryos (D) or *msgn1*$^{-/-}$ mutants (E) at 48hpf.

Figure 2.2

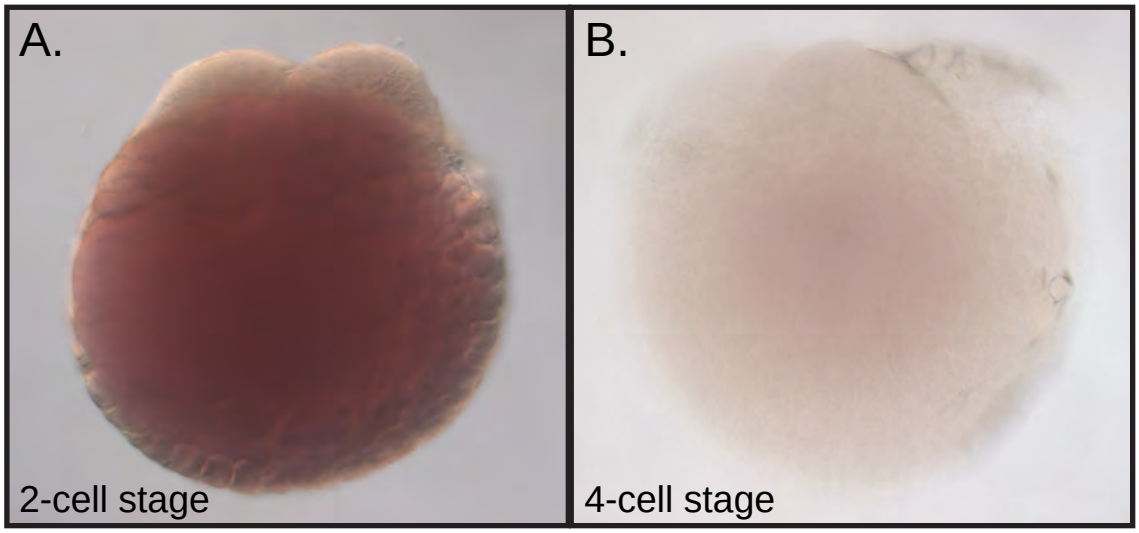

C.

male *msgn1* het X female *msgn1* mutant		
pairwise cross	WT	*msgn1*
1	21	25
2	4	3

D.

female *msgn1* het X male *msgn1* mutant		
pairwise cross	WT	*msgn1*
1	29	27
2	17	17

Figure 2.2. **There is no evidence of maternal *msgn1* contribution**

Embryos at the 2-cell (A) or 4-cell (B) stage were hybridized with a *msgn1* riboprobe to detect maternal transcript. (C and D) Tables showing the number of *msgn1* mutants recovered from a cross of *msgn1*$^{-/-}$ females with *msgn1*$^{+/-}$ males (C) or *msgn1*$^{+/-}$ females with *msgn1*$^{-/-}$ males (D). The fish were mated pairwise and their progeny were scored as either wildtype or *msgn1* based on their tailbud morphology.

Figure 2.3

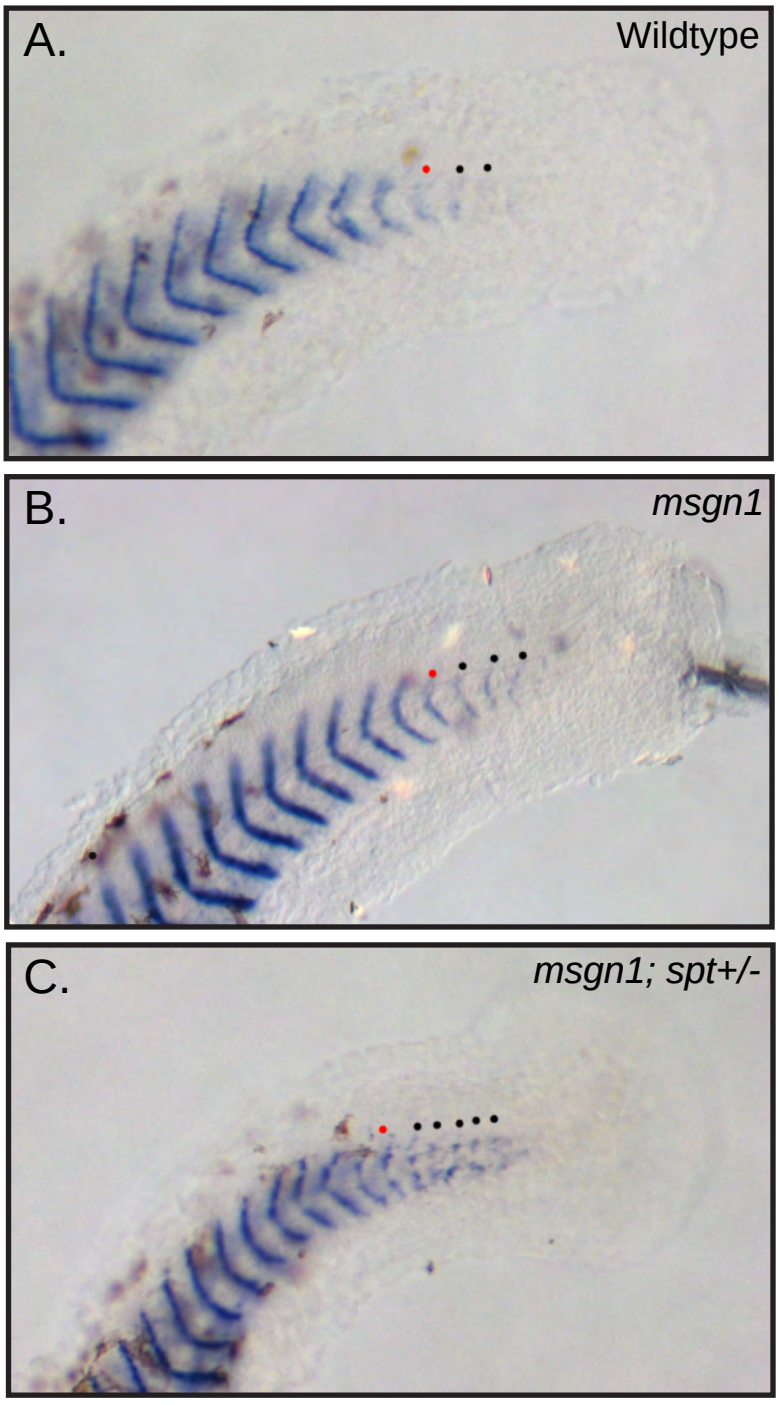

Figure 2.3. ***cb1045* staining of somite boundaries in wildtype and *msgn1*$^{-/-}$ embryos**

Wildtype (A), *msgn1* (B) or *msgn1-enhanced* (C) embryos at 36hpf once all somite boundaries have formed. Somite boundaries were visualized by wholemount *in situ* hybridization with a dig-labeled *cb1045* probe. The red dot marks the posterior boundary of the 30th somite in all embryos. Black dots mark the posterior boundary of each additional somite formed after somite 30. The more posterior somite boundaries in *msgn1-enhanced* embryos are slightly disrupted compared to those in WT or *msgn1* embryos.

Figure 2.4

A.

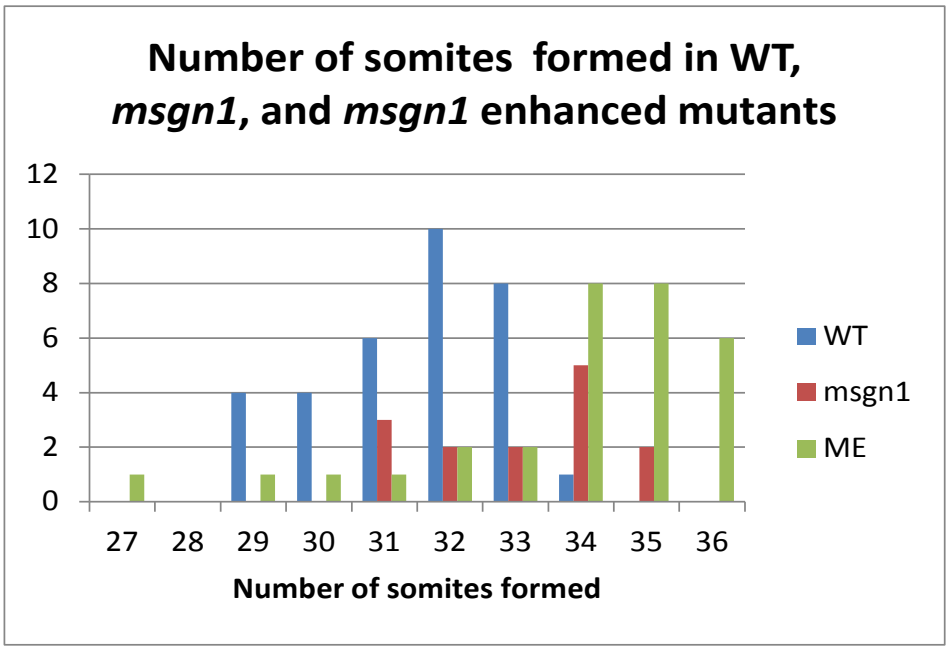

B.

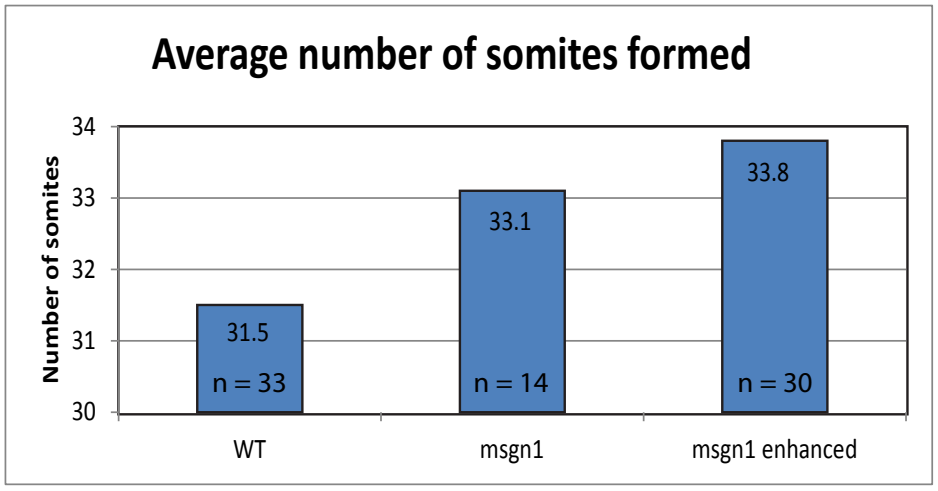

C.

	WT vs *msgn1*	WT vs *msgn1* enhanced	*msgn1* vs *msgn1* enhanced
p	0.002*	0.00001*	0.179

Figure 2.4. ***msgn1* mutants generate more somites than wildtype embryos**

(A) Histogram showing the number of somites formed in WT (blue, n=33), *msgn1* (red, n=14), and *msgn1-enhanced* (green, n=30) embryos. (B) The average number of somites formed in WT, *msgn1* and *msgn1-enhanced* embryos. (C) The average number of somites formed in WT, *msgn1* and *msgn1-enhanced* embryos was compared using a two-tailed student's T-test. The p value for each comparison is indicated. Asterisk indicates the difference between two groups was significant.

Figure 2.5

Figure 2.5. ***spt* and *msgn1* exhibit functional redundancy in the paraxial mesoderm**

Live images of 24hpf embryos (A-E) and enlarged images of their tails (A'-E') in a wildtype embryo (A,A'), *msgn1* mutant (B, B'), *msgn1-enhanced* mutant (C, C'), *spt* mutant (D,D'), and *spt*;*msgn1* double mutant (E, E') embryos. Asterisks mark somites formed in the tail. The subtle enlargement of the tailbud in *msgn1* mutants as compared to wildtype embryos (B' vs A') becomes progressively larger as *spt* function is removed in *msgn1-enhanced* (*msgn1*$^{-/-}$;spt$^{+/-}$) mutants, and *spt* single mutants. Loss of both *msgn1* and *spt* is more severe than loss of *spt* alone. In addition to having a larger tailbud than *spt* single mutants, *spt*;*msgn1* double mutants fail to form somites (E' vs D').

Figure 2.6

A.

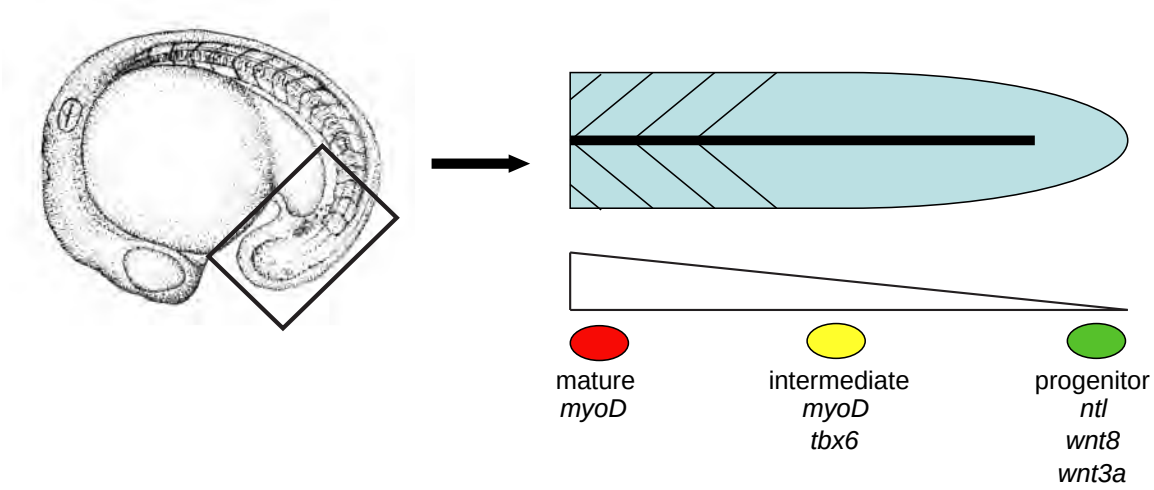
mature
myoD
intermediate
myoD
tbx6
progenitor
ntl
wnt8
wnt3a

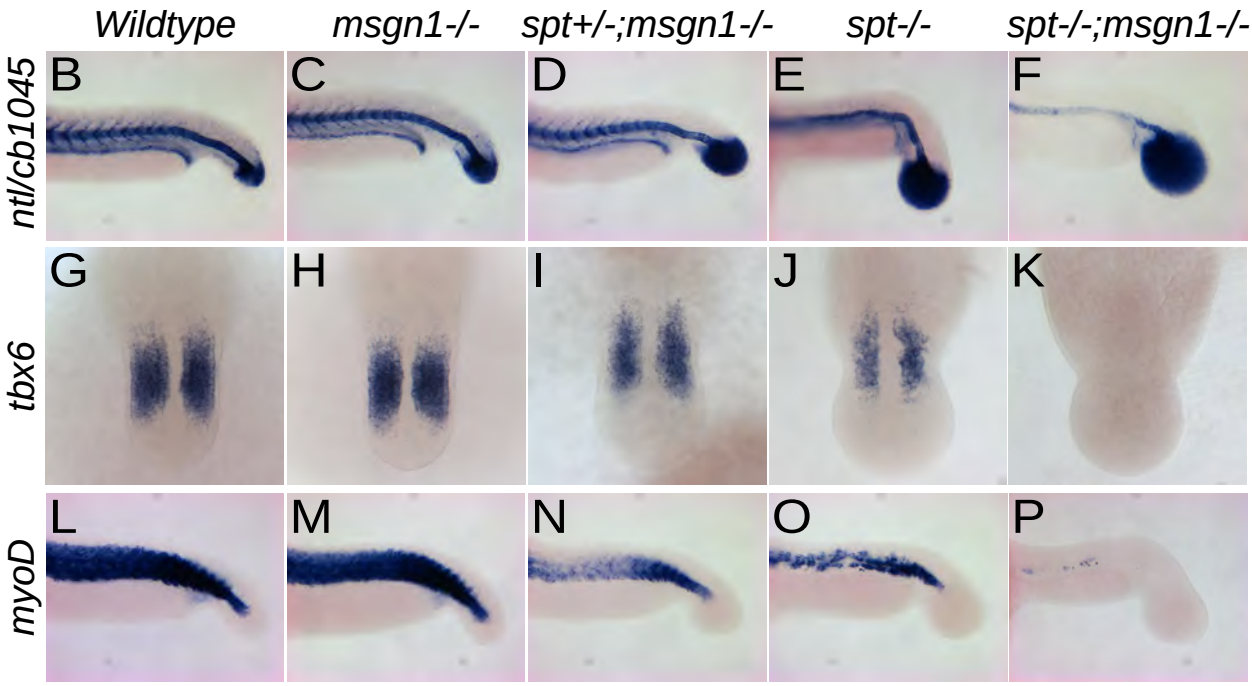
Wildtype
msgn1-/-
spt+/-;msgn1-/-
spt-/-
spt-/-;msgn1-/-
ntl/cb1045
tbx6
myoD
B
C
D
E
F
G
H
I
J
K
L
M
N
O
P

Figure 2.6. ***msgn1* and *spt* are required for mesodermal progenitors to transition from the tailbud to the PSM**

(A) The left shows an embryo during mid-segmentation (17-18 somites). The posterior end of the embryo containing the tailbud, paraxial mesoderm, and recently formed somites is highlighted and schematized on the right. Beneath the diagram of the posterior end I've shown the progression of differentiation from the tailbud to the somites based on genes being expressed by cells in each region. The green cell represents progenitor cells in the tailbud which express *ntl*, *wnt8* and *wnt3a*. As cells migrate out of the tailbud and become displaced anteriorly in the PSM, they turn off *ntl* and express markers of intermediate paraxial mesoderm, *myoD* and *tbx6* (yellow cell). Cells turn off *tbx6* and continue to express *myoD* once they are incorporated into somitic mesoderm (red cell). Staining of *ntl*/*cb1045*, *tbx6*, and *myoD* in wildtype (B,G,L), *msgn1* mutant (C,H,M), *msgn1*-enhanced mutant (D,I,N), *spt* mutant (E,J,O), and *spt;msgn1* double mutant embryos (F,K,P). *ntl* marks the larger tailbud compartment due to accumulation of progenitor cells in each mutant. *cb1045* staining marks the trunk somite boundaries. Tail somite boundaries have not matured but do stain for *cb1045* in all but the *spt;msgn1* double mutants by 36 hpf (data not shown). *tbx6* is eventually expressed by cells in the intermediate PSM in all embryos except *spt;msgn1* double mutants. Unlike in *spt* mutants *myoD* expression does not recover in *spt;msgn1* double mutants, and no somites are formed. B-F are lateral views at 24hpf. G-K are dorsal views at 15-16 somites. L-P are lateral views at 15-16 somites.

Figure 2.7

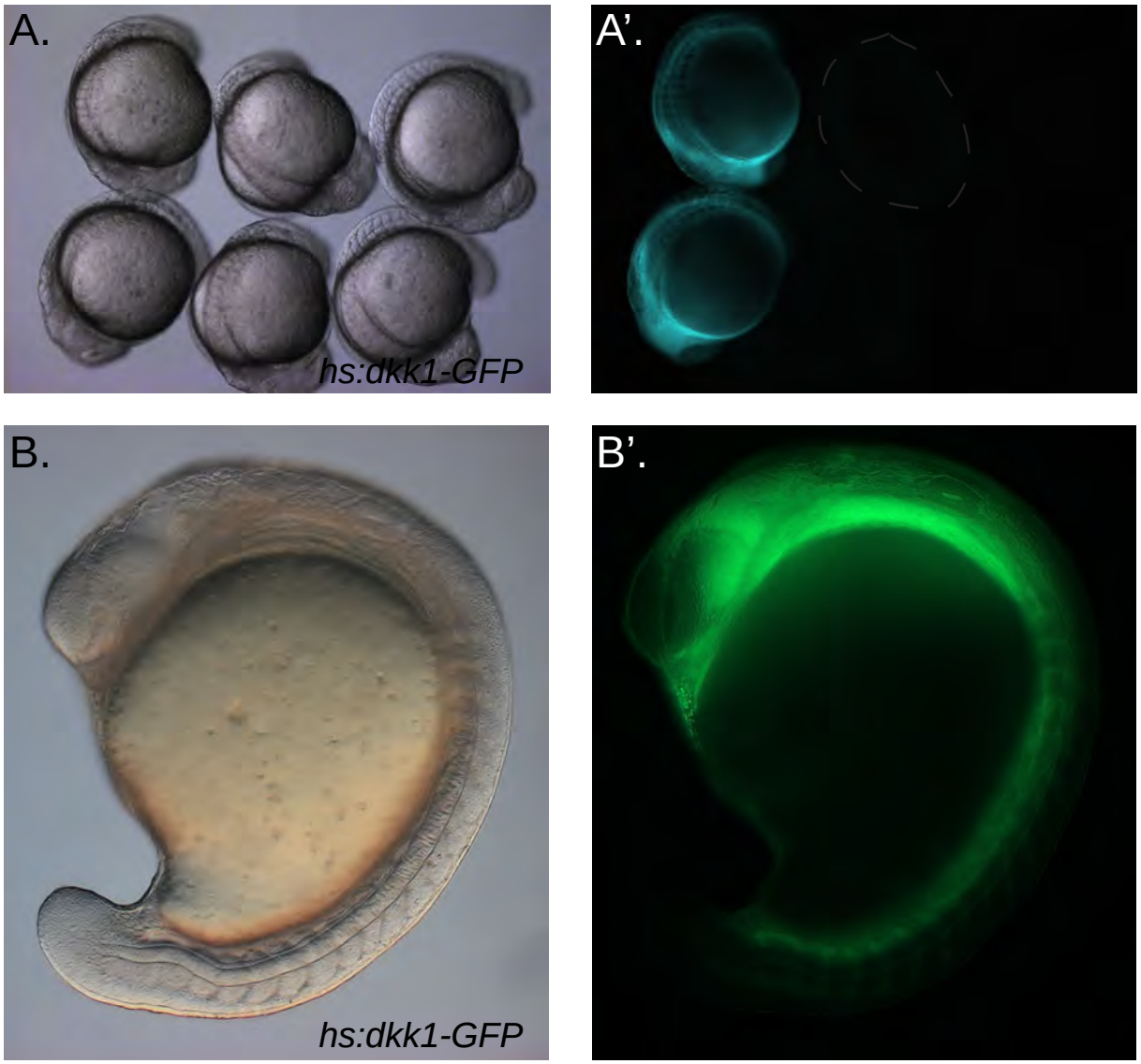

Figure 2.7. **Scoring *hs:dkk1-GFP* embryos by fluorescence**

(A) Brightfield image of *hs:dkk1-GFP* embryos that were heat-shocked at 5 somites and allowed to recover for 4 hours. GFP+ embryos express *dkk1*, an inhibitor of Wnt signaling. (A') The embryos in (A) were sorted based on GFP fluorescence. The two on the left were sorted as being strongly GFP positive, the two in the middle (one is outlined) were scored as being less GFP positive, and the two on the right were scored as being GFP negative. (B and B') Larger magnifications of a strongly GFP positive embryo from (A).

Figure 2.8

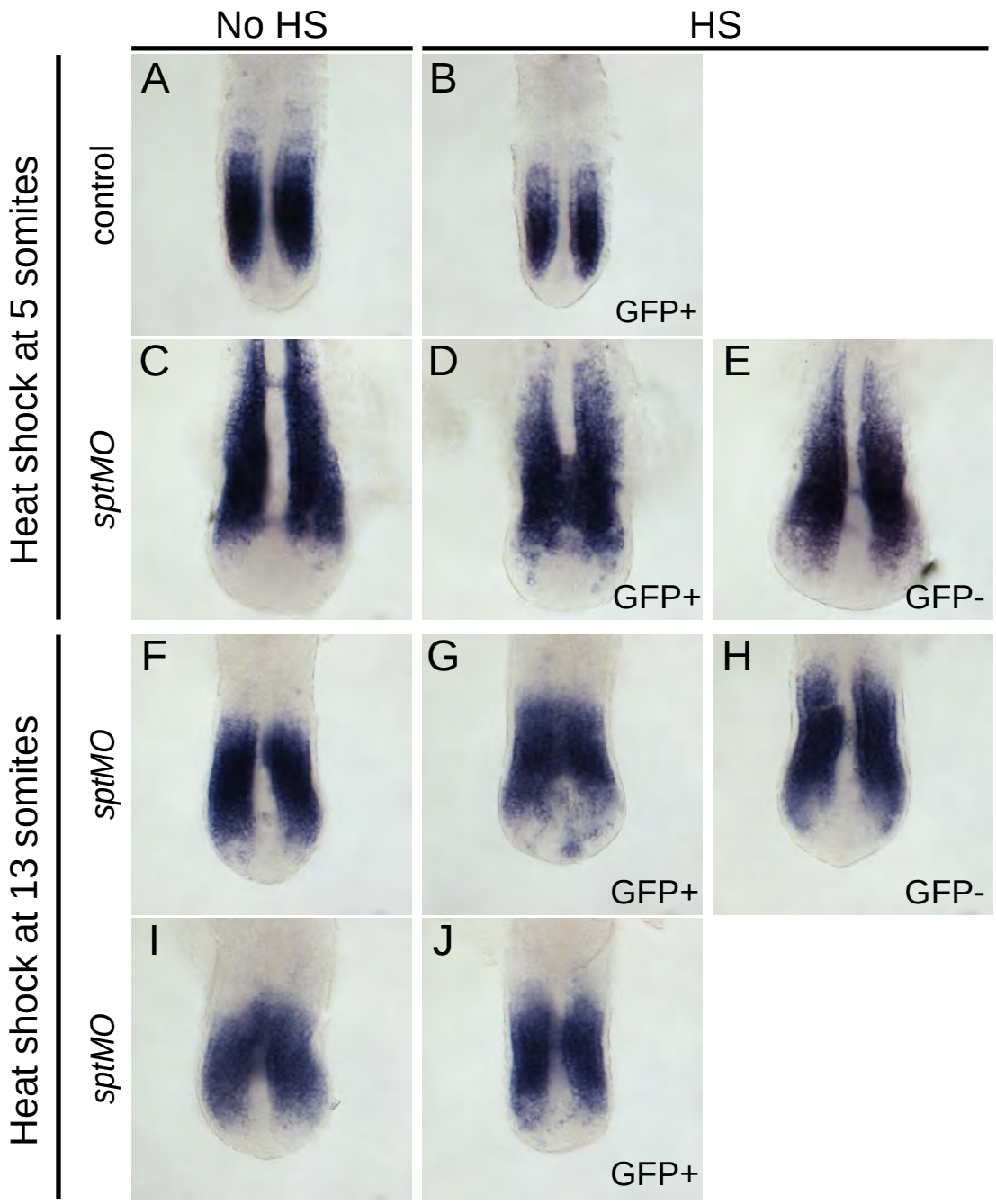
No HS
HS
Heat shock at 5 somites
Heat shock at 13 somites
control
sptMO
sptMO
sptMO
A
B
GFP+
C
D
GFP+
E
GFP-
F
G
GFP+
H
GFP-
I
J
GFP+

Figure 2.8 **Loss of progenitor markers is not sufficient to induce *tbx6* expression in the tailbud**

Embryos carrying the *hs:dkk1-GFP* transgene were injected with 0.2M KCl (control) (A, B) or *spt* MO (C-J) and heat-shocked for 1 hour at the 5-somite stage (A-E) or 13-somite stage (F-J) and recovered for 7 hours at 25°C. No-HS controls (A, C, F, I) were left at 28.5°C for 1 hour and then recovered for 7 hours at 25°C. In all embryos *tbx6* expression was detected by wholemount *in situ* hybridization. *tbx6* expression does not expand when Wnt signaling is intact (A and B). Ectopic *tbx6* expression is only seen in the tailbud and midline of embryos with decreased Wnt signaling in combination with loss of *spt* function (compare D,G, and J with C,E,F,H, and I).

Figure 2.9

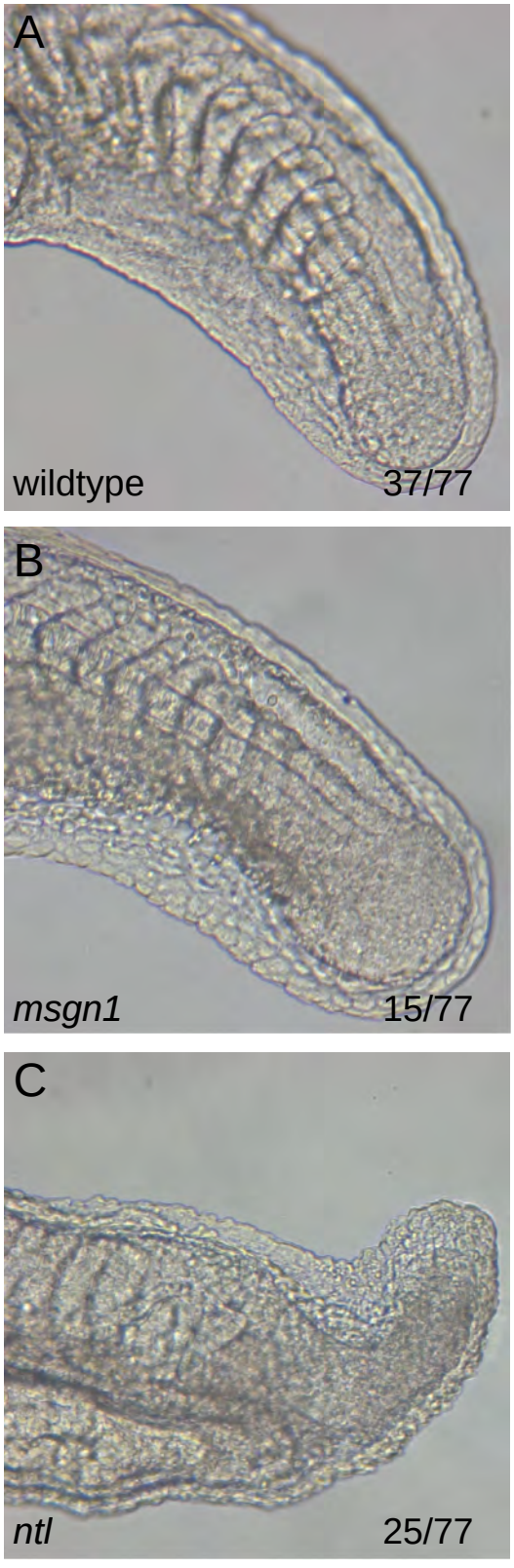

Figure 2.9 **There is no genetic interaction between *msgn1* and *ntl***

The progeny of an intercross between *ntl*$^{+/-}$;*msgn*$^{+/-}$ fish were raised to 22hpf and scored for defects in morphology. All embryos were scored as being wildtype (A), *msgn1* (B), or *ntl* (C). Genotyping revealed that 11 out of the 25 *ntl* mutants were *ntl*;*msgn1* double mutants. They were indistinguishable from *ntl* single mutants.

Table 2.1

HS Stage	Injected	Score as	n	*tbx6* expression
5som*	---	Mch +	8	0 (0%)
5som*	---	Mch-	18	0 (0%)
5som	control	No HS	21	0 (0%)
5som	control	GFP +	19	0 (0%)
5som	control	GFP +/-	10	0 (0%)
5som	control	GFP -	22	0 (0%)
5som	sptMO	No HS	29	1 (3%)
5som	sptMO	GFP +	30	21 (70%)
5som	sptMO	GFP +/-	4	0 (0%)
5som	sptMO	GFP -	6	0 (0%)
13som	control	No HS	11	0 (0%)
13som	control	GFP +	13	0 (0%)
13som	control	GFP -	5	0 (0%)
13som	sptMO	No HS	13	3 (23%)
13som	sptMO	GFP +	28	22 (79%)
13som	sptMO	GFP +/-	6	2 (33%)
13som	sptMO	GFP -	5	0 (0%)
5 som	---	No HS	53	0 (0%)
5 som	---	GFP +	53	0 (0%)
5 som	---	GFP +/-	25	0 (0%)
5 som	---	GFP -	36	0 (0%)
13 som	---	No HS	53	0 (0%)
13 som	---	GFP +	34	0 (0%)
13 som	---	GFP +/-	19	0 (0%)
13 som	---	GFP -	39	0 (0%)

Table 2.1 ***tbx6* expression requires the absence of progenitor markers and *spt***

This table lists the conditions tested in inducing *tbx6* ectopically in the tailbud. Embryos were heat shocked, separated based on their fluorescence and then scored for ectopic expression of *tbx6* transcripts. The frequency with which ectopic expression was seen is indicated in the column on the right. Regardless of the stage that Wnt signaling was reduced, *tbx6* expression was only seen in conjunction with loss of *spt* function.

Chapter 3: Potential role of Tbx6l during mesoderm development

Background

T-box genes belonging to the T/Brachyury and Tbx6 subfamilies are important for mesoderm development and patterning in all vertebrates examined to date. While *Brachyury* orthologs have very similar expression domains and functions in the organisms investigated, the *Tbx6* subfamily is less conserved, but still appears to regulate the same developmental processes. Zebrafish *tbx6l* is expressed in the paraxial mesoderm, similar to mouse and *Xenopus Tbx6*. Although all of these genes group within the Tbx6 subfamily, phylogenetic analysis indicates that zebrafish *tbx6l* is a paralog of other vertebrate *Tbx6* genes (Ruvinsky et al., 1998). *Tbx6* loss of function experiments in mouse and *Xenopus* yield distinct phenotypes, but several developmental roles are conserved, including specification of paraxial mesoderm, inhibition of neural fate, and establishment of somite boundaries through interactions with proteins belonging to the Mesp family of transcription factors and Ripply family of co-repressors (Kawamura et al., 2008; Dunty et al., 2008; Oginuma et al., 2008; Moreno et al., 2008; Hitachi et al., 2008). Although zebrafish *tbx6* (previously *tbx24/fused somites*) is expressed in the anterior PSM and only briefly overlaps with expression domains of other T-box genes, it is more closely related to mouse and *Xenopus Tbx6* than *tbx6l* in the T-domain and shares a role in patterning somites through interactions with Mesp and Ripply proteins (Nikaido et al., 2002; Kawamura et al., 2008; Yasuhiko et al., 2008).

Despite its identification in 1997, relatively little is known about the function of zebrafish *tbx6l*. A previous attempt to knock down Tbx6l function with morpholinos reported mild axial defects (“data not shown”), but no loss of paraxial mesoderm comparable to loss of Spt or Ntl function (Goering et al., 2003). That study reported that Tbx6l was capable of antagonizing Ntl function, possibly through competitive binding to Ntl targets. No other studies regarding Tbx6l function have been reported. Based on their phylogeny and nearly identical expression patterns, Tbx6l has long been thought to be partially functionally redundant with Spt (Griffin et al., 1998), perhaps in a similar way that Ntlb function overlaps with that of Ntla (Martin and Kimelman, 2008). Consistent with a functional overlap of Spt and Tbx6l, one might propose that tail somites form in a *spt* mutant because *ntl* activates *tbx6l* expression which can then compensate for the lack of *spt* (Griffin et al., 1998; Amacher et al., 2002). However, since *tbx6l* expression is down-regulated in *spt* mutants (Garnett et al., 2009), it is also possible that anterior paraxial mesoderm formation is dependent on *tbx6l* function.

tbx6l expression overlaps with *spt* and *ntl* expression in the ventrolateral margin during gastrulation and later in the presumptive mesoderm of the tailbud (Fig 1.2, 1.3) (Hug et al., 1997; Amacher et al., 2002). The ventral margin of zebrafish has been shown to act as a tail organizer (Agathon et al., 2003). Expression of *bmp2/4*, *wnt8a*, and components of the Nodal signaling pathway overlap in the tail organizer and, when co-injected into early blastula stage embryos, are capable of inducing a secondary tail containing ventrolateral mesoderm derivatives, paraxial mesoderm and blood, and neural structures, but lacking axial mesoderm derivatives (Agathon et al., 2003). *tbx6l* is directly regulated by both the Wnt and Bmp signaling pathways (Szeto and Kimelman,

2004) and thus may be important for specifying tail mesoderm. Because *tbx6l* is dramatically down-regulated in *spt;ntl* double mutants (Garnett et al., 2009), I was interested in determining the function of Tbx6l in zebrafish, particularly whether it functioned mainly as a mediator of *ntl* and *spt* functions, or if it had an altogether independent function and set of targets. Using antisense morpholino oligonucleotides to knockdown *tbx6l* expression, I show that Tbx6l is required for posterior mesoderm development and that its loss-of-function phenotype is distinct from that of Ntl and Spt.

Materials and Methods

Microinjection

See Materials and Methods from Chapter 2.

In situ hybridization and imaging

See Materials and Methods from Chapter 2.

Morpholinos

For *spt* MO, see Materials and Methods from Chapter 2. *tbx6l* MOs were designed by and ordered from GeneTools. The translation-blocking MO sequence (5'-CAGGCCGTTCCTCTGGGAGATACAT-3') targets the start site of the *tbx6l* coding region. The MO was diluted to a 50 ng/nL stock solution in nuclease free molecular biology grade water (Gibco). For injection solutions, the stock MO was diluted to 1-7 ng/nL in 0.2M KCl, 0.1% Phenol Red. 2-5 nL was injected into embryos at the 1-cell stage. The splice-blocking *tbx6l* MO (sbMO) targeted the splice junction between intron 1 and exon 2 (5'-GTCCGGCAATCTAATCCATACAATT-3'). The sbMO was diluted and injection solutions were prepared as described for the translation-blocking *tbx6l* MO.

RNA preparation to analyze *tbx6l* sbMO-induced splicing events

Embryos injected with the control solution or *tbx6l* sbMO were harvested for RNA at 50-80% epiboly. Embryos were transferred to 1.5mL tubes and 200ul Trizol was added to each. Tubes were then vortexed until embryos were dissociated. Samples were stored at -70°C or processed immediately. Trizol (300ul) was added to each tube and samples were incubated at room temperature for 5 minutes. This was followed by adding 125ul chloroform, vortexing for 30 seconds, and centrifuging at 4°C for 15 minutes. The supernatant was transferred to new 1.5mL tubes and extracted a second time with an equal volume of Trizol and 100ul chloroform. The samples were vortexed for 30 seconds and centrifuged 15 minutes at 4°C. The supernatant was transferred to a new tube and precipitated by addition of 1ul glycogen (20mg/mL) (Roche) and 0.7 volumes of isopropanol overnight at -20°C. The samples were centrifuged for 20 minutes at 4°C. The supernatant was aspirated and replaced with 300ul 70% ethanol. The tubes were centrifuged for 2 minutes and the ethanol was removed. The RNA pellets were air-dried and resuspended in 15ul of nuclease free water (Gibco). DNAse treatment of the RNA pellet was performed by adding the following mixture to each tube of RNA:

2.4ul	10X NEB1 buffer
0.4ul	DNAseI (NEB)

1.25ul 20mM DTT
0.5ul RNAse inhibitor (Roche)
5.4ul nuclease free water

The 25ul reaction was incubated at 37°C for 30 minutes. 175ul of nuclease free water was added and the samples were extracted with an equal volume of phenol-chloroform. The supernatant was collected and extracted with an equal volume of chloroform. The supernatant was precipitated with 20ul ammonium acetate and 500ul ethanol at -70°C for 2 hours. The samples were centrifuged for 20 minutes at 4°C, washed with 70% ethanol and air-dried. The RNA pellet was resuspended in 11.5ul nuclease free water.

To analyze aberrant splicing events, I used the following primers flanking the target site in exons 1 and 4: tbx6In1Ex2_F5 (5'-TGTGCTGGACTTACCCTACCAGA TG-3'), tbx6In1Ex2_R5 (5'- AACGGCACCATGTCCATTATCAC-3') and tbx6In1Ex2_R6 (5'- GTTGGGCAGGTGCGGATCAGATG-3'). Embryos injected with the *tbx6l* sbMO were harvested for cDNA synthesis, and 0.25ul of cDNA was used as a template for each 25ul PCR reaction. The thermocycler program used was:

1) 95°C 2:00
2) 95°C 0:30
3) 55°C 0:30
4) 72°C 4:00
5) Repeat step 2-4 for 30 cycles
6) 72°C 10:00
7) 4°C

All centrifugation steps were performed at 13,500rpm.

cDNA synthesis

Complementary DNA was synthesized using an RNA template as follows:

1ul Oligo(dT) (500ug/ml)
10ul RNA
1ul 10mM dNTP mix

The mixture was heated to 65°C for 5 minutes and chilled on ice before adding the following:

4ul 5X first-strand buffer
2ul 0.1mM DTT
1ul RNAse inhibitor

The samples were mixed by gently pipetting. After a 2 hour incubation at 42°C, 1ul of SuperScript II RT (200U/ul) (Invitrogen) was added and the samples were mixed again. The samples were incubated at 42°C for 50 minutes, followed by a 15 minute incubation at 70°C to inactivate the reverse transcriptase. The cDNA was stored at -20°C.

Cloning *tbx6l* coding sequence for *in vitro* transcription

The *tbx6l* coding sequence was amplified from a plasmid containing the *tbx6l* cDNA (bq116) with Phusion DNA polymerase (Fermentas) using the primer pair

tbx6_FL_Fwd (5'-ATTAGGATCCATGAATCATTTGGCTAATAACTATGGATAC-3') and tbx6_FL_Rev (5'-ATTAGAATTCATCAGTACTCAGTTAGTGGCCTC-3') and the following thermocycler program:

1) 98°C 0:30
2) 98°C 0:15
3) 57°C 0:30
4) 72°C 0:45
5) Repeat steps 2-4 for 30 cycles
6) 72°C 10:00
7) 4°C

The *tbx6l* PCR fragment and pCS2+ vector were digested with restriction endonucleases BamHI and EcoRI, column purified using QIAGEN PCR purification kits, and eluted in 25ul water. The *tbx6l* coding region and linearized pCS2+ vector were ligated using T4 DNA ligase (NEB) and overnight incubation at 16°C. 5ul of the ligation mixture was added to 100ul of TOP10 chemically competent *E. coli* (Invitrogen) and transformed using the following protocol:

10:00 min on ice
0:45 sec heat-shock at 42°C
5:00 min on ice
Add 250ul LB
Incubate at 37°C for 1 hour

50ul and 100ul of the transformation were plated on LB plates containing 100ug/mL carbenicillin (carb) and incubated overnight at 37°C. 3 clones were cultured in 5mL LB+carb. The bacteria were harvested and lysed, and the plasmid was purified using QIAGEN mini prep kits.

***hsp70l:tbx6l-2A-GFP* over-expression construct**

To generate the *hsp70l*:*txb6l-2A-GFP* transgene, the *hsp70l* promoter, *tbx6l* coding sequence, *2A* viral peptide sequence, *GFP* sequence, and polyadenylation signal were subcloned from plasmids using Phusion DNA polymerase. The primers used are as follows: Vector_hsp_F (5' ACAGGGTAATCTCGAGTCAGGGGTGTCGCTT GGTTAT-3') and Inf_hsp70_R (5'-CGGTGCAATTGTTTCATTATGAAAGG-3') were used to amplify the *hsp70l* promoter sequence; hsp_tbx6_F (5'-GAAACAATTGCACC GATGTATCTCCCAGAGGAACGGC-3') and Inf_tbx6_R (5'-GTACTCAGTTAGTGGCC TCATATGTG-3') were used to amplify the *tbx6l* coding sequence; tbx6_2A_F (5'-CCAC TAACTGAGTACATGAGATCTGGCGGCGGAGA-3') and Inf_2A_R (5'-GTCCATCCTA GGGCCGGGATT-3') were used to amplify the *2A* viral peptide sequence; 2A_eGFP_F (5'-GGCCCTAGGATGGACATGGTGAGCAAGGGCGAGGA-3') and Vec_pA_R (5'-CC GCTCTAGAACTAGTCGCCTTAAGATACATTGATGAGTTTGG-3') were used to amplify the *GFP* and polyadenylation signal sequence. The *hsp70l* and *GFP* plasmids were a gift from the lab of Kenneth Poss. Each fragment was run on a 1% agarose gel and purified using QIAGEN gel extraction kits. The pBSKI2 plasmid was linearized with SpeI and XhoI restriction enzymes and column-purified using the QIAGEN PCR purification kit. The vector and inserts were combined in the following In-Fusion cloning reaction (Clontech):

1.55 ul	64.6ng/ul	pBSKI2 vector
0.78 ul	83ng/ul	*hsp70l*
0.78 ul	83.1ng/ul	*tbx6l*
2.40 ul	10ng/ul	*2A*
0.25 ul	184ng/ul	*GFP-pA*
2.00 ul	5x In-Fusion Mix (Clontech)	
	Millipore water to a volume of 10 ul	

This reaction was incubated at 50°C for 15 minutes. I then added 40 ul of 1x TE buffer and aliquoted the 50ul mixture into 4 tubes of 10 ul each to be stored at -20°C. 3 ul of the remaining cloning reaction were used to transform 50 ul of stellar competent cells (Clontech). The cells were plated on LB+carb plates. Colonies were picked to determine transformation of the plasmid by colony PCR. The *hsp70l:tbx6l-2A-GFP* construct was purified from four independent clones numbered 1 and 3-5. Clones 1 and 4 were prepped using QIAGEN plasmid preps and sent for sequencing. Wildtype embryos were injected with Clone 1 and the I-SceI meganuclease to facilitate integration into the genome. Once the fish reach sexual maturity they can be scored for germline transmission.

Bacterial stocks

For long-term storage of bacterial stocks carrying specific plasmids, a colony was picked to inoculate a 25 mL LB+carb culture for a large scale prep of the plasmid. 500 ul of the 25 mL culture was mixed with 500 ul 80% glycerol and stored at -70°C.

Colony PCR

To identify bacterial clones transformed with plasmids carrying the transgene insert, colonies from transformation plates were picked with a pipette tip, swirled in 25 ul of a PCR mix and then used to inoculate 40 ul of LB+carb. Primers and thermocycler programs used to identify the insert were the same as those used to generate the fragment. The 40 ul LB+carb inoculants of clones shown to be carrying the recombinant plasmid were used to inoculate 5 mL of LB+carb.

Tbx6l antibody

A polyclonal antibody against zebrafish Tbx6l was generated by Strategic Diagnostics (SDIX). The DNA sequence encoding residues 310-409 was used to immunize rabbits. Preimmune sera samples from 2 rabbits were collected prior to immunization. The rabbits were exsanguinated and the antiserum was affinity purified to yield 1.84 mL of Tbx6l antibody.

Immunohistochemistry

Conditions for testing non-affinity purified Tbx6l antiserum and pre-inoculation serum are as follows: Embryos were fixed in 4% PFA (1:1 2xPBS:8%PFA), Carnoy's fixative (3 mL 100% ethanol, 1.5 mL glacial acetic acid, 500 ul chloroform), or trichloroacetic acid for 2 hours at room temperature or 4°C overnight, rinsed 2 times with PBST and dechorionated manually. Embryos were washed 5 times for 5 minutes in PBST. In some cases an additional permeabilization step was added by incubating

embryos in 2% PBT(1x PBS, 2% Triton) for 105 minutes on a flatbed rocker (for non-affinity purified Tbx6l antisera and preimmunized sera) or incubating embryos in cold acetone for 7 minutes at -20°C (affinity purified Tbx6l antibody). Embryos not permeabilized were incubated in PBST for the same time. Embryos were blocked for 2 hours in PBT Block (1x PBX, .1% Triton, 50 mg/mL BSA). The Block was removed and replaced with 1:20, 1:100, 1:200, 1:1000, or a 1:5000 dilution of Tbx6l antiserum, pre-inoculation sera, or affinity purified Tbx6l antibody and incubated at 4°C overnight. Embryos were rinsed with PBT (1x PBS, 0.1% Triton-100x) and washed 8 times for 15 minutes with PBT. The embryos were blocked 15 minutes in PBT and incubated at 4°C overnight in a goat anti-rabbit IgG secondary antibody conjugated to horse radish peroxidase (HRP) or Alexa Fluor® 568 (Molecular Probes). Embryos were rinsed with PBT and washed 8 times for 15 minutes with PBT. Embryos incubated with the HRP-conjugated secondary were stained in diaminobenzidine (DAB), a peroxidase substrate, for 3-10 minutes. Embryos incubated with the Alexa Fluor® 568-conjugated secondary were scored by fluorescence.

Protein extraction

Wildtype embryos and *tbx6l* morphants were harvested at 10-15 somites (n=48) or 4dpf (n=30) for deyolking and protein extraction. Embryos were dechorionated manually prior to removing the yolks. For deyolking, embryos were placed in 1.5 mL tubes and 200 ul Ringer's solution (without $CaCl_2$) was added. Using a P200 pipettor, embryos were pipetted up and down 2-3 times, followed by a 5-minute wash on a flatbed rocker. Embryos were spun down at 300 x rcf for 1 minute. The pellet was resuspended in 500 ul of Ringer's solution (without $CaCl_2$). Embryos were pipetted, rocked, and centrifuged two more times. The tube was put on ice, and 1 mL of homogenization buffer (20 mM HEPES,pH 7.5, 10 mM EGTA, 2.5 mM $MgCl_2$, 1x protease inhibitor cocktail, Roche) was added; embryos were then homogenized with a pestle and pelleted at 14000rpm. 100 ul of sample buffer (63 mM Tris-HCl, pH 6.8, 2% SDS, 10 mM DTT, 10% glycerol) was added to each pellet and the samples were homogenized by passage through an 18-guage needle 15 times. Samples were boiled at 95°C for 5 minutes and spun down at 14000rpm for 5 minutes. The supernatant was stored at -70°C or run immediately on an SDS-polyacrylamide gel.

Western blot

Protein samples were run on a polyacrylamide gel (4% 19:1 acrylamide:bisacrylamide (BioRad) stacking gel and 12% 19:1 acrylamide:bisacrylamide resolving gel) in a mini-vertical gel electrophoresis unit (Hoefer SE 250) for 1 hour at a constant current of 40 mA. Proteins were transferred to Hybond-P PVDF membranes (GE) by a semi-dry transfer method according to manufacturer protocol. The PVDF membranes were washed 10-15 minutes in TBST buffer (1x TBS [0.5M Tris-HCl, pH 8, 1.5M NaCl] 0.1% Tween), blocked 1 hour in 5% non-fat dairy milk (NFDM), and incubated in Tbx6l antibody dilutions of 1:1000 or 1:5000 overnight at 4°C. Dilutions were made in 5% NFDM. Primary antibody was removed and membranes were rinsed with TBST quickly, and then again for 15 minutes. The membranes were incubated in HRP-conjugated goat anti-rabbit IgG secondary for 1 hour at room temperature and rinsed 3 x 5 minutes with TBST. ECL Plus chemiluminescent substrate was added to

blots as outlined in the manufacturer protocol and protein bands were detected by Amersham Hyperfilm ECL (GE).

Results

Depleting *tbx6l* reveals a role for Tbx6l in patterning and specifying mesoderm

To understand the functional requirement of *tbx6l* in zebrafish embryos, we knocked down *tbx6l* expression using a translation-blocking morpholino (*tbx6l* MO) (Fig 3.1 A,B). Embryos injected with several doses of *tbx6l* MO were scored near the end of gastrulation (9-10hpf) and segmentation (24hpf). During gastrulation I frequently observed that *tbx6l* morphants were often elongated in shape (Fig 3.1 C,D), a defect commonly associated with mutations in genes required for dorsal-ventral patterning (Mullins et al., 1996). The severity and frequency of elongated embryos increased with higher doses of *tbx6l* MO (data not shown). *tbx6l* morphants also displayed a broadening of the dorsal mesoderm domain as evidenced by *ntl* expression (Fig 3.1 E-G). *tbx6l* morphants were assessed for trunk and tail mesoderm formation at 24hpf, and displayed a variety of phenotypes ranging from mild and severe truncations of the body axis to complete dorsalization (Fig 3.2, data not shown). This range of phenotypes was observed in nearly all doses, with the more severe phenotypes occurring more frequently at the higher doses (Fig 3.2 E). Communications with David Grunwald's lab revealed similar dose-dependent, though variable, phenotypes were observed with attempts to deplete Tbx6l function with different *tbx6l* MOs.

To address the target specificity of *tbx6l* MO and to verify the loss-of-function phenotype of *tbx6l*, a second morpholino against *tbx6l* was tested. *tbx6l* sbMO is a splice-blocking morpholino which targets the splice junction between intron 1 and exon 2 (Fig 3.3 A). Sequence encoding the ~190 aa T-box domain begins in exon 2, so disruption of the first intron-exon boundary should increase the chance of introducing an early stop codon or frameshift, resulting in a null *tbx6l* phenotype. *tbx6l* sbMO was injected at doses ranging from 3-28 ng and embryos were scored at 24hpf or 48hpf for defects. At 10-20 ng there were several abnormalities which occurred more frequently in *tbx6l* sbMO injected embryos than in their uninjected siblings, namely, blisters in the median fin fold at the end of the tail, curled tails, and loss of fin fold mesenchyme (Fig 3.3 B-F). These phenotypes were strikingly different and less severe than morphant phenotypes observed following injection of the translation-blocking *tbx6l* MO, and we reasoned that *tbx6l* sbMO may not be affecting a large pool of *tbx6l* transcript in the embryo. To test the effectiveness of *tbx6l* sbMO at altering the splicing profile of *tbx6l,* primers were designed flanking the *tbx6l* sbMO target site. The forward primer tbx6In1Ex2_F5 (F5) binds in exon 1 and the reverse primer tbx6In1Ex2_R5 (R5) binds in exon 3 (Fig 3.3 A). Embryos were injected with 3-4 nL of mock carrier solution, or *tbx6l* sbMO at 1ng/nL or 5ng/nL concentrations. At 60%-80% epiboly embryos were harvested for RNA extraction and cDNA synthesis. Primer pair F5 and R5 is predicted to amplify a 288bp fragment in WT cDNA. Mock-injected cDNA yielded bands of expected size for the primer set (Fig 3.3 G, lane 1). In embryos injected with 3-4ng or 15-20ng *tbx6l* sbMO, additional bands were detected migrating at roughly ~950 bp and ~700 bp (Fig 3.3 G, lanes 2-4). Inclusion of intron 1, which is 701 bp may explain the 950 bp band, while an off-target splicing event at a cryptic splice sight may explain the

second aberrant band. Although injection of the *tbx6l* sbMO resulted in two larger alternative splice forms, the dominant splice form was the same as in control embryos (Fig 3.3, lanes 2-4). Because knockdown therefore appeared inefficient, the *tbx6l* sbMO-dependent bands were not sequenced to identify the molecular nature of the splice forms generated.

Given the range of phenotypes observed with the translation-blocking MO, and the mild defects observed using the splice-blocking MO, we decided to forgo extensive phenotypic characterization of knockdown embryos and instead collaborate with the David Grunwald to characterize a *tbx6l* mutant being generated by his lab. The Grunwald lab used TALEN-mediated mutagenesis (Huang et al., 2011; Cade et al., 2012) to recover several mutations resulting in severe truncations of Tbx6l that effectively abolish the T-box binding domain. Initial crosses of mutants and preliminary analysis of transheterozygous progeny indicate a subtle change in tailbud morphology (David Grunwald and Kazuyuki Hoshijima, personal communication) but full analysis of these potential *tbx6l* null mutants has not been performed.

Attempted rescue of *tbx6l* morphants by over-expressing *tbx6l*

Without a zebrafish *tbx6l* null mutant to verify the *tbx6l* morphant data, I attempted to validate the *tbx6l* MO induced defects by rescuing the effects of *tbx6l* MO injected embryos with MO-resistant *tbx6l* mRNA. *tbx6l* MO and *tbx6l* mRNA were co-injected at the 1-cell stage. The majority of the embryos died or failed to gastrulate properly, while those that progressed to segmentation did not show signs of rescue (data not shown). Given the lack of success with attempts at over-expressing *tbx6l* by injecting it as mRNA at the 1-cell stage, I constructed a transgene that would allow for temporal induction of *tbx6l* expression. A transgene was generated using the *heat-shock cognate 70-kd protein, like* (*hsp70l*) zebrafish promoter to drive expression of the *tbx6l* coding sequence and the fluorescent reporter *GFP*. The *tbx6l* and *GFP* coding sequences were separated by the *2A* viral peptide ribosomal stutter sequence, generating a bicistronic transcript (Ryan and Drew, 1994; Trichas et al., 2008) (Fig 3.4 A). Separate translation of the Tbx6l and GFP proteins from the heat-shock-induced bicistronic transcript precludes the potential problem of the reporter interfering with the folding or activity of the protein of interest, a well-known caveat of fusion proteins. This allowed me to identify which cells had received the transgene based on GFP expression.

The *hsp70l:tbx6l-2A-GFP* transgene was cloned into the pBSKI2 vector (Thermes et al., 2002) using a recombination cloning method. The transgene is flanked by I-SceI sites in the vector to facilitate integration into the zebrafish genome using the I-SceI meganuclease (Thermes et al., 2002 Four independent clones were injected into 1- to 4-cell stage embryos, heat-shocked at the shield stage for 1 hour, and assayed for expression of the fluorescent reporter 3 hpHS. More than 50% of the heat-shocked embryos injected with clone 1, 4, or 5 exhibited mosaic GFP expression. Only 16% of heat-shocked embryos injected with clone 3 expressed GFP. Clone 1 and 3 did not have leaky expression while clones 4 and 5 each had one embryo express GFP without HS (Fig 3.4A). Clone 1 had the highest percentage of GFP-expressing heat-shocked embryos and no GFP-expressing non heat-shocked embryos, and this clone was used in the experiments described below.

Validating the loss of Tbx6l

The patterning and posterior defects observed in *tbx6l* morphants were indicative of a role for Tbx6l in mesoderm formation and patterning, but it was still necessary to show that truncation and dorsalization were a result of depleted Tbx6l protein. To firmly establish the link, we contracted with Strategic Diagnostics Inc (SDIX) to design an antibody against zebrafish Tbx6l. To avoid possible cross-reactivity with other members of the T-box protein family, the immunogen used was a 100 aa peptide near the C-terminus of the protein, a peptide with little homology to other T-box proteins (Fig 3.5).

The antiserum and the affinity-purified antibodies were tested for their ability to detect Tbx6l by immunohistochemistry. Wildtype embryos were fixed between gastrulation and early somite stages when *tbx6l* mRNA expression is concentrated at the margin or in the tailbud and paraxial mesoderm. After a number of conditions were tested (Table 3.1), embryos were incubated in a hydrogen peroxidase (HRP)-conjugated secondary antibody, and the antigen was detected by chromogenic staining with DAB and hydrogen peroxide. Neither the antiserum nor the affinity purified Tbx6l antibody detected a tissue-specific or nuclear antigen. Instead, there was a diffuse brown staining over the entire embryo. This staining was Tbx6l antibody-dependent as it was absent in embryos that were incubated in block instead of the antibody (data not shown). The amount of staining decreased as the antibody concentration decreased. To determine if the antibody staining was reflecting the presence of Tbx6l, embryos were injected with *tbx6l* MO and sorted for the dorsalized phenotype at 2-3 somites. Along with their uninjected siblings, the embryos were stained using a 1:1000 dilution of Tbx6l antibody and processed as before. While there was still neither punctate or regionalized staining, the *tbx6l* morphants with dorsalized morphology had a less intense diffuse brown staining than either the uninjected embryos or the *tbx6l* MO-injected embryos with wild-type morphology (data not shown). The difference in DAB staining between *tbx6l* morphants and wildtype embryos indicated some degree of recognition of the antigen, despite considerable background.

Next, I wanted to determine whether the antibody was capable of detecting high levels of Tbx6l protein. Embryos were injected with the *hsp70l:tbx6l-2A-GFP* construct and *tbx6l* was induced by shifting to 40°C for 30 minutes. Using GFP fluorescence as an indicator of ectopic Tbx6l expression, co-localization of the Tbx6l antibody was detected by immunohistochemistry using a secondary antibody conjugated to Alexa Fluor® 568, which emits a signal in the red channel. Embryos injected with the *tbx6l* over-expression construct and their uninjected siblings were heat-shocked and incubated in Tbx6l primary antibody or block (as a control). No Tbx6l antibody-independent staining was observed, and GFP was only detected in cells of injected embryos (Fig 3.6). At dilutions of 1:20, 1:100, and 1:500 80-100% of embryos containing GFP+ cells also showed considerable red fluorescence overlapping with GFP signal (Table 3.2, Figure 3.7 D-I, data not shown). At the 1:1000 dilution of Tbx6l antibody, all GFP+ embryos had some overlap with cells in which Tbx6l was detected, but there was a higher proportion of GFP+ cells that did not exhibit co-localization with the Tbx6l signal than was observed in the more concentrated antibody dilutions (Table 3.2, Figure 3.7 J-L). At the 1:5000 antibody dilution, the Alexa Fluor signal detected Tbx6l in less than half of the embryos expressing GFP (Table 3.2, Fig 3.7 M-O). I did

not detect obvious nuclear or localized Tbx6l signal in the uninjected embryos incubated in Tbx6l primary antibody (Fig 3.7, Table 3.2). Based on these results I conclude the Tbx6l antibody is capable of recognizing Tbx6l *in vivo* but not at endogenous levels or under the conditions I tested.

The above results indicate the Tbx6l antibody recognized the protein encoded by the *tbx6l* gene, but immunohistochemistry was not the best way to validate loss of Tbx6l in *tbx6l* MO-injected embryos. The Tbx6l antibody was then tested via western blot to determine if the antibody was better suited to determining loss of Tbx6l using this technique. Preliminary results with the Tbx6l antibody indicated it was capable of recognizing a GST-tagged form of Tbx6l, detecting a band between 75-100KDa. The predicted weight of the Tbx6l-GST fusion protein is 79 KDa. Protein extracts from segmentation stage embryos, when *tbx6l* transcripts are detectable, and 4dpf embryos, when *tbx6l* transcripts are not detected (Hug et al., 1997), were run on an SDS-PAGE gel and probed with a 1:1000 and 1:5000 dilution of the *tbx6l* antibody. The banding patterns for segmentation stage and 4dpf embryo protein extracts indicated non-specific binding of the Tbx6l antibody (Fig 3.8 lanes 2,4,7,8).

Although I am unable to detect endogenous levels of Tbx6l at this point using the Tbx6l antibody, the design of the *hsp70l:tbx6l-2A-GFP* over-expression construct is suited to assay whether the *tbx6l* MO is targeting and preventing expression from the *tbx6l* transcript. The *2A* viral peptide sequence separating the *tbx6l* and *GFP* coding regions allows for the use of GFP fluorescence as a readout of *tbx6l* MO activity. Unlike the internal ribosomal entry site (IRES) sequence, which facilitates binding of a second ribosome to the transcript in order to translate the second encoded gene (Jang et al., 1988), the 2A sequence allows both genes to be translated by the same ribosome (Ryan and Drew, 1994). Instead, the 2A sequence acts as a ribosomal stutter sequence, disrupting peptide bond formation between residues in the 2A peptide sequence (Donnelly et al, 2001). The ribosome proceeds with synthesis of the second peptide, resulting in the separation of the two proteins. Embryos were injected with either the *tbx6l* over-expression construct alone or in combination with the *tbx6l* MO, heat-shocked at 40°C at shield stage, and assayed for GFP expression 2 hpHS. Of the embryos injected solely with *hsp70l:tbx6l-2A-GFP*, 63% were scored as having GFP positive cells (n=41, Table 3.3). In contrast only 8% of the embryos co-injected with *hsp70l:tbx6l-2A-GFP* and *tbx6l* MO contained GFP positive cells (n=37, Table 3.3). The loss of GFP expression suggests that the *tbx6l* MO is preventing translation of the bicistronic *tbx6l*-2A-GFP transcript, thereby blocking production of both Tbx6l and GFP proteins. Thus, the *tbx6l* MO is likely inhibiting translation of the endogenous *tbx6l* transcript as well, indicating the mesoderm defects observed in *tbx6l* morphants are caused by a decrease in Tbx6l.

tbx6l functions with *spt* to induce paraxial mesoderm fate

Tbx6l is thought to have partial functional redundancy with Spt in addition to being one of its transcriptional targets. While the *tbx6l* morphants display a range of phenotypes, they are all part of an assortment of defects one might expect to see from decreasing the expression of a gene required for posterior mesoderm development. For this reason, I used the *tbx6l* MO to investigate the proposed genetic interaction between *spt* and *tbx6l* by depleting Tbx6l function in a *spt* mutant background. The progeny of a

spt$^{+/-}$ heterozygous cross were injected with a moderate dose (9-12 ng) of *tbx6l* MO and scored for mesoderm defects at 24 hpf. As expected, uninjected *spt* mutants from the *spt*$^{+/-}$ heterozygote cross formed tail somites; however, spt$^{-/-}$ mutants injected with *tbx6l* MO often failed to form tail somites (Fig 3.9). I attempted to verify these results by co-injecting *tbx6l* and *spt* MOs, but the *spt* MO used resulted in a hypomorphic phenotype—although enlarged tailbuds were present, trunk somites formed in most of the embryos. Even so, co-injection of *spt* and *tbx6l* MOs resulted in a more severe phenotype (fewer somites) than either MO alone (data not shown), consistent with the result described above. Additionally, wholemount *in situ* hybridization of *spt* morphants and *spt*/*tbx6l* morphants at 24 hpf showed *tbx6* expression was down-regulated in the PSM of *spt/tbx6l* compared to *spt* morphants (data not shown), whereas *tbx6* expression is not reduced in *tbx6l* morphants when compared to their uninjected siblings (data not shown). These results suggest Tbx6l has an overlapping function with Spt in the differentiation of posterior mesoderm.

Discussion

The Tbx6l antibody detects zebrafish Tbx6l but not at endogenous levels

My data using the *tbx6l* translation-blocking MO would be more convincing if I had been able to detect a significant decrease in Tbx6l protein in embryos displaying patterning and posterior mesoderm defects. I was able to use the Tbx6l antibody made by SDIX to detect over-expression of Tbx6l, but was not able to detect endogenous levels of protein in wildtype embryos. Using both immunohistochemical (DAB staining) and fluorescent detection methods, I observed only ubiquitous signal without any specific or nuclear localization. Despite varying the fixatives, fixation times, and permeabilization protocols, I always observed the same ubiquitous signal. The fact that tailbud stage *tbx6l* MO injected embryos displaying a dorsalized morphology had a less intense signal than wildtype embryos suggests that upon further optimization of the protocol, the antibody may be able to detect endogenous Tbx6l.

tbx6l plays a role in patterning and specifying mesoderm during zebrafish development

Tbx6l depletion with the translation-blocking MO results in elongated embryos with expanded axial domains during gastrulation. This is similar to phenotypes resulting from mutations in dorsal-ventral patterning genes (Mullins et al., 1996) and suggests a role for *tbx6l* in inhibiting the dorsal mesoderm domain during development. The majority of *tbx6l* morphants injected with a moderate dose complete gastrulation and are able to generate trunk and some tail somites. However, higher doses of *tbx6l* MO cause dorsalization in a percentage of embryos and no paraxial mesoderm is present at 24hpf. Goering et al. (2003) reported that Tbx6l was capable of antagonizing Ntl activity. Injection of RNA encoding either full-length *tbx6l* or the DNA binding T-box domain of *tbx6l* had similar effects as expressing a repressor form of *ntl*. Similarly, in *Xenopus*, over-expression of *Xtbx6* prevents formation of a proper notochord and disrupts neural tube formation (Uchiyama et al., 2001). Thus, there may be functional conservation between Tbx6l and the other vertebrate Tbx6 paralogs.

The later segmentation phenotypes exhibited when depleting Tbx6l support a role for Tbx6l in tail organizer function. *tbx6l* is a direct target of Wnt and Bmp signaling pathways and shares overlapping expression of Wnt and Bmp ligands in the ventral-lateral margin and tailbud of developing embryos (Kelly et al., 1995; Hug et al 1997; Hwang et al., 1997; Kishimoto et al., 1997; Szeto and Kimelman, 2004). Wnt is a molecular component of the tail organizer and studies in mouse, *Xenopus* and fish demonstrated that loss of *wnt3a*/*wnt8* function results in posterior truncations, including loss of notochord and paraxial mesoderm (Takada et al., 1994; Hoppler et al., 1996; Agathon et al., 2003; Thorpe et al., 2005). Based on the truncations observed in *tbx6l* morphants, it is tempting to speculate that a subset of posterior mesoderm defects resulting from knocking down Wnt signaling may be due to the decrease in *tbx6l* expression and subsequent loss of Tbx6l function. If *tbx6l* is required downstream of the Wnt, Bmp and Nodal signaling pathways in the tail organizer, I would expect the ventral margin of an embryo lacking functional Tbx6l to be incapable or less efficient at inducing a secondary tail when grafted onto a host embryo. However, the anterior truncations of the body axis (including the notochord) occasionally observed in the trunk region of *tbx6l* morphants would suggest a requirement for *tbx6l* in specifying trunk mesoderm as well. While not observed in mouse Tbx6 mutants, posterior truncations and loss of notochord do occur in the Mouse *Wnt3a* null mutant.

Tbx6l has distinct functions from mesodermal T-box proteins Ntl and Spt, but shares at least one overlapping function with Spt

Though we have yet to verify that the *tbx6l* MO phenotype is caused by loss of Tbx6l expression, the defects generated through MO injections point towards Tbx6l playing a role in posterior mesoderm development in zebrafish. It is worth noting that the phenotypes observed during gastrulation and segmentation for *tbx6l* morphants are distinctly different from those observed in either *spt* or *ntl* mutants (Kimmel et al., 1989; Halpern et al., 1993), which is surprising considering that this gene is clearly down-regulated in the absence of *spt* and *ntl* (Garnett et al., 2009). Likewise, the 24 hpf phenotypes of *tbx6l* morphants suggest that *tbx6l* functions in a different manner from Spt and Ntl. Unlike *spt* mutants, *tbx6l* morphants do not develop enlarged tailbuds due to unspecified paraxial mesoderm. Instead, the *tbx6l* morphants' tails terminate prematurely, most likely due to a diminishing pool of mesodermal progenitors in the tailbud. This is also observed in *ntl* and *wnt3/8* loss-of-function studies where the signals responsible for proliferation and maintenance of the progenitor pool are not expressed (Halpern et al., 1993; Lekven et al., 2001; Thorpe et al., 2005; Martin and Kimelman, 2010). If Tbx6l does share overlapping function with Spt, similar to the one I've described with Msgn1, one would expect the loss of both *tbx6l* and *spt* genes to be more severe than the *spt* mutant, possibly resembling the *spt;msgn1* double mutant. Injection of a moderate dose of *tbx6l* MO into a *spt* heterozygote cross appears to inhibit the formation of tail somites, suggesting functional overlap of the two T-box genes. Although the Tbx6l-depleted *spt* mutant phenotype is clearly more severe from that of *spt* single mutants, further analysis is needed to determine how loss of Tbx6l function enhances the *spt* phenotype. The *tbx6l* MO dose used in these experiments is predicted to mimic a partial loss of *tbx6l* expression and causes a minor deficit of tail mesoderm when injected into wildtype embryos. One would expect this same dose to reflect a

stronger *tbx6l* loss-of-function phenotype in *spt* mutants because *tbx6l* expression during gastrulation in *spt* mutants is already severely reduced (Griffin et al., 1998). If *tbx6l* in the tail functions similarly to *spt* in trunk mesoderm, then loss of *tbx6l* function during tail formation in a *spt* mutant background would be expected to result in a larger tailbud, in addition to fewer tail somites being formed. Indeed, I observed that *spt* mutants appeared to have smaller tailbuds and produced fewer somites than *tbx6l* MO-injected *spt* mutants, supporting the idea that Tbx6l and Spt have at least one overlapping function during posterior mesoderm development.

Tbx6l and Ntl may regulate similar target genes during tail formation

Distinguishing the role of *tbx6l* during tail paraxial mesoderm formation from the role of *ntl* during tail mesoderm formation is more difficult given that they affect the same region. Depending on the dose of morpholino injected, *tbx6l* morphants can exhibit axis truncations as severe as those exhibited by *ntl* mutants. This could be due to *ntl* and *tbx6l* acting in parallel or *tbx6l* acting downstream of *ntl*. Studies from the Kimelman lab have shown that Ntl and zebrafish Bra are required for maintaining a population of undifferentiated mesodermal progenitors in the tailbud via a positive feeback loop with *wnt3a* and *wnt8a* (Martin and Kimelman, 2008, 2010). The tail truncations and reduced tailbuds exhibited by *tbx6l* morphants point toward a role for Tbx6l in maintaining mesodermal progenitor cells but whether this activity is downstream of *ntl* or the tail organizer has yet to be determined. One way to address this question would be to assess the ability of ventral margins from Tbx6l-depleted embryos to induce secondary tails in wildtype embryos (Agathon et al., 2003). Goering et al. (2003) showed that the T-box DNA binding domain of Tbx6l could antagonize Ntl function, supporting the idea that Tbx6l may function alongside Ntl through regulation of an overlapping set of target genes during the tail segmentation program. Accordingly, assessing the formation of tail paraxial mesoderm in a *ntl* mutant following the over-expression of *tbx6l* during segmentation would indicate which roles ascribed to *ntl* are potentially mediated by *tbx6l*.

A potential null *tbx6l* mutant generated using targeted mutagenesis strategies

Distinguishing between putative null versus hypomorphic loss-of-function *tbx6l* phenotypes would be better addressed using a *tbx6l* null genetic mutant. Concurrently with the progress of my work, the Grunwald lab was attempting to generate a *tbx6l* mutant by targeting mutations to the *tbx6l* locus using zinc finger nuclease (ZFN) and transcription activator–like effector nuclease (TALEN)-mediated strategies (Doyon et al., 2008; Miller et al., 2011; Huang et al., 2011; Cade et al., 2012). Recently, they have isolated several mutant alleles which induce early stop codons within the first 30 residues of the ~190 amino acid T-box DNA binding domain. The preliminary analysis of transheterozygous mutants by the Grunwald lab did not show mesoderm defects similar to the *tbx6l* MO defects reported here (David Grunwald, personal communication). Further characterization of these mutants is necessary in order to verify *tbx6l* loss-of-function phenotypes described to date.

Figure 3.1

A.

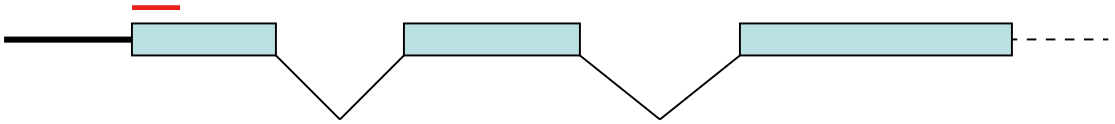

B.

AGTTTGTAGCTTCAGTCTGGTGGACATGTATCTCCCAGAGGAACGGCCTGTGCTGGACTTACCCTACCAGATGAATC

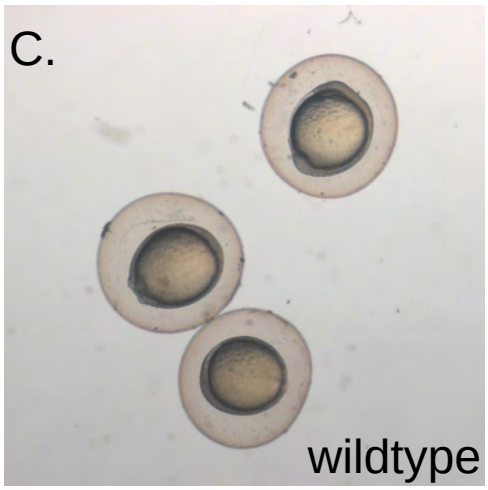

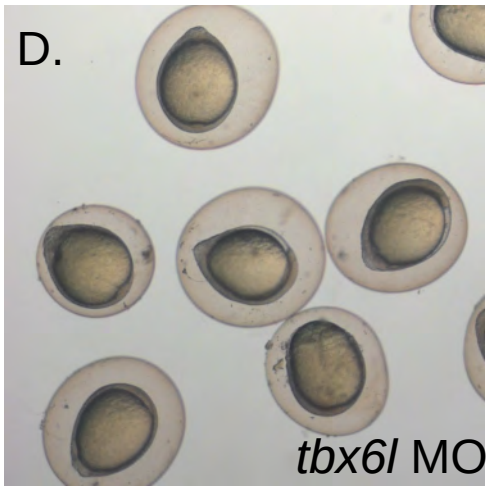

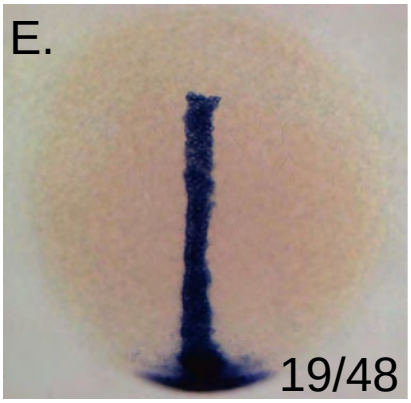

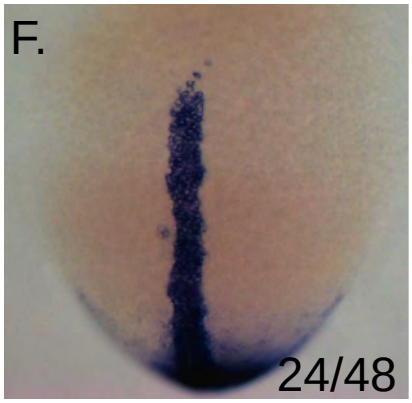

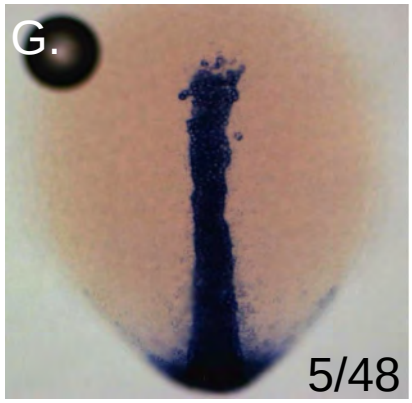

Figure 3.1 **Knocking down *tbx6l* causes dorsal patterning defects during gastrulation**

(A) A diagram of the *tbx6l* gene showing the 5' UTR (heavy black line), exons 1-3 (blue boxes) and the first two introns (lines connecting the boxes). The red line represents the translation-blocking *tbx6l* MO which is positioned over its target sequence located in the first exon. (B) 5'UTR (bold) and exon1 sequence flanking the *tbx6l MO* target sequence (overlined in red). Tailbud stage embryos in wildtype (C) and *tbx6l* MO-injected embryos (D). Notice the oval shape of yolks and pointed tailbuds in (D) as compared to (C). (E-G) Wholemount *in situ* hybridization staining of *ntl* in *tbx6l* MO-injected embryos. Embryos were sorted into classes based on the size of the axial domain. Class I embryos were relatively wildtype in size (E), class II embryos were slightly broader (F), and class III embryos were broadest (G). The seemingly larger domain of *ntl* staining in the posterior of embryos in (F) and (G) is due to the tailbud protruding away from the embryo instead of wrapping around the embryo as in (E).

Figure 3.2

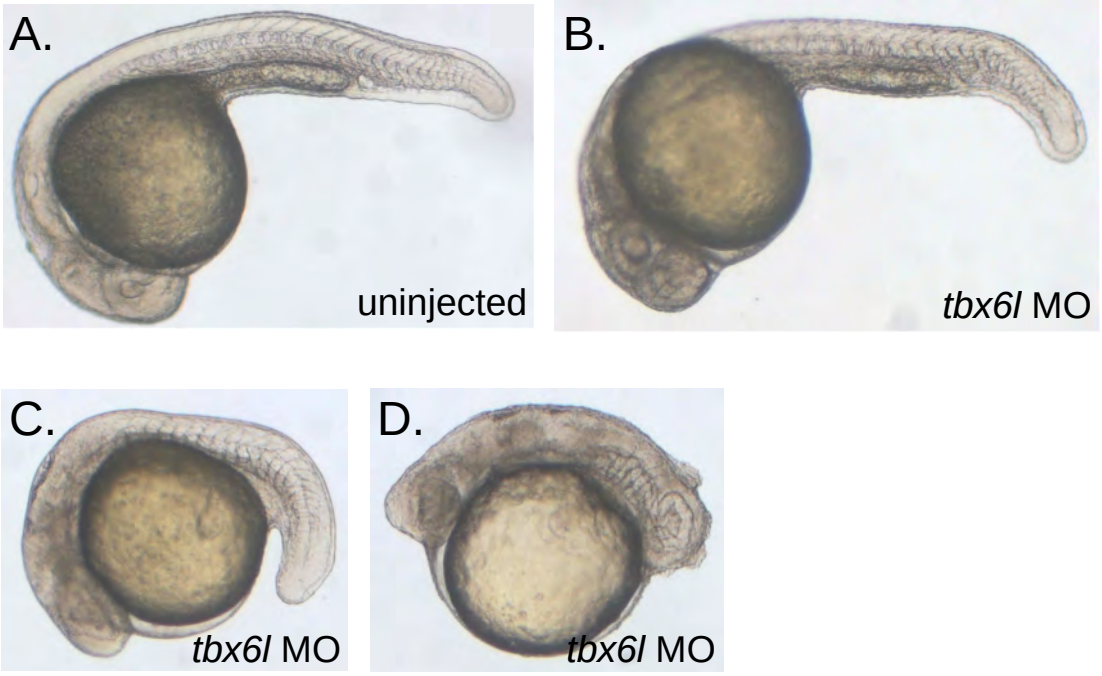
A.
uninjected
B.
tbx6l MO
C.
tbx6l MO
D.
tbx6l MO

E.

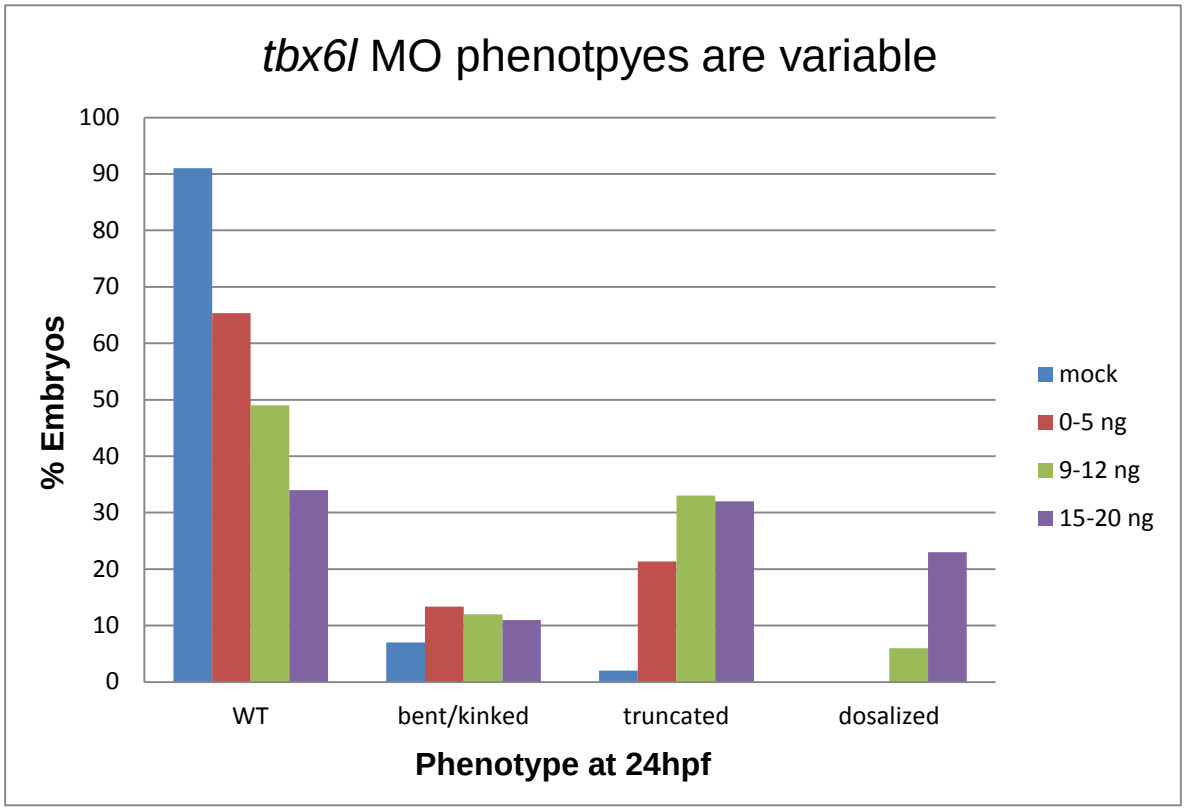
tbx6l MO phenotpyes are variable
% Embryos
100
90
80
70
60
50
40
30
20
10
0
WT
bent/kinked
truncated
dosalized
Phenotype at 24hpf
mock
0-5 ng
9-12 ng
15-20 ng

Figure 3.2 ***tbx6l* is required for trunk and tail mesoderm formation**

(A) Uninjected wildtype embryo at 24hpf. (B-D) Phenotypes seen with progressively higher doses of *tbx6l MO*. Low doses of MO results in mostly wildtype embryos with bent and skinny tails (B), while higher doses result in truncations (C and D) or dorsalization (data not shown). (E) Graph showing that all of the described phenotypes are seen at each dose but that the more severe defects are seen most often at higher doses of *tbx6l* MO.

Figure 3.3

A.

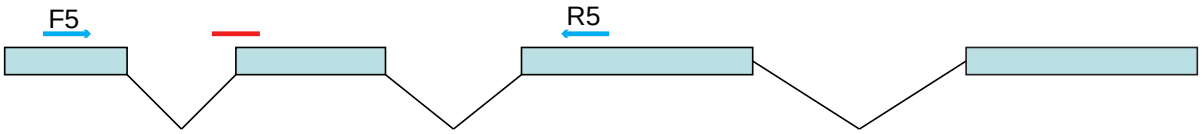

G.

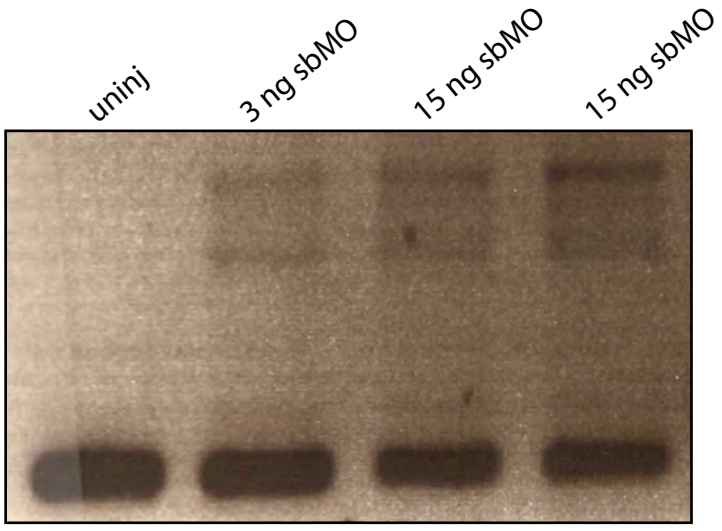

Figure 3.3 **Splice-blocking *tbx6l MO* does not effectively knock down *tbx6l* expression**

(A) Gene model of *tbx6l* including the first 4 exons and the first 3 introns. *tbx6l* sbMO is shown in red over its target sequence, the intron1-exon2 junction in the *tbx6l* pre-mRNA. The primers used in splice analysis are represented in blue. (B-C) *tbx6l* sbMO injected embryos at 24hpf. Note the failure of the tail to extend in (B) and the stumpy bifurcated tail in (C). (D-F) Control-injected (D) and *tbx6l* sbMO-injected embryos (E-F) at 48hpf. The embryo in (E) displays the blisters seen in a portion of embryos while (F) exhibits the curved body and reduced fin mesenchyme. (G) Analysis of *tbx6l* splice variants resulting from *tbx6l* sbMO injection. cDNA was made from RNA extracted from control-injected or *tbx6l* sbMO-injected embryos. Primers F5 and R5 were used to amplify *tbx6l* mRNA from cDNA and products were run on an agarose gel and stained with ethidium bromide. Lane 1 uninjected embryos, lane 2: embryos injected with 3ng *tbx6l* sbMO, lane 3 and 4: embryos injected with 15 ng of *tbx6l* sbMO. All RNA samples extracted from *tbx6l* morphants contain similar aberrant splice profiles compared to mock injected controls.

Figure 3.4

A.

clone	HS	GFP+	No HS	GFP+
1	37	25 (68%)	15	0 (0%)
3	25	4 (16%)	11	0 (0%)
4	30	22 (73%)	17	1 (6%)
5	15	13 (87%)	16	1 (6%)

B.

clone	HS	GFP+	DsRed+	No HS	GFP+	DsRed+
1*	21		19 (90%)			
12*	24		16 (67%)			
13*	25		10 (40%)	11		0 (0%)
5*	22	16 (73%)				
6*	24	20 (83%)		19	0 (0%)	

Figure 3.4 **Heat-inducible *tbx6l* over-expression constructs**

(A) Schematic of the *tbx6l* over-expression transgene. The *hsp70l* promoter drives the full *tbx6l* and *gfp* coding sequences separated by a *2A* viral ribosomal stutter sequence. The *tbx6l* sequence contains the target for the translation-blocking *tbx6l MO*. Below the construct, a table indicates the relative GFP expression from each of four clones with and without heat-shock induction. (B) Schematic of *tbx6l* over-expression transgenes generated that lack the *tbx6l MO* target sequence. Below the construct, a table indicates the reporter expression from each clone tested with and without heat-shock induction.

Figure 3.5

MYLPEERPVLDLPYQMNHLANNYGYYPQDCRTQYSRMNSAEAELTSLPVH

VSLQDRELWDKFSSIGTEMLITKSGRRMFPSCKVTVTGLNPKVKYVVIMD

MVPFDNHKYKWNKDCWEVNGSSDPHLPNRFFIHPDSPAPGQKWMQYPISF

HKLKLTNNTLNSNGLVVLHSMHKYQPRLHIVQSPDPCTPHNPGAYLRFTF

PEAAFIAVTAYQNQEITKLKIDNNPFAKGFRDNGLNRKRFRDKGTQEMQD

TDRQVKLDLTANECAAGMSQMVEDVDVSVSSSVDCRDTQNSSSVSLNPFI

SAFTNPSSAGGAAAHQTHTLLSLSNRHFSSPRESNLNSVCAALPVSQLST

GHTSFSRLNPQETHHNSRPKIQLQPPHPSLQCHDLELRLPLPPKLSRVQL

SESALRNLEMSPLSDCANPRPLTNILNRSCFRASTPSGKLLPNPPQPEQF

LRGSEREIYPAVQEYTDQQFTLNSQTEHRPHMRPLTEY

Figure 3.5 **Peptide sequence of Tbx6l**

The Tbx6l protein is 488 amino acids. The amino terminal T-box domain is underlined in black and the antigen sequence used to generate the polyclonal Tbx6l antibody is underlined in green.

Figure 3.6

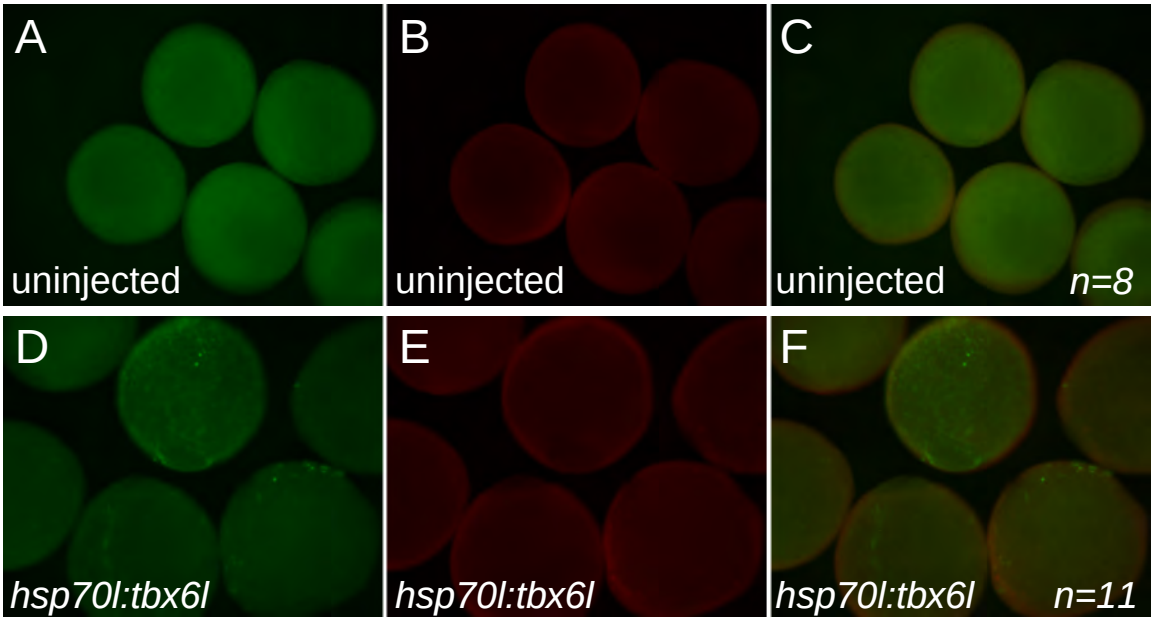
A
uninjected
B
uninjected
C
uninjected
n=8
D
hsp70l:tbx6l
E
hsp70l:tbx6l
F
hsp70l:tbx6l
n=11

Figure 3.6 **Detection of the Tbx6l antigen signal is dependent on the Tbx6l primary antibody**

Uninjected (A-C) or *hsp70l*:*tbx6l-2A-GFP* injected (D-F) embryos were heat-shocked for 1 hour at shield stage, raised to late gastrula stage and fixed. Immunohistochemistry was performed and embryos were incubated in block instead of the Tbx6l primary antibody. Ectopic Tbx6l expression is indicated by green fluorescence (A,D). An Alexa Fluor® 568 -conjugated secondary antibody was used to detect Tbx6l binding of the Tbx6l primary antibody (B,E). (C) and (F) are merges of panels (A) and (B), and (D) and (E), respectively. Anti-Tbx6l immunohistochemistry does not detect an antigen signal in no primary antibody control embryos.

Figure 3.7

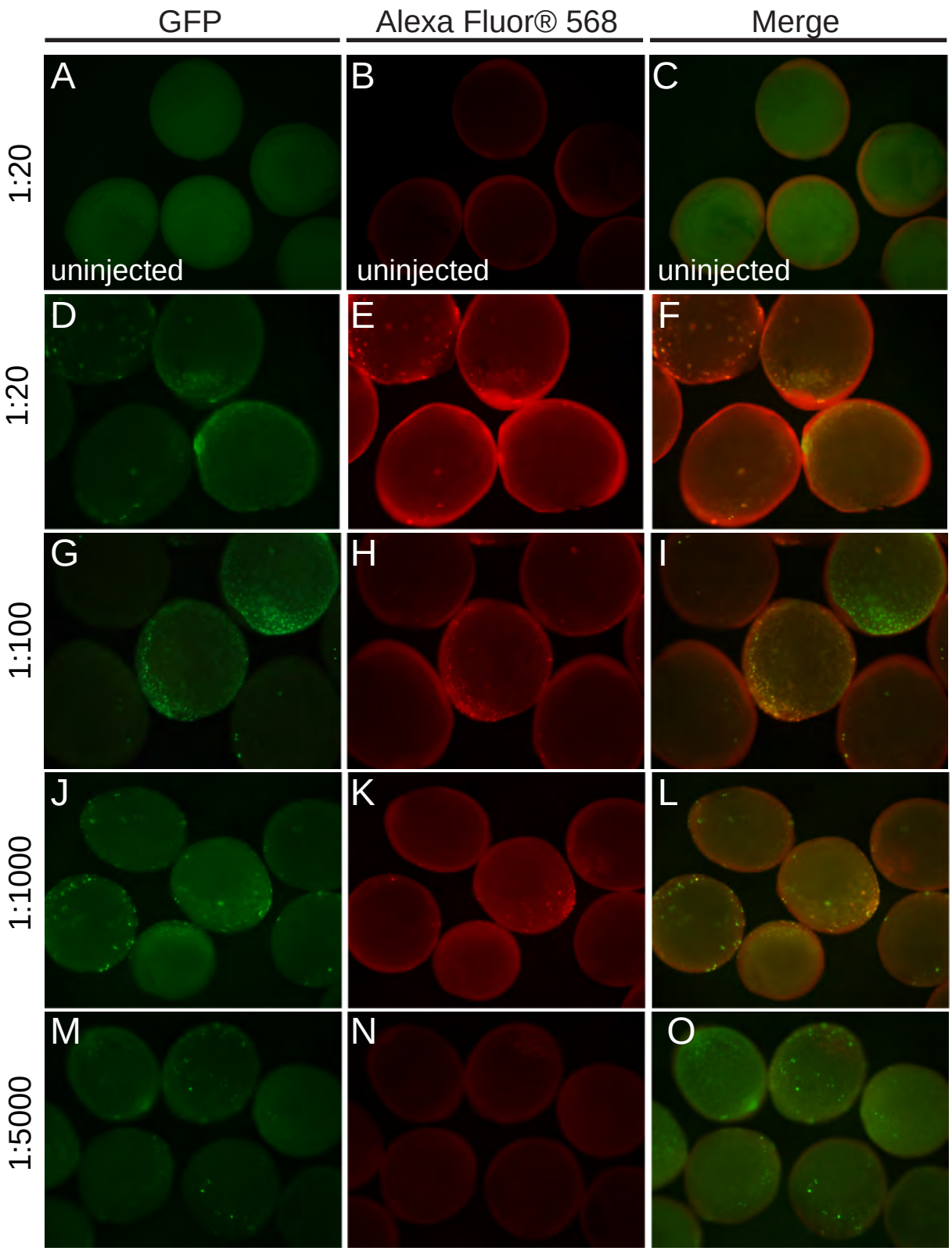
GFP
Alexa Fluor® 568
Merge
1:20
1:20
1:100
1:1000
1:5000
A
B
C
uninjected
uninjected
uninjected
D
E
F
G
H
I
J
K
L
M
N
O

Figure 3.7 **Tbx6l primary antibody detects Tbx6l by immunohistochemistry but not at endogenous levels**

Uninjected (A-C) or *hsp70l*:*tbx6l-2A-GFP* injected (D-O) embryos were heat-shocked for 1 hour at shield stage, raised to tailbud stage and fixed. Immunohistochemistry was performed and embryos were incubated in a 1:20 (A-F), 1:100 (G-I), 1:1000 (J-L), or 1:5000 (M-O) dilution of the Tbx6l primary antibody. Ectopic Tbx6l expression is indicated by green fluorescence (A,D,G,J,M). An Alexa Fluor® 568-conjugated secondary antibody was used to detect bound anti-Tbx6l antibody (B,E,H,K,N). Panels on the right (C,F,I,L,O) are merges of panels to the left. Note that endogenous Tbx6l is not detected in uninjected embryos at the lowest antibody dilution (A-C).

Figure 3.8

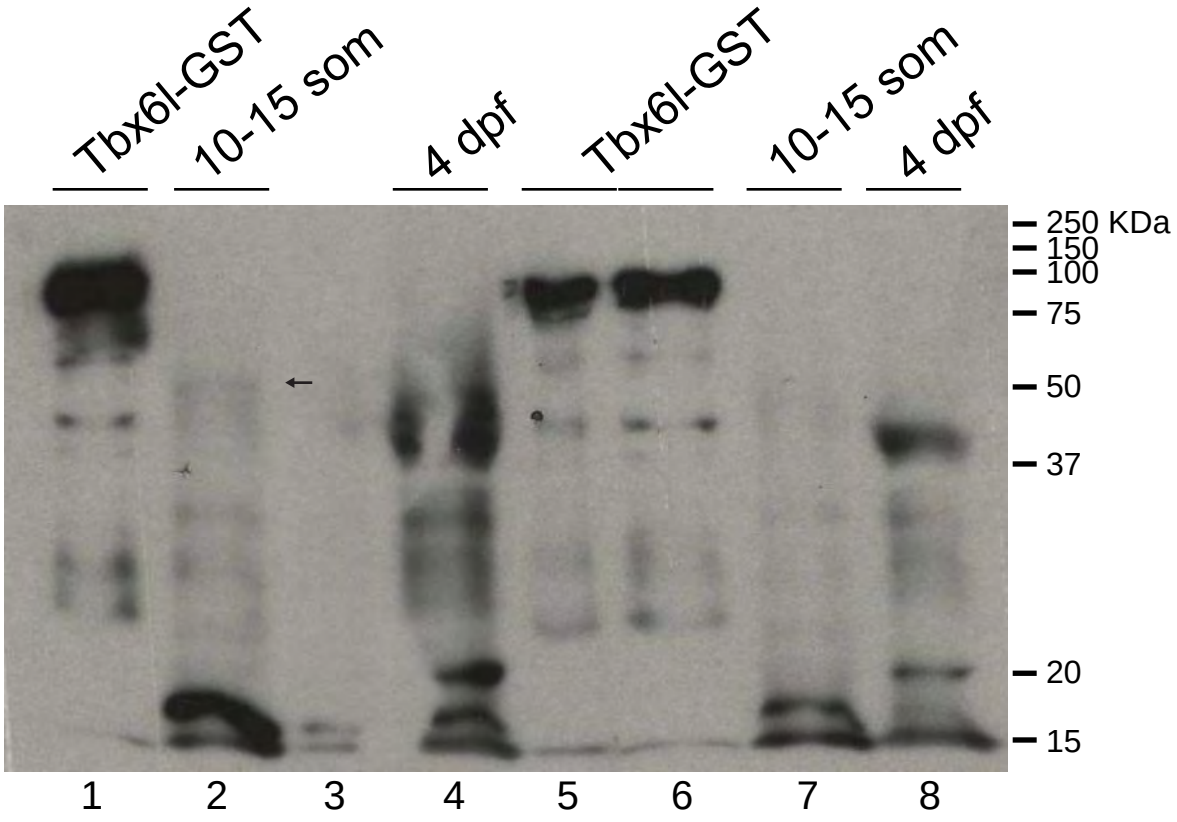
Tbx6l-GST
10-15 som
4 dpf
Tbx6l-GST
10-15 som
4 dpf
250 KDa
150
100
75
50
37
20
15
1
2
3
4
5
6
7
8

Figure 3.8 **Tbx6l antibody detects multiple bands on a western blot**

Western blot incubated in rabbit polyclonal anti-Tbx6l antibody and HRP-conjugated goat anti-rabbit IgG secondary antibody. Lanes 1,5 and 6 were loaded with 30ul purified recombinant Tbx6l-GST. Lanes 2 and 7 were loaded with 25-30 ul protein extract from 10-15 somite staged embryos. Lanes 4 and 8 were loaded with 20-25 ul protein extract from 4dpf embryos. Lanes 1-4 were incubated in 1:1000 dilution of the Tbx6l antibody and lanes 5-8 were incubated in 1:5000 dilution of the Tbx6l antibody. The band sizes are indicated in kilodaltons (KDa) on the right. Arrow indicates band corresponding to predicted size of endogenous Tbx6l.

Figure 3.9

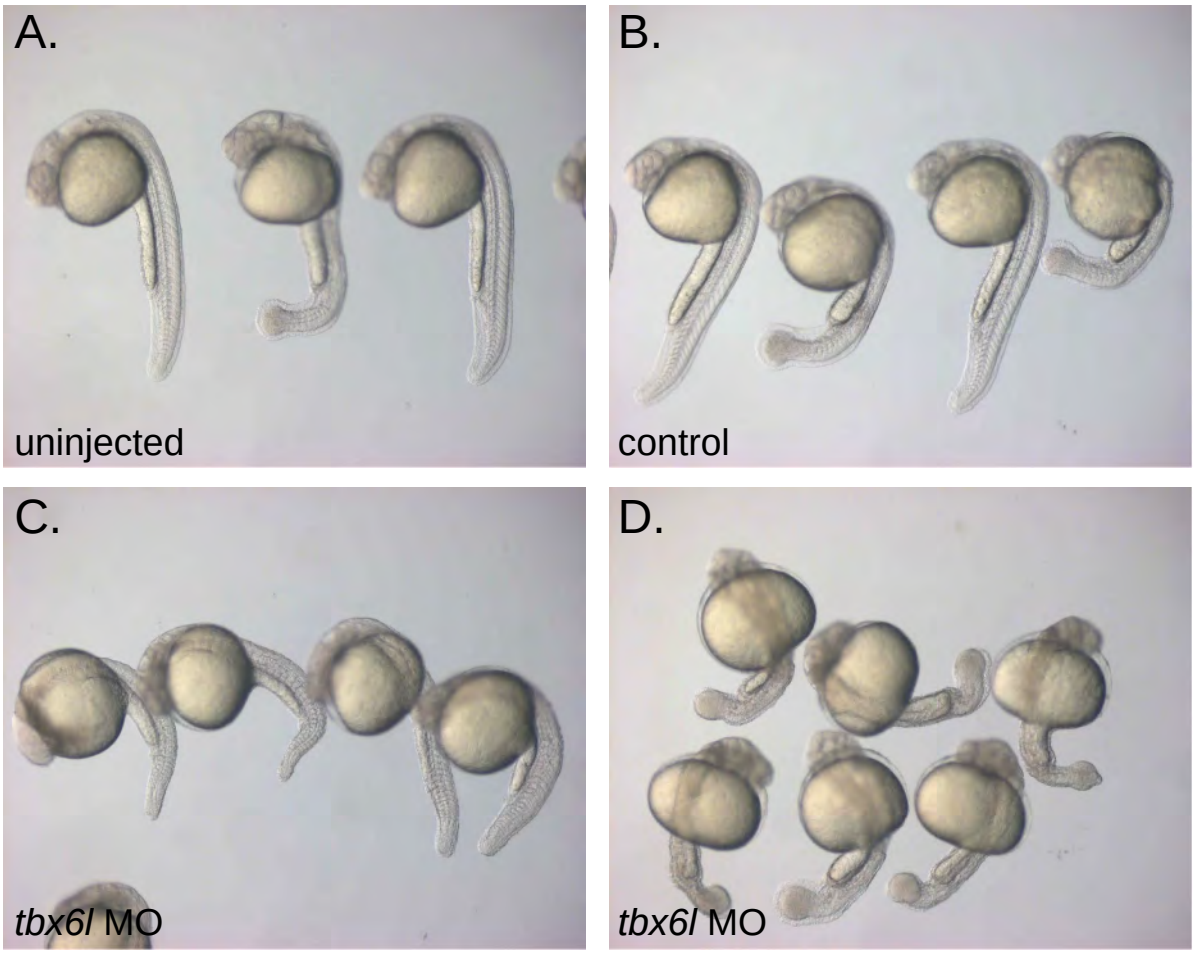

Figure 3.9 **Depleting *tbx6l* function in a *spt* mutant background results in loss of paraxial mesoderm in the tail**

Live images of 24hpf uninjected (A), control-injected (B), and *tbx6l MO*-injected (C and D) $spt^{+/-}$ intercross progeny. Uninjected (A) and control-injected (B) *spt* mutants lack trunk somites but do form tail somites, and form the characteristic spadetail. Wildtype embryos from both groups are identical. (C) The moderate dose of *tbx6l MO* used causes tail truncations but tail somites are present past the yolk extension. The same MO dose in a *spt* mutant background appears to cause a complete loss of paraxial mesoderm, demonstrated by the absence of somites (D).

Table 3.1

		Fixative			Fix time		Permeabilized			Perm.		Tbx6l Antibody				Antibody dilution						
		PFA	C.F.	TCA	2hr	O/N	No	Ac.	Triton	7min	2hr	Cont.	Anti	Abs	AP	No 1°	1:20	1:100	1:200	1:500	1:1000	1:5000
1	WT	x				x			x		x	x							x		x	x
2	WT	x				x			x		x		x						x		x	x
3	WT	x				x			x		x			x					x		x	x
4	WT	x				x	x					x							x		x	x
5	WT	x				x	x						x						x		x	x
6	WT	x				x	x							x					x		x	x
7	WT	x			x		x									x						
8	WT	x			x		x					x									x	
9	WT	x			x		x						x								x	
10	MO	x			x		x						x								x	
11	WT	x			x		x								x	x		x		x	x	x
12	WT	x			x			x		x					x	x		x		x	x	x
13	WT		x		x		x								x	x		x		x	x	x
14	WT		x		x			x		x					x	x		x			x	x
15	WT			x		x	x								x		x	x		x	x	
16	WT	x				x	x								x	x	x	x		x	x	x
17	HS	x				x	x								x	x	x	x		x	x	x

Table 3.1 **Conditions used for Tbx6l antibody immunohistochemistry**

A chart indicating the conditions used to detect the Tbx6l antigen with the Tbx6l antibody by immunohistochemistry. Columns indicate the fixative used (PFA-4% paraformaldehyde, C.F.-Carnoy's Fixative, TCA-Trichloroacetic acid), duration of the fixation (O/N indicates an overnight fixation for 14-16 hours at 4°C), method used for permeabilizing embryos (No-no extra permeabilization step, Ac.-embryos incubated in 100% acetone at -20°C, Triton-PBT block with 2% triton), duration of permeabilization step (Perm.), the Tbx6l primary antibody used (Cont.-serum from a pre-immunized rabbit, Anti- Tbx6l antisera, Abs- Tbx6l antibody preabsorbed in 4dpf zebrafish embryos, AP- Affinity purified Tbx6l antibody), and the dilutions of the antibody used for the incubation. WT-wildtype embryos, MO-embryos injected with 9-15ng *tbx6l* MO, HS-embryos injected with *hsp70l:tbx6l-2A-GFP* and heat-shocked at 40°C. Embryos were incubated in HRP-conjugated secondary antibody (rows 1-15) or Alexa Fluor® 568-labeled secondary antibody (rows 16-17).

Table 3.2

	condition	n	GFP	AF568	overlap
Wildtype	No 1	8	0	0	0
hs:tbx6l	No 1	11	11	0	0
Wildtype	1:20	9	0	1	0
hs:tbx6l	1:20	11	9	9	9
Wildtype	1:100	9	0	2	0
hs:tbx6l	1:100	11	10	8	8
Wildtype	1:500	10	0	1	0
hs:tbx6l	1:500	13	12	12	12
Wildtype	1:1000	10	0	2	0
hs:tbx6l	1:1000	13	11	11	11
Wildtype	1:5000	10	0	4	0
hs:tbx6l	1:5000	12	12	3	3

Table 3.2 **Results for anti-Tbx6l immunohistochemistry visualized with Alexa Fluor® 568 conjugated secondary antibody**

From left to right, the columns list (1) the background of the embryos (2) the Tbx6l antibody dilution used to detect Tbx6l expression in whole embryos (3) the number of embryos tested in each condition (4) the number of embryos which expressed GFP (5) the number of embryos exhibiting punctate localization of the Alexa Fluor® 568 signal (6) the number of embryos in which the GFP expression and Alexa Fluor® 568 signal co-localized.

Table 3.3

	condition	n	GFP+	% GFP+
B1	uninjected	25	0	0
	hs:tbx6l	22	13	59
	hs:tbx6l and MO	17	0	0
B2	*hs:tbx6l*	6	3	50
	hs:tbx6l and MO	14	1	7
B3	*hs:tbx6l*	13	10	77
	hs:tbx6l and MO	6	2	33
total	***hs:tbx6l***	**41**	**26**	**63**
total	**hs:tbx6l and MO**	**37**	**3**	**8**

Table 3.3 **The translation-blocking *tbx6l* MO targets and inhibits translation of the *tbx6l* transcript**

This table contains results from three experiments where embryos were injected with either the *hsp70l:tbx6l-2A-GFP* overexpression construct alone (*hs:tbx6l*) or in combination with the *tbx6l* MO (MO). The *tbx6l* MO blocks translation from the *tbx6l* transcript ($p<0.001$, chi square statistical test).

Chapter 4: Regulation of other potential Ntl/Spt targets

Background

RNA binding motif protein 38 (*rbm38*) was identified in the Amacher lab as a potential downstream target of *ntl* and *spt* and has been shown by others to be a direct target of Ntl (Garnett et al., 2009; Morley et al., 2009). The zebrafish *rbm38* gene produces two transcripts, both of which encode proteins containing the RNA recognition motif (RRM) domain. RNA binding proteins have been shown to be important in a number of processes including the transcription, splicing, 3' end modification, localization, stability and translation of mRNA (reviewed by Dreyfuss et al., 2002).

Cloning and functional analysis of *rbm38* was first achieved in studies of the *Xenopus* ortholog, *Xseb4R*. *Xseb4R* is expressed early on in the oocyte and throughout the tadpole stage, as detected by RT-PCR. Transcripts are first detected by *in situ* hybridization around the blastopore margin and underlying paraxial mesoderm, excluding the dorsal region. During somite formation *Xseb4R* is expressed in the tailbud as well as the more ventral mesoderm derivatives, the blood island, and pronephros (Boy et al., 2003). In addition to mesodermal tissue, *Xseb4R* is also expressed in neural and head structures including the neural plate, trigeminal and otic placodes, forebrain, midbrain, hindbrain, and retina, as well as being expressed in the liver and gastrointestinal tract (Boy et al., 2003). Loss-of-function studies in *Xenopus* indicate *Xseb4R* promotes neural differentiation. Global MO knockdown of *Xseb4R* with 10-20ng of *Xseb4R* MO decreases the expression of neural differentiation marker *N-tubulin*. Additionally, Souopgui et al. (2008) showed that by promoting the stability and translation of the *VegT* transcript through interaction with its 3' UTR, Xseb4R functions during early development to promote the specificiation of mesoderm and endoderm germ layers. Consistent with these results, embryos injected with 100ng of the same *Xseb4R* MO and assayed by *in situ* hybridization showed decreased expression of mesodermal gene *Xbra* and endoderm gene *Sox17β* (Souopgui et al., 2008). However, these embryos were not raised past the gastrulation stage and the extent of their effect on embryonic development was not determined. In order to knock down Xseb4R expression in the eye, Boy et al. (2003) used lipofection to introduce the *Xseb4R* morpholino into retinoblasts, and showed that targeted knockdown of Xseb4R in the eye inhibits retinal cell differentiation (Boy et al., 2003).

Functional studies in cell culture assays have demonstrated that human and mouse *Rbm38* orthologs act downstream of the p53 family of tumor supressors to promote cell cycle arrest (Chen et al., 2003; Shu et al., 2006; Miyamoto et al., 2009; Leveille et al., 2011). Like zebrafish *rbm38*, the human *Rbm38*/*Rnpc1* gene produces two transcripts: *Rnpc1a* encodes 239 amino acids, while *Rnpc1b* encodes 121 amino acids that are identical to the N-terminal of Rnpc1a. Both proteins encode the RRM domain and are capbable of binding transcripts of the cell cycle regulator p21 in the 3'UTR. However, only the Rnpc1a isoform is capable of inducing cell cycle arrest and inhibiting cell proliferation in cell culture by stabilizing *p21* transcripts (Shu et al., 2006). In addition to regulating *p21* stability, murine *Rbm38*, along with its paralog *Rbm24*, was shown to promote myogenic differentiation when over-expressed in cell culture (Miyamoto et al., 2009). Thus, in vertebrates, Rbm38 may have a conserved role in

stabilizing its targets through interaction with the 3' UTR in addition to promoting differentiation by inhibition of proliferation.

Another downstream target of *ntl* and *spt*, *integrin beta 5* (*itgb5*), is only down-regulated in the absence of both Ntl and Spt expression (Garnett et al., 2009; Morley et al., 2009; Shestopalov et al., 2012). Integrins are heterodimer membrane-spanning receptors that link the cytoskeleton to the extracellular matrix and relay signals from both sides of the plasma membrane (reviewed by Takada et al., 2007). Each integrin is comprised of an alpha integrin and beta integrin and binds different ligands depending on its subunits. *itgb5* encodes the beta subunit of an integrin adhesion molecule which, to date, has only been show to interact with the *alphaV* (*αV*) alpha subunit. The αVβ5 integrin binds ECM proteins containing the RGD(S) amino acid motif (reviewed by Takada et al., 2007). Although the integrin family has been shown to be important in a variety of developmental process, the role of *itgb5* in mesoderm development has yet to be addressed (reviewed by Arcangelis and Georges-Labouesse, 2000). Mice homozygous for an *Itgb5* null allele develop normally and do not display defects in wound healing or increased susceptibility to adenovirus infection, processes attributed to the αVβ5 integrin (Huang et al., 2000). In mouse knock-out models lacking both *Itgb3* and *Itgb5*, tumors injected into the mouse display increased growth and increased angiogenesis, indicating a role for αVβ3 and αVβ5 integrins in regulating this process (Reynolds et al., 2002; Taverna et al., 2003).

I chose to investigate the functional roles of *rbm38* and *itgb5* for several reasons. Firstly, down-regulation of expression of *itgb5* and *rbm38* in *spt*;*ntl* double mutants (*rbm38* ~7-fold; *itgb5* ~3-fold) when compared to their expression in either *spt* (*rbm38* and *itgb5* ~ <1.5-fold) or *ntl* (*rbm38* ~2-fold down-regulation; *itgb5* ~ <1.5-fold) single mutants indicates they are regulated by both *ntl* and *spt*, making them likely genes to function during trunk and tail mesoderm formation. Secondly, whereas transcription factor targets lead to more downstream transcriptional targets, *rbm38* and *itgb5* are likely to affect processes downstream of gene induction that are required for mesoderm formation. As an RNA-binding protein, *rbm38* may elucidate post-transcriptional mechanisms involved in mesoderm development, as well as uncover genes in the mesoderm gene regulatory network that are indirectly regulated by *ntl* and *spt* function. *itgb5* may be involved in cytoskeletal rearrangements that precede cell shape changes and morphogenetic movements prevalent during gastrulation and segmentation stages (reviewed by Hynes, 2002; Holley et al., 2009). As a first step to analyzing the respective roles of *itgb5* and *rbm38* during zebrafish development, I characterized their expression during the first 24 hours of development. For *rbm38*, I also attempted to knock down its function using a splice-blocking MO. I have shown that expression of *rbm38* and *itgb5* during gastrulation support a role for these genes in mesoderm patterning downstream of *ntl* and *spt,* whereas their expression in non-mesodermal tissues during later stages of segmentation indicate additional roles in zebrafish development.

Materials and Methods

Zebrafish husbandry

Wildtype embryos used were from the AB genetic background. For scoring the left-right position of the liver, I used fish embryos homozygous for the "*gut:gfp"* transgene [Tg(XlEef1a1:GFP)^{s854}; line generously provided by the Stainier lab] (Field et al., 2003). All fish were raised at 28.5°C unless otherwise noted.

Probe synthesis

To generate a probe against *itgb5*, I designed primers to amplify an 1104 bp fragment containing the 3' end of the transcript including a portion of the 3' untranslated region and the first 5 exons: itgb5-5'1 (5'-ATCTACGGCACCTTCTGCGAATGTG-3') and itgb5R1 (5'-ATAATGTGTGGGAGGTACGGTTAGAAATG-3'). This fragment was amplified from gastrula stage cDNA, cloned into a dual promoter TOPO® vector (Invitrogen) and sent for sequencing to verify the insertion of the *itgb5* sequence. The resulting plasmid was then used to generate sense and antisense digoxigenin-labeled RNA riboprobes (See Materials and Methods from Chapter 2). To generate a digoxigenin-labeled *in situ* probe for *rbm38*, a plasmid containing the full-length *rbm38* cDNA (constructed by Xiao Xu, an honors undergraduate student in the lab) was used as the template for the *in vitro* transcription reaction. To linearize the plasmid templates for sense and antisense probes against *itgb5* and *rbm38* the following digests were performed: *itgb5* sense (BamHI), *itgb5* antisense (NotI), *rbm38* sense (NotI), *rbm38* antisense (EcoRI). Sp6 RNA polymerase was used in reactions for the *rbm38* sense probe and *itgb5* antisense probe. T7 RNA polymerase was used in reactions for the *rbm38* antisense probe and *itgb5* sense probe. Probes were diluted 1:200 in pre-hybridization buffer for *in situ* hybridizations.

in situ hybridization and imaging

See Materials and Methods from Chapter 2.

Microinjections

See Materials and Methods from Chapter 2.

Morpholino injections

The *rbm38* MO sequence is 5'-CGGTTGTTTTTACTCACAAAGCCGT-3'. The MO was dissolved in nuclease free water to make a 50ng/nL stock, and diluted to a working concentration of 1ng/nL, 3ng/nL, or 5ng/nL in a 0.2M KCl, 0.1% phenol red carrier solution. Embryos were injected at the 1-cell stage with 2-4nL of MO. The *itgb5* MO sequence ordered is 5'-TCACCAAACACAGCGCTTACCTTTG-3'.

Results

itgb5 and *rbm38* are expressed in the mesoderm during gastrulation and segmentation

The zebrafish *itgb5* gene produces 4 transcripts, two of which encode proteins, *itgb5-001* and *itgb5-004*. *Itgb5-001* encodes a protein of 807 amino acids (aa). The

shorter transcript, *itgb5-004* encodes a 138aa protein identical to the N-terminal portion of Itgb5-001. There was no published expression profile of *itgb5* in zebrafish embryos, so I first wanted to determine if this gene was expressed in the same tissues and at the same developmental time as *ntl* and *spt*. Wildtype embryos were collected, fixed at multiple time points during development and assayed for *itgb5* mRNA expression by *in situ* hybridization using the *itgb5* riboprobe. *itgb5* is expressed in all cells of a 16-cell embryo prior to activation of zygotic transcription, indicating maternal supply of the transcript, and continues to be expressed ubiquitously in the blastula after zygotic transcription has commenced (Fig 4.1 A,B). By shield stage, *itgb5* expression is confined to the margin (Fig 4.1 C). As gastrulation proceeds, expression is detected in margin cells, including those in the dorsal midline, as well as in the hypoblast (Fig 4.1 D). Early during somitogenesis *itgb5* is weakly expressed in the PSM, the head, and along the body. Later during segmentation, expression is barely detected in the PSM and is more strongly expressed in head tissues (Fig 4.1 F).

The zebrafish *rbm38* gene encodes two transcripts, *rbm38-001* and *rbm38-002*, which encode proteins of 234aa and 211aa, respectively. Each protein contains an RNA recognition motif (RRM) domain, the most prevalent RNA binding domain in vertebrates (Clery et al., 2008) (Fig 4.4 A). The two transcripts are identical through the RRM domain, but exon 2 in *rbm38-001* terminates prematurely, while its last exon is 100 bp longer than *rbm38-002* (Fig 4.4 A). Wildtype embryos were collected, fixed at different developmental stages, and processed for expression of *rbm38* transcripts. The *rbm38* transcript is maternally provided and evident at 8-16 cell stage (data not shown). Between dome and 30% epiboly, expression is ubiquitous in the animal pole, but appears faint (Fig 4.2 A,B). Because this is nearly one hour after initiation of zygotic transcription, it appears that there is a lag between depletion of maternal transcript and induction of zygotic *rbm38*. By shield stage, *rbm38* is expressed robustly around the margin but not in the axial mesoderm (data not shown). During gastrulation, *rbm38* continues to be expressed in the ventral and lateral margin, and in the underlying hypoblast, but is excluded from the dorsal-most mesoderm (Fig 4.2 C). As gastrulation concludes, expression is detected in the tailbud and paraxial mesoderm of the PSM, where it continues to be expressed throughout segmentation (Fig 4.2 D,F,H). At the 4-5 somite stage, *rbm38* is also expressed in the lateral plate mesoderm and the head (Fig 4.2 E). By 20 somites, *rbm38* appears to be expressed in the forebrain, midbrain and hindbrain as well as in two stripes along the body axis that may represent lateral mesoderm, paraxial mesoderm, and/or neural crest cells (Fig 4.2 G), which could be definitively identified by double *in situ* hybridization with known markers. At 26-28 hpf, there is still detectable expression in the forebrain as well as in the blood island posterior and dorsal to the yolk tube (Fig 4.2 H). Based on these results, I conclude that zebrafish *rbm38* is expressed in many of the same tissues as its *Xenopus* ortholog.

Ntl and Spt are necessary for expression of *itgb5* and *rbm38*

My expression analyses show that both *itgb5* and *rbm38* expression overlap with *ntl* and *spt* expression in the margin and hypoblast during gastrulation as well as in the tailbud throughout somitogenesis. The overlapping expression with T-box genes as well as the transcriptional regulation by *spt* and *ntl* reported by Garnett et al. (2009) indicate that these genes may be direct targets of Spt and Ntl. To determine the necessity of *spt*

and *ntl* in expression of *itgb5* and *rbm38* as well as verify the microarray results, embryos were depleted of Spt and/or Ntl expression using MOs and assayed for *itgb5* and *rbm38* expression during mid-gastrulation. Consistent with the microarray data, during gastrulation, *itgb5* expression is not affected by the loss of either Spt or Ntl alone, but is nearly absent from the margin and underlying hypoblast when both Spt and Ntl are depleted (Fig 4.3). Likewise, *rbm38* was predicted to be a *ntl*-regulated target and expression was only decreased in *ntl* MO-injected embryos and *ntl* MO/*spt* MO-injected embryos. This supports the idea that down-regulation of these transcripts during gastrulation, as reported by Garnett et al. (2009), may be due to their regulation by *ntl* and *spt*. Recently, two groups have published efforts to identify targets of Ntl. Using chromatin immunoprecipitation and genomic microarrays, Morley et al. (2009) identified known and novel targets bound *in vivo* by the Ntl transcription factor. They reported that *rbm38* was bound by and is most likely a direct target of Ntl, but did not report an interaction between Ntl and the *itgb5* promoter (Morley et al., 2009). Shestopalov et al. (2012) employed the use of a caged *ntl* MO and fluorescein marker, both of which are photoactivatable, to compare the transcriptional profiles of wildtype notochord precursor cells (within the shield) to Ntl-depleted notochord precursor cells. Both *itgb5* and *rbm38* were identified as being downstream targets of *ntl* (Shestopalov et al., 2012).

rbm38-depleted embryos do not have an overt phenotype

To determine the role of *rbm38* in zebrafish development, I used a splice-blocking morpholino to knock down expression of Rbm38. The MO binds at the exon1-intron1 junction, which corresponds to the C-terminal portion of the RNA-binding RRM domain (Fig. 4.4 A,B). Since the two *rbm38* transcripts are identical until just after the RRM motif, the splice-blocking MO should target both. Embryos were injected at the 1-cell stage and scored at 24hpf for morphological defects. *rbm38* morphants displayed two noticeable defects: decreased or absent median fin fold and pooled blood or poor blood circulation (Fig. 4.5 A,B; data not shown). The median fin fold mesenchyme extends from the end of the yolk extension to the posterior end of the fish. However, control-injected embryos showed median fin fold mesenchyme defects at a similar frequency to the MO-injected embryos, indicating an overall defect with the genetic background of the fish or an artifact of the injection technique (Fig 4.5 C). In two of the three experiments, the embryos exhibited slowed blood circulation or pooling of the blood in the tail. This occurred in roughly 10% of the *rbm38* morphants but was not detected in control-injected embryos (Fig 4.5 C; data not shown). Finally, in one of the three experiments, *rbm38* morphants also showed slightly cupped or “scooped” tails (Fig 4.5 C; data not shown).

Spt and Ntl have been shown to be required for formation and function of Kupffer’s vesicle, an organ which functions in specifying the left-right axis, and s*pt* and *ntl* mutants show randomized symmetry of left lateral mesoderm markers (Essner et al., 2005; Amack et al., 2007). To determine if *rbm38* may have a role in left-right patterning, *rbm38* MO or a control solution was injected into embryos carrying the gut:*gfp* transgene, which marks the gut endoderm including the liver, pancreas, swim bladder and intestine (Field et al., 2003). Injected embryos were raised to 48hpf and the position of the liver was scored. Normally, the liver is positioned on the left side of the embryo. Control-injected embryos showed the liver developing on the right side of

the embryo 25% of the time compared to 7% in uninjected embryos (p=0.003). When compared to control-injected embryos, *rbm38* morphants did not display a significant difference in the left-right asymmetry of the liver (<10ng p=0.492; 9-15ng p=0.072). These results indicate that the left-right patterning defect observed is a result of the injection method and not the loss of *rbm38* (Fig 4.5 D).

Discussion

Rbm38 orthologs regulate cell cycle progression and promote mesoderm and neural differentiation

rbm38 is expressed maternally; expression in the paraxial mesoderm, blood island and neural tissues in zebrafish is very similar to the expression reported for *Xseb4R*, suggesting the genes may function similarly in both organisms. *Xseb4R* is able to stabilize and promote translation of its RNA targets through binding to sequences in the 3'UTR. Based on the studies in *Xenopus* embryos and cell culture, *rbm38* likely functions in multiple processes, depending on its upstream regulators and downstream targets. In neural tissues, *rbm38* expression is regulated by the proneural genes *XNgnr1* and *XNeuroD* (Boy et al., 2003) while its expression in mesoderm is regulated by *ntl* (Garnett et al., 2009; Shestopalov et al., 2012). Additionally, studies have demonstrated that human *Rbm38* is capable of inducing p21-dependent and -independent cell cycle arrest as well as promoting differentiation (Shu et al., 2006; Miyamoto et al., 2009; Cho et al., 2012). Based on these studies, Rbm38 may be induced in multiple cell types where it has a permissive role in promoting differentiation; by negatively regulating cell proliferation, Rbm38 establishes an environment in which tissue-specific transcription factors can then induce the expression of genes responsible for terminal differentiation. Interestingly, Xseb4R stabilizes the expression of *VegT* mRNA, the *Xenopus spt* ortholog, which is expressed maternally and required for establishing the endoderm and mesoderm germ layers. If the same is true in zebrafish, *rbm38* and *spt* may form a negative feedback loop that functions in the differentiation of paraxial mesoderm. Alternatively, if the *rbm38* function in endoderm development is conserved between *Xenopus* and zebrafish, *rbm38* may act to stabilize the transcript encoding *eomes*, the T-box transcription factor which functions upstream of endoderm specification in zebrafish.

rbm38 MO does not reveal definitive role of Rbm38 in zebrafish mesoderm development

To study the role of *rbm38* during zebrafish mesoderm development, I designed a MO to block proper splicing of the *rbm38* transcript in order to knock down Rbm38 expression. The median fin fold and blood defects were realistic phenotypes to expect considering the expression of *rbm38* in the ventral margin and blood island. Though initially promising, the median fin fold defects were not restricted to the *rbm38*-depleted embryos and the blood circulation defects were not observed in morphants in all three experiments performed (Fig 4.5 C). Given the well-documented role of Ntl and Spt in patterning the left-right axis of the zebrafish embryo, the left-sided orientation of the liver was also assayed to determine if *rbm38* functions downstream of *ntl* and *spt* in left-right patterning. There was no significant difference between the frequency of left-sided livers

in *rbm38* MO-injected embryos compared to control-injected embryos. Surprisingly, the data collected while scoring median fin-fold and left-right patterning defects showed that control-injected embryos exhibited defects at a similar frequency to *rbm38* MO-injected embryos. While they could be the result of an unknown factor in the genetic background of the wildtype embryos injected, they are more likely to be artifacts of the injection process. For instance, the control solution used for injections as well as dilution of the MO may have been contaminated. Additionally, the size or placement of the needle, as well as the volume of solution injected, may have disrupted localization of cellular components required later in establishing left-right asymmetry. Repeating the experiments would be the best way to determine if the defects were caused by solutions used or the actual injection process.

One caveat to using MOs for loss-of-function studies is that they may not result in a complete knock down of expression from the targeted transcript. By using splice-blocking morpholinos, the efficiency of the MO can be assayed by primers designed to amplify the aberrant transcript produced when splicing at the targeted exon-intron junction is blocked. For this reason, primers were designed to flank the targeted region of the *rbm38* transcript, as well as the sequences predicted to result from off-target splicing events. The efficiency of the *rbm38* MO needs to be tested before proceeding with additional injections. RNA was extracted from *rbm38* MO-injected embryos but has not been processed or sequenced to determine if the splicing of *rbm38* is significantly altered in morphants displaying defects when compared to control embryos.

itgb5 expression in the presumptive mesoderm prior to 24 hpf supports its potential role in migratory events during zebrafish development

Integrins are important for somite formation and somite boundary morphology in vertebrates. Zebrafish mutants for *integrin alpha 5* (*itga5*) have disrupted or absent somite boundaries in the first 6-8 anterior somites, and altered somite morphology in the somites that form (Julich et al., 2005). Similarly, knocking down *Itga5* in *Xenopus* embryos disrupts somite boundary formation (Kragtorp and Miller, 2007). Zebrafish *itgb5* is expressed maternally and in the head, suggesting that its role in development is not restricted to the mesoderm. However, its expression in the margin and hypoblast during gastrulation, as well as the severe decrease of its expression in these regions in the *spt*;*ntl* double mutant (Fig 4.3), is consistent with its regulation by mesoderm-inducing factors Ntl and Spt (Garnett et al., 2009; Morley et al., 2009). β5 interacts with αV to form integrin αVβ5 (reviewed by Takada et al., 2007). *itgaV* is expressed in and required for the migration of the dorsal forerunner cells, the precursor to Kupffer's vesicle (Ablooglu et al., 2010). Although this particular migratory event is mediated through dimerization with the β1 subunit, β5 may still mediate migratory or cell-cell interactions occurring during gastrulation. β5 may also function in αV integrin-mediated formation of blood vessels (Bader et al., 1998). An MO targeting the exon2-intron2 junction of *itgb5* was ordered but remains to be tested (Fig 4.4 D).

Figure 4.1

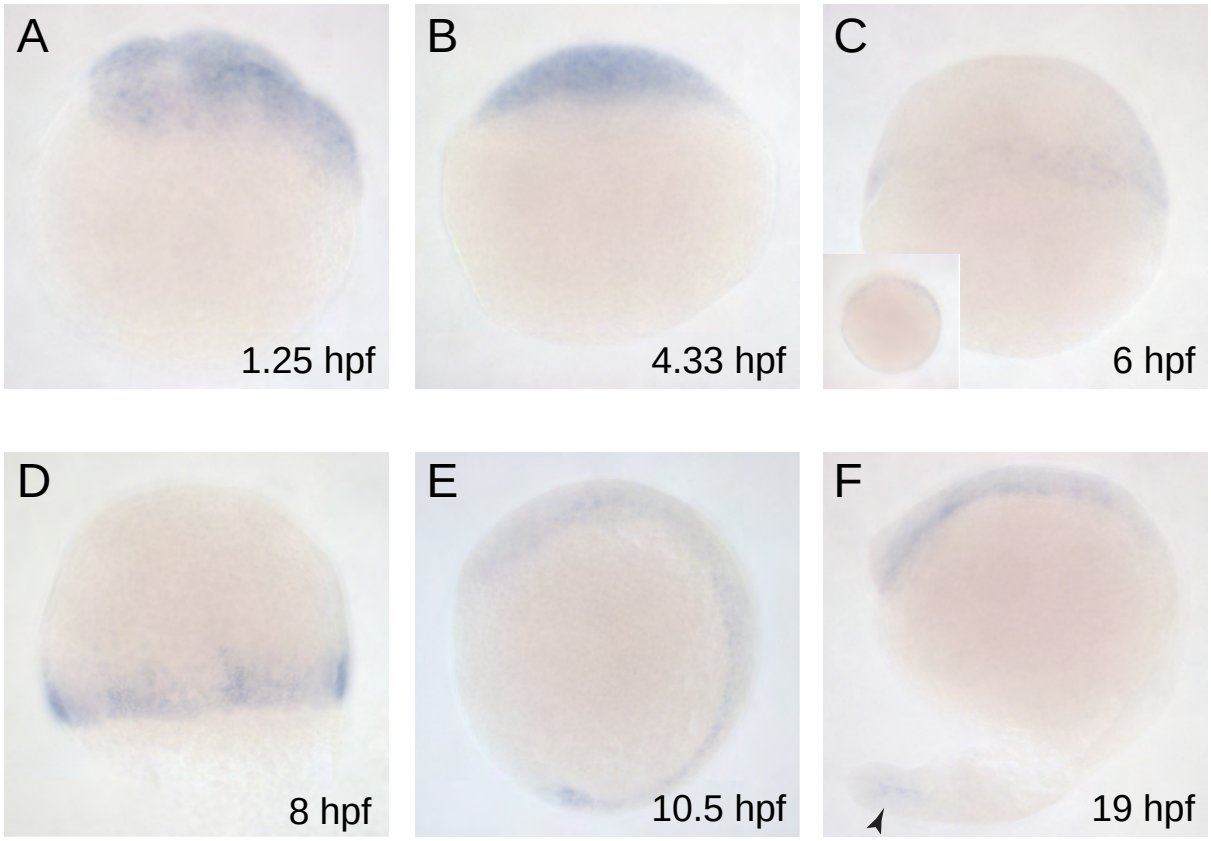

Figure 4.1 ***itgb5*** **expression during the first day of zebrafish development**

Expression of i*tgb5* in zebrafish wildtype embryo at (A) 8-16 cell, (B) dome stage, (C) shield stage (50% epiboly), (D) mid-gastrulation (70-80% epiboly), (E) 1-2 somite stage, and (F) 20-22 somite stage. The arrowhead in (F) marks the *itgb5* expression in the PSM. The hours post fertilization (hpf) is indicated in the bottom right of each panel. Zygotic transcription begins at 2.75 hpf. Animal pole is to the top (A-D). Anterior is to the top (E and F). (D) is a dorsal view. Dorsal is to the right (C, E, and F). The inset in (C) is a view from the animal pole with the dorsal side positioned to the top.

Figure 4.2

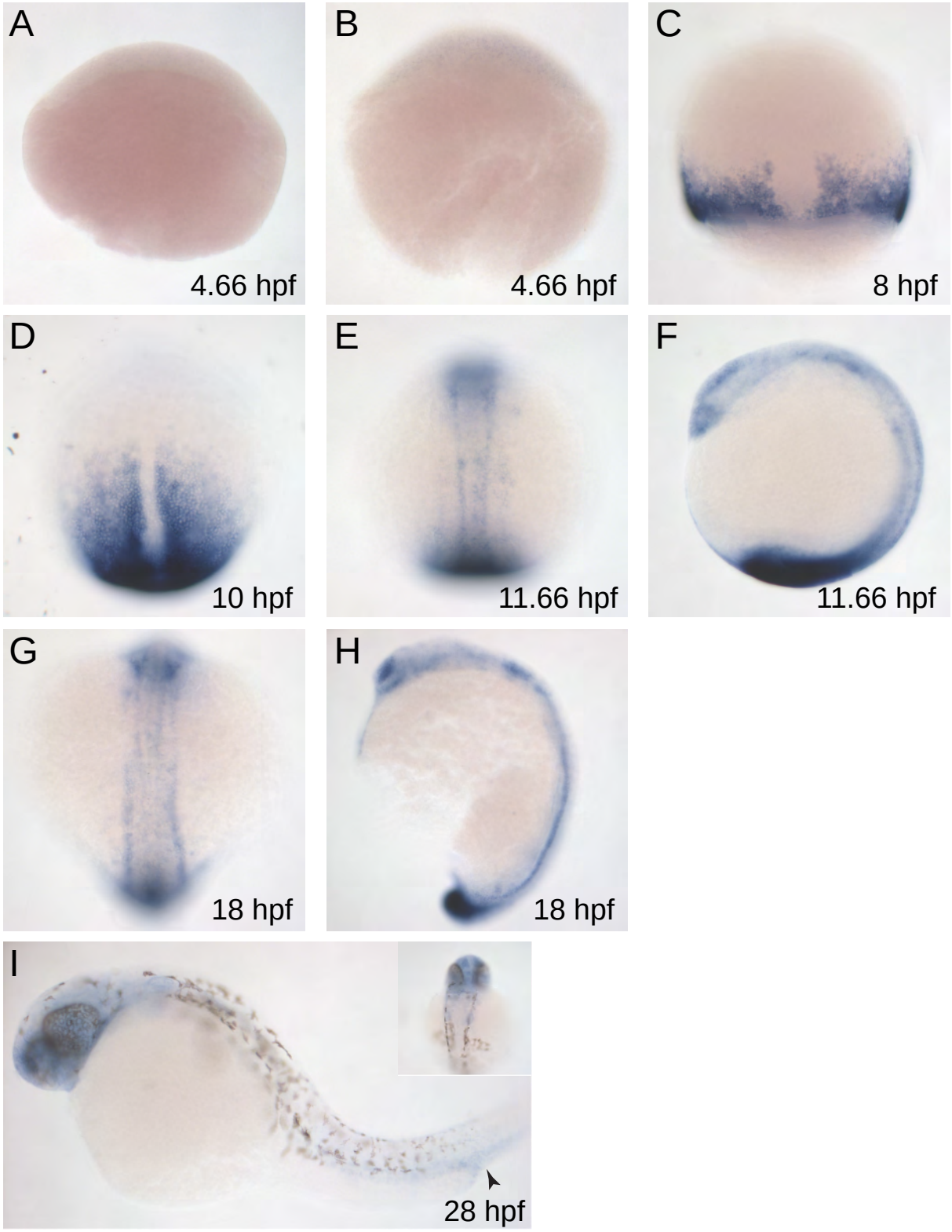
A
4.66 hpf
B
4.66 hpf
C
8 hpf
D
10 hpf
E
11.66 hpf
F
11.66 hpf
G
18 hpf
H
18 hpf
I
28 hpf

Figure 4.2 ***rbm38* expression during the first day of zebrafish development**

Expression of *rbm38* in zebrafish embryo at (A,B) 30% epiboly, (C) mid-gastrulation, (D) bud stage (100% epiboly), (E, F) 4-5 somites, (G,H) 17-18 somites, and (I) 28hpf. The arrowhead in (I) marks the *rbm38* expression in the blood island. The hpf is indicated in the bottom right of each panel. Animal pole is to the top in (A-C). Anterior is to the top in (D-H), and to the left in (I). C, D, E and G are dorsal views. F, H and I are lateral views with dorsal to the right (F and H) or top (I). The inset in (I) is a dorsal view of the head.

Figure 4.3

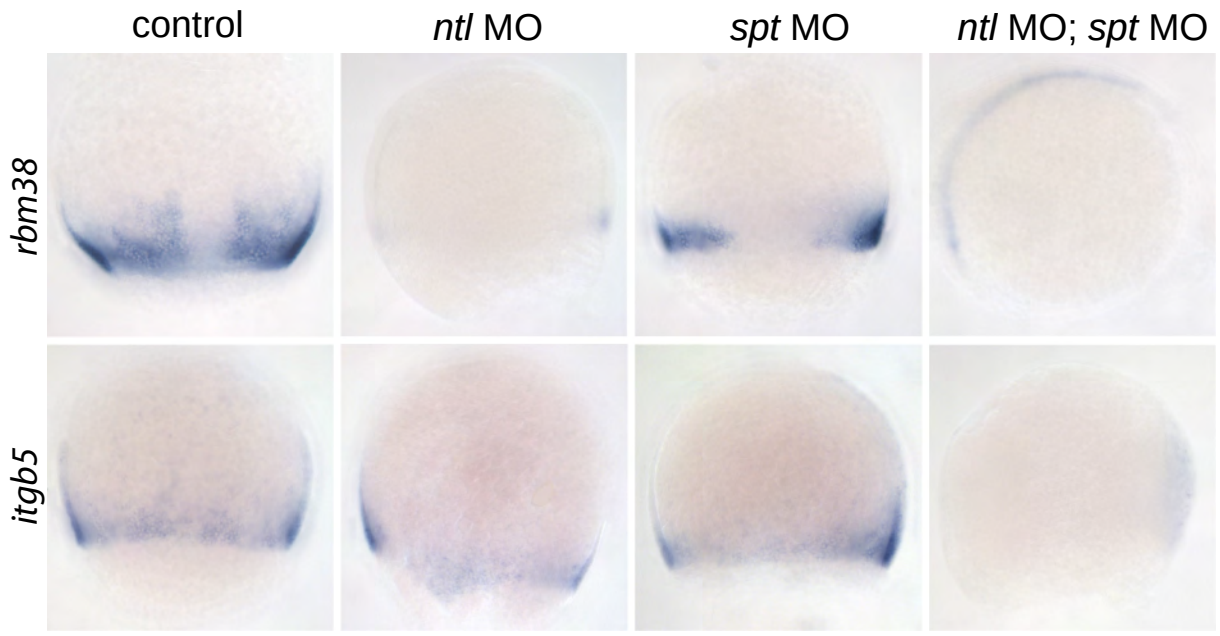

Figure 4.3 **Ntl and Spt are required for expression of *itgb5* and *rbm38***

itgb5 is a class III redundantly-regulated target. *itgb5* expression is unaffected in *ntl* MO- and *spt* MO-injected embryos, but margin expression is absent in embryos injected with both *ntl* MO and *spt* MO. *rbm38* is a class II Ntl-regulated target. *rbm38* expression in the margin is decreased in *ntl* MO-injected and *ntl* MO*;spt* MO-injected embryos but is relatively unaffected in *spt* MO-injected embryos. The altered *rbm38* expression in *spt* MO injected in the dorsal-lateral margin is due to defective dorsal convergence of cells in *spt*-depleted embryos. Embryos were fixed at 70-80% epiboly.

Figure 4.4

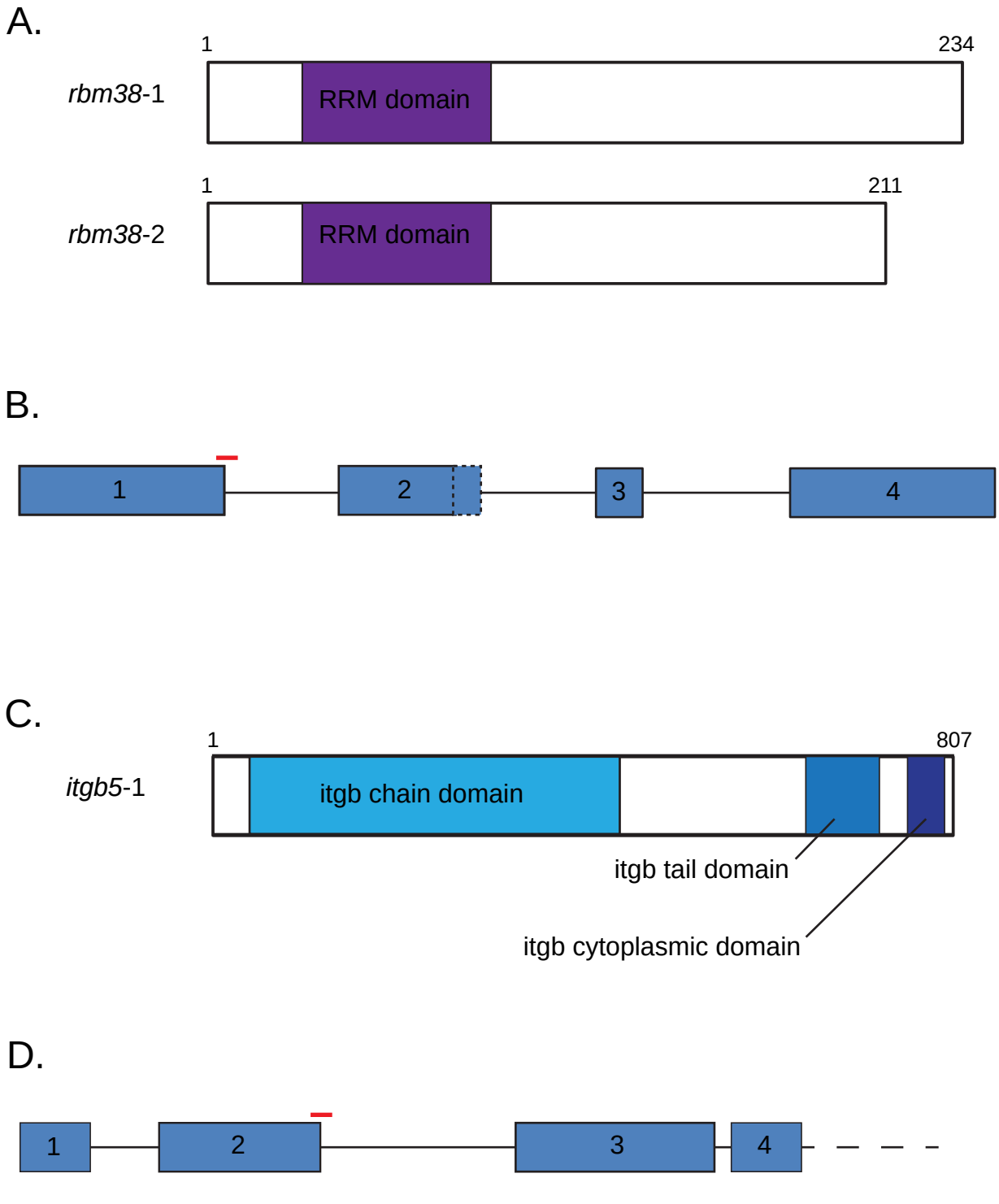
A.
1
234
rbm38-1
RRM domain
1
211
rbm38-2
RRM domain
B.
1
2
3
4
C.
1
807
itgb1-1
itgb chain domain
itgb tail domain
itgb cytoplasmic domain
D.
1
2
3
4

Figure 4.4 **Amino acid sequence and morpholino targets for *rbm38* and *itgb5***

(A) Amino acid sequence of the two *rbm38* transcripts. *rbm38*-1 and *rbm38*-2 are identical through the first half of the second exon, which includes the RNA-binding RRM domain. (B) A diagram of the *rbm38* mRNA transcript. The dashed region in exon 2 is only present in the *rbm38*-2 transcript. The red line represents the *rbm38* MO over its target sequence at the exon1-intron1 junction. (C) The amino acid sequence for the longer *itgb5*-1 transcript. The shorter *itgb5*-2 transcript is identical to the longer transcript until it truncates at 138 amino acids. (D) A diagram depicting the first four exons of *itgb5.* The red line represents the *itgb5* MO where it targets the exon2-intron 2 junction.

Figure 4.5

C.

	n	WT	bl. circ.	MFF	scooped tail
control	27	70%		30%	
3-5ng	65	63%	6%	31%	
9-15ng	147	67%	11%	30%	35%
15-20ng	37	65%	8%	35%	

D.

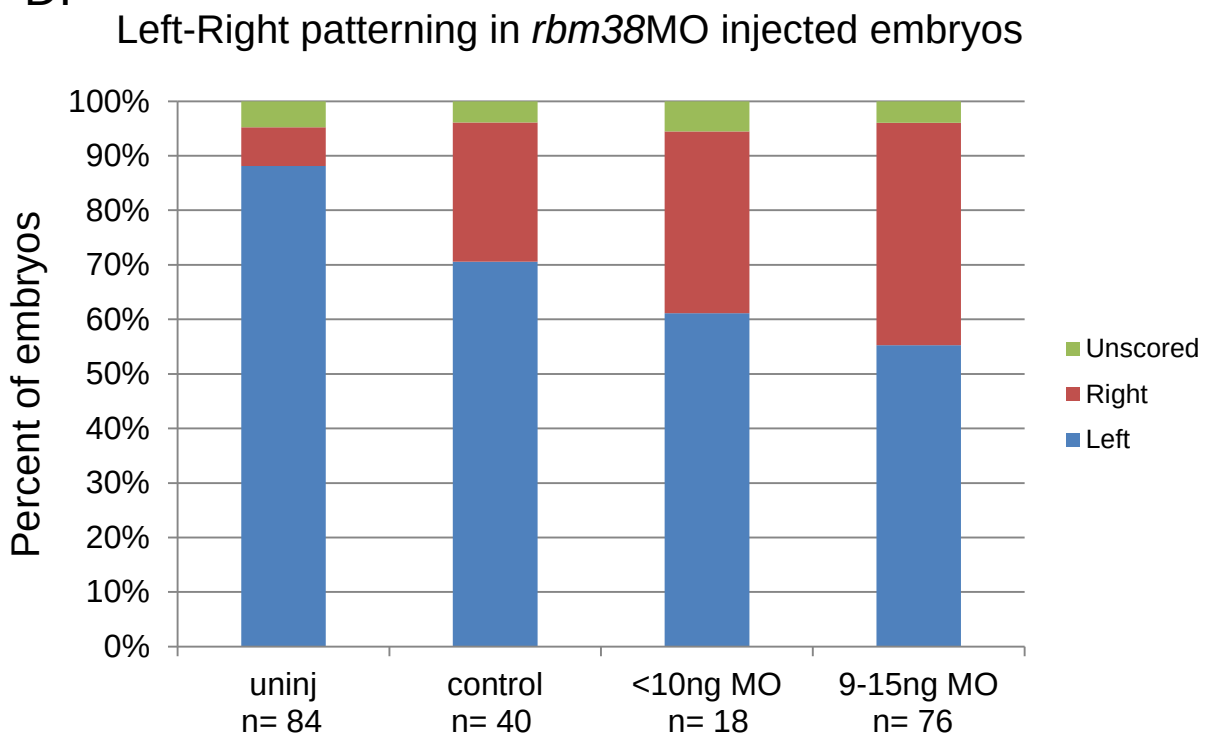

Figure 4.5 ***rbm38* loss-of-function results**

Embryos injected with 10-15ng of *rbm38* MO displaying wild-type median fin fold (A) and a loss of median fin fold (B). The asterisks mark the end of the yolk extension and beginning of the fin fold. (C) A table showing the amount of 0.2M KCl control solution or *rbm38 MO* injected and the frequency of observed phenotypes. WT = wildtype morphology, bl. circ = blood circulation defects, MFF = median fin fold defects. (D) A graph representing the frequency of left- or right-sided livers in control- or *rbm38* MO-injected embryos. There is a significant difference between uninjected and control-injected embryos (p=0.003), but not between control-injected and the *rbm38* MO-injected embryos (<10ng p=0.492; 9-15ng p=0.072)

Chapter 5: Future directions and closing remarks

Future directions

Gene Regulatory Network for tailbud to PSM transition

Loss of *msgn1* function enhances the *spt* phenotype such that *spt*;*msgn1* double mutants do not form somites because mesoderm progenitors fail to migrate out of the tailbud. Row et al. (2011) reported that unlike the wildtype cells, *spt*$^{-/-}$ cells fail to down-regulate cell-cell contacts and protrusions prior to migrating from the tailbud. They were able to partially rescue the cell extension activity and more caudal trunk somites with a pulse of *spt* expression. However, they were unable to identify the gene(s) repsponsible for this Spt-dependent behavior. Identifying Msgn1 targets would enable us to focus on genes regulated by Msgn1, Spt, and possibly Nodal signaling, that will uncover the molecular mechanism employed as cells transition from the tailbud to the PSM. Since development is negligibly affected by loss of *msgn1*, presumably because *spt* is sufficient to regulate expression of mutual targets, a ChIP-seq approach to identifying Msgn1 targets may prove to be more effective than methods which rely on changes in transcript abundance. For example, if a gene required for the tailbud-PSM transition is co-regulated by Spt and Msgn1, the change in its transcript levels in a Msgn1 mutant may be negligible due to the continued function of Spt. As a result, this gene would show no change in expression in a Msgn1 mutant when compared to its expression in a wildtype embryo and thus would not be detected as a Msgn1 target. Using the ChIP-seq approach, as long as the promoter of the gene is bound by Msgn1, following the sequencing of DNA fragments immunoprecipitated with the Msgn1 transcription factor, the gene would be identified as a potential target of Msgn1.

Progress toward obtaining a *tbx6l* mutant for functional analysis of Tbx6l

The *tbx6l* morphant data to date points toward a role for *tbx6l* in posterior mesoderm development. However, without validating the loss of Tbx6l expression, it is difficult to make more than a general speculation of the role of *tbx6l* due to the range of defects observed in *tbx6l* morphants. I suspect the truncations and dorsalization defects observed are caused by depleting Tbx6l but cannot rule out the possibility that they result from off-target effects of the *tbx6l* MO. These issues as well as the *tbx6l* loss-of-function phenotype can be addressed through the generation of a true *tbx6l* null mutant. We are working in collaboration with David Grunwald to characterize a *tbx6l* mutant. In addition to verifying the *tbx6l* MO results, a *tbx6l* mutant would prove extremely valuable in dissecting the genetic interactions between *tbx6l* and the T-box genes *ntl* and *spt* through generation and characterization of double mutant lines. If one of the roles of *tbx6l* is to inhibit dorsal mesoderm, one might predict that the patterning defects in a *ntl*;*tbx6l* double mutant would be less severe than the *tbx6l* single mutant. Additionally, if *tbx6l* does exhibit functional overlap with *spt* in tail mesoderm as my experiments suggest, I would expect the *spt*;*tbx6l* double mutant to be reminiscent of the *spt*;*msgn1* phenotype. While T-box genes do share overlapping expression patterns and functions in the specification and patterning of the trunk and tail mesoderm, they have also been shown to perform distinct roles from one another. In addition to shedding light on the actual function of *tbx6l* during zebrafish development, characterization of the *tbx6l*

mutant will allow for its unique functions, if they exist, to be distinguished from those shared by other T-box genes.

Using a *tbx6l* over-expression construct and Tbx6l antibody to detect loss of Tbx6l following *tbx6l* MO-mediated knockdown

I have been unable to validate the loss of endogenous Tbx6l protein in *tbx6l* MO-injected embryos. Optimizing the conditions for detection of the endogenous Tbx6l protein using the Tbx6l antibody will allow us to evaluate the level of protein knockdown observed in the more severe *tbx6l* morphants. The Tbx6l antibody we have can detect very high levels of Tbx6l via immunohistochemistry assays and can detect a purified recombinant Tbx6-GST protein on a western blot. However, both protocols need to be optimized for detection of endogenous Tbx6l protein.

I have used the *hsp70l:tbx6l-2A-GFP* over-expression construct to demonstrate that the *tbx6l* MO was indeed targeting and inhibiting translation from the *tbx6l* transcript. Embryos collected from a stable line of transgenic *hsp70l:tbx6l-2A-GFP* fish can be injected with *tbx6l* MO and scored for loss of *tbx6l* expression based on the amount of GFP fluorescence. In this way, I can demonstrate whether the truncations and more severe dorsalizations in *tbx6l* morphants reported here result from less and more complete knock down of Tbx6l*,* respectively. Additionally, a *tbx6l* over-expression construct can be used to perform rescue experiments in *tbx6l* MO injected embryos. While the construct used in experiments above contains the *tbx6l* MO target sequence, I have also generated two heat-inducible *tbx6l* over-expression constructs which lack the *tbx6l* MO target sequence (Fig 3.4 B).

Over-expressing *tbx6l* in *ntl* and *spt* mutants to distinguish the role of Tbx6l in mediating trunk and tail development downstream of *spt* and *ntl*

The results in this thesis have focused primarily on demonstrating the role of Tbx6l based on loss-of-function phenotypes. However, the *hsp70l:tbx6l-2A-GFP* construct can be used to address the role of *tbx6l* as it functions downstream of *ntl* and *spt*. By inducing *tbx6l* expression in *spt* or *ntl* mutant embryos prior to trunk or tail somitogenesis we can address the extent to which the *spt* and *ntl* mutant defects are the result of decreased *tbx6l* expression. If Tbx6l is capable of replacing Spt in the trunk mesoderm, one might expect that over-expressing *tbx6l* during gastrulation may rescue migration of trunk mesodermal precursors, leading to partial rescue of trunk somite formation in *spt* single mutants. Based on the antagonistic relationship shown to exist between Ntl and Tbx6l (Goering et al., 2003), in addition to the fact that the *ntl* mutant appears to result from decreased proliferation and thus premature exhaustion of the mesodermal progenitor pool, it is more difficult to predict the result of over-expressing *tbx6l* in a *ntl* mutant. If Tbx6l function in tail development requires a Ntl-dependent mesodermal progenitor population, I would expect over-expression of *tbx6l* induced during tail segmentation stages to have no effect in a *ntl* mutant. Additionally, based on the *tbx6l* over-expression in wildtype embryos reported by Goering et al. (2003), one could predict that in the absence of Ntl, Tbx6l may be capable of binding and inhibiting expression from additional promoters, resulting in more severe truncations than those exhibited by *ntl* mutants or embryos injected with *tbx6l* mRNA (Halpern et al., 1993; Goering et al., 2003).

Interaction of Ntl and Spt Targets

Tbx6l is a direct target of Ntl and Spt, but as a member of the same T-box family of transcription factors it may also be capable of binding and regulating genes identified as Ntl and Spt targets. Using F1 embryos carrying the *hsp70l:tbx6l-2A-GFP* transgene we can over-express *tbx6l* during mesoderm development, collect RNA from transgenic and wildtype embryos, and compare differential expression of genes by RNA-seq or microarray analysis. This dataset can then be compared to previous lists of genes reported to be regulated or bound by Ntl and Spt. Identification of genes similarly regulated by *tbx6l*, *spt*, and *ntl* will give us insight into which processes are regulated by which T-box genes during mesoderm development.

When comparing *msgn1* and *spt* single mutant phenotypes to the *spt;msgn1* double mutant phenotype, it seems likely that Msgn1 shares a set of transcriptional targets with Spt, the main mediator of the switch from progenitor to PSM identity. Preliminary experiments depleting Tbx6l in a *spt* mutant background indicated that Tbx6l-deficient *spt* mutants may be similar in morphology to *spt*;*msgn1* mutants. If these results are reproducible, then the next question is whether or not *tbx6l* and *msgn1* interact with *spt* in the same pathway to regulate mesoderm progenitor maturation. This question can be addressed by a *msgn1*;*tbx6l* double mutant. If the two transcription factors converge on the same targets or pathways with Spt as cells migrate from the tailbud to the PSM, I expect loss of *tbx6l* function in a *msgn1* background to enhance the *msgn1* phenotype similar to what I observe in the *msgn1*-enhanced ($msgn1^{-/-}$; $spt^{+/-}$) phenotype.

Using splice-blocking MOs to study the developmental function of *rbm38* and *itgb5*

Although *Rbm38* has been reported to induce myogenesis in cell culture (Miyamoto et al., 2009), there have been few reports to indicate a role for *rbm38* or *itgb5* in early mesoderm development and patterning. *rbm38* and *itgb5* were reported to be likely targets of Ntl and Spt and are expressed in overlapping regions with the T-box genes during gastrulation and somitogenesis stages (Garnett et al., 2009). Splice-blocking morpholinos targeting *rbm38* and *itgb5* were ordered to deplete gene function and assess the role of each in the developing mesoderm. Preliminary results from the *rbm38* MO were inconclusive regarding its function. The deficit in median fin fold observed in *rbm38* morphants was a plausible phenotype to expect after depleting expression of a gene expressed in the tailbud of developing embryos, although it may not be consistent with loss-of-function phentoypes reported for *rbm38* in *Xenopus*. Until the experiment can be repeated with reliable controls, I can neither accept nor negate the requirement of *rbm38* for development of the median fin fold. However, the blood circulation defects observed were not present in control embryos and a requirement for *rbm38* in blood development would be supported by its expression in the blood island at 28 hpf (Fig 4.2 I). The *itgb5* MO has not yet been tested. Without the existence of a *rbm38* or *itgb5* mutant for comparison, the efficiency of both the *rbm38* MO and *itgb5* MO needs to be validated in knocking down expression by analyzing the splicing pattern generated in MO-injected embryos. If injecting the MO results in depletion of the wildtype transcript, either due to an increased abundance of an aberrant transcript or

nonsense-mediated decay, then I can be more confident in the characterization of *rbm38* and *itgb5* loss-of-function phenotypes.

Closing remarks

Ntl and Spt are transcription factors that play a significant role in formation of the posterior body mesoderm through regulation of their many gene targets (Amacher et al., 2002). While they have distinct roles in development as revealed by their respective single mutant phenotypes, the *spt*;*ntl* double mutant phenotype highlights the shared role of the T-box genes in establishing mesodermal fate. This is consistent with their overlapping expression in a few rows of cells in the margin. For my thesis, I was interested in identifying and characterizing the role of Ntl/Spt targets mediating the shared functions of Spt and Ntl. These genes would presumably function in paraxial mesoderm development over the entire body axis as opposed to being required in the trunk vs tail mesoderm development. To this end, I used mutant and antisense oligonucleotide methods to knock down expression of transcription factors Msgn1 and Tbx6l, respectively, the genes most highly down-regulated in *spt*;*ntl* double mutants (Garnett et al., 2009). I have shown that Msgn1 is required for the normal progress of cells from the tailbud to the PSM, and that loss of *msgn1* function in a *spt* mutant background results in a failure to specify both trunk and tail paraxial mesoderm. For this reason, the *spt*;*msgn1* double mutant will be a useful tool for future dissection of the mechanism controlling migration of cells out of the tailbud. I have also demonstrated that Tbx6l is required for early dorsal-ventral patterning in gastrula stage embryos in addition to being required for posterior mesoderm formation. My work to date clearly demonstrates that the role of Tbx6l during trunk and tail mesoderm development is distinct from that of Spt and Ntl, although it may share an overlapping set of targets. Additionally, these results show that, aside from being required for paraxial mesoderm development, Tbx6l function is not conserved with mouse and *Xenopus* Tbx6, supporting the paralogous relationship between the proteins.

References

Ablooglu, A. J., Tkachenko, E., Kang, J. and Shattil, S. J. (2010). Integrin alphaV is Necessary for Gastrulation Movements that Regulate Vertebrate Body Asymmetry. *Development* **137,** 3449-3458.

Agathon, A., Thisse, C. and Thisse, B. (2003). The Molecular Nature of the Zebrafish Tail Organizer. *Nature* **424,** 448-452.

Amacher, S. L., Draper, B. W., Summers, B. R. and Kimmel, C. B. (2002). The Zebrafish T-Box Genes no Tail and Spadetail are Required for Development of Trunk and Tail Mesoderm and Medial Floor Plate. *Development* **129,** 3311-3323.

Amack, J. D., Wang, X. and Yost, H. J. (2007). Two T-Box Genes Play Independent and Cooperative Roles to Regulate Morphogenesis of Ciliated Kupffer's Vesicle in Zebrafish. *Dev. Biol.* **310,** 196-210.

Bader, B. L., Rayburn, H., Crowley, D. and Hynes, R. O. (1998). Extensive Vasculogenesis, Angiogenesis, and Organogenesis Precede Lethality in Mice Lacking all Alpha v Integrins. *Cell* **95,** 507-519.

Beddington, R. S. (1994). Induction of a Second Neural Axis by the Mouse Node. *Development* **120,** 613-620.

Bjornson, C. R., Griffin, K. J., Farr, G. H.,3rd, Terashima, A., Himeda, C., Kikuchi, Y. and Kimelman, D. (2005). Eomesodermin is a Localized Maternal Determinant Required for Endoderm Induction in Zebrafish. *Dev. Cell.* **9,** 523-533.

Boy, S., Souopgui, J., Amato, M. A., Wegnez, M., Pieler, T. and Perron, M. (2004). XSEB4R, a Novel RNA-Binding Protein Involved in Retinal Cell Differentiation Downstream of bHLH Proneural Genes. *Development* **131,** 851-862.

Buchberger, A., Bonneick, S. and Arnold, H. (2000). Expression of the Novel Basic-Helix-Loop-Helix Transcription Factor cMespo in Presomitic Mesoderm of Chicken Embryos. *Mech. Dev.* **97,** 223-226.

Cade, L., Reyon, D., Hwang, W. Y., Tsai, S. Q., Patel, S., Khayter, C., Joung, J. K., Sander, J. D., Peterson, R. T. and Yeh, J. R. (2012). Highly Efficient Generation of Heritable Zebrafish Gene Mutations using Homo- and Heterodimeric TALENs. *Nucleic Acids Res.*

Casey, E. S., O'Reilly, M. A., Conlon, F. L. and Smith, J. C. (1998). The T-Box Transcription Factor Brachyury Regulates Expression of eFGF through Binding to a Non-Palindromic Response Element. *Development* **125,** 3887-3894.

Casey, E. S., Tada, M., Fairclough, L., Wylie, C. C., Heasman, J. and Smith, J. C. (1999). Bix4 is Activated Directly by VegT and Mediates Endoderm Formation in Xenopus Development. *Development* **126,** 4193-4200.

Chalamalasetty, R. B., Dunty, W. C.,Jr, Biris, K. K., Ajima, R., Iacovino, M., Beisaw, A., Feigenbaum, L., Chapman, D. L., Yoon, J. K., Kyba, M. et al. (2011). The Wnt3a/beta-Catenin Target Gene Mesogenin1 Controls the Segmentation Clock by Activating a Notch Signalling Program. *Nat. Commun.* **2,** 390.

Chapman, D. L., Agulnik, I., Hancock, S., Silver, L. M. and Papaioannou, V. E. (1996). Tbx6, a Mouse T-Box Gene Implicated in Paraxial Mesoderm Formation at Gastrulation. *Dev. Biol.* **180,** 534-542.
Chapman, D. L., Cooper-Morgan, A., Harrelson, Z. and Papaioannou, V. E. (2003). Critical Role for Tbx6 in Mesoderm Specification in the Mouse Embryo. *Mech. Dev.* **120,** 837-847.
Chapman, D. L. and Papaioannou, V. E. (1998). Three Neural Tubes in Mouse Embryos with Mutations in the T-Box Gene Tbx6. *Nature* **391,** 695-697.
Chen, X., Liu, G., Zhu, J., Jiang, J., Nozell, S. and Willis, A. (2003). Isolation and Characterization of Fourteen Novel Putative and Nine Known Target Genes of the p53 Family. *Cancer. Biol. Ther.* **2,** 55-62.
Cho, K. W., Blumberg, B., Steinbeisser, H. and De Robertis, E. M. (1991). Molecular Nature of Spemann's Organizer: The Role of the Xenopus Homeobox Gene Goosecoid. *Cell* **67,** 1111-1120.
Cho, S. J., Jung, Y. S., Zhang, J. and Chen, X. (2012). The RNA-Binding Protein RNPC1 Stabilizes the mRNA Encoding the RNA-Binding Protein HuR and Cooperates with HuR to Suppress Cell Proliferation. *J. Biol. Chem.* **287,** 14535-14544.
Clery, A., Blatter, M. and Allain, F. H. (2008). RNA Recognition Motifs: Boring? Not quite. *Curr. Opin. Struct. Biol.* **18,** 290-298.
Conlon, F. L., Fairclough, L., Price, B. M., Casey, E. S. and Smith, J. C. (2001). Determinants of T Box Protein Specificity. *Development* **128,** 3749-3758.
Conlon, F. L., Sedgwick, S. G., Weston, K. M. and Smith, J. C. (1996). Inhibition of Xbra Transcription Activation Causes Defects in Mesodermal Patterning and Reveals Autoregulation of Xbra in Dorsal Mesoderm. *Development* **122,** 2427-2435.
Conlon, F. L. and Smith, J. C. (1999). Interference with Brachyury Function Inhibits Convergent Extension, Causes Apoptosis, and Reveals Separate Requirements in the FGF and Activin Signalling Pathways. *Dev. Biol.* **213,** 85-100.
Corbo, J. C., Levine, M. and Zeller, R. W. (1997). Characterization of a Notochord-Specific Enhancer from the Brachyury Promoter Region of the Ascidian, Ciona Intestinalis. *Development* **124,** 589-602.
Cunliffe, V. and Smith, J. C. (1992). Ectopic Mesoderm Formation in Xenopus Embryos Caused by Widespread Expression of a Brachyury Homologue. *Nature* **358,** 427-430.
De Arcangelis, A. and Georges-Labouesse, E. (2000). Integrin and ECM Functions: Roles in Vertebrate Development. *Trends Genet.* **16,** 389-395.
Donnelly, M. L., Luke, G., Mehrotra, A., Li, X., Hughes, L. E., Gani, D. and Ryan, M. D. (2001). Analysis of the Aphthovirus 2A/2B Polyprotein 'Cleavage' Mechanism Indicates Not a Proteolytic Reaction, but a Novel Translational Effect: A Putative Ribosomal 'Skip'. *J. Gen. Virol.* **82,** 1013-1025.
Doyon, Y., McCammon, J. M., Miller, J. C., Faraji, F., Ngo, C., Katibah, G. E., Amora, R., Hocking, T. D., Zhang, L., Rebar, E. J. et al. (2008). Heritable Targeted Gene Disruption in Zebrafish using Designed Zinc-Finger Nucleases. *Nat. Biotechnol.* **26,** 702-708.

Draper, B. W., McCallum, C. M., Stout, J. L., Slade, A. J. and Moens, C. B. (2004). A High-Throughput Method for Identifying N-Ethyl-N-Nitrosourea (ENU)-Induced Point Mutations in Zebrafish. *Methods Cell Biol.* **77,** 91-112.
Dreyfuss, G., Kim, V. N. and Kataoka, N. (2002). Messenger-RNA-Binding Proteins and the Messages they Carry. *Nat. Rev. Mol. Cell Biol.* **3,** 195-205.
Du, S., Draper, B. W., Mione, M., Moens, C. B. and Bruce, A. (2012). Differential Regulation of Epiboly Initiation and Progression by Zebrafish Eomesodermin A. *Dev. Biol.* **362,** 11-23.
Dubrulle, J. and Pourquie, O. (2004). Coupling Segmentation to Axis Formation. *Development* **131,** 5783-5793.
Dunty, W. C.,Jr, Biris, K. K., Chalamalasetty, R. B., Taketo, M. M., Lewandoski, M. and Yamaguchi, T. P. (2008). Wnt3a/beta-Catenin Signaling Controls Posterior Body Development by Coordinating Mesoderm Formation and Segmentation. *Development* **135,** 85-94.
Eckner, R., Ewen, M. E., Newsome, D., Gerdes, M., DeCaprio, J. A., Lawrence, J. B. and Livingston, D. M. (1994). Molecular Cloning and Functional Analysis of the Adenovirus E1A-Associated 300-kD Protein (p300) Reveals a Protein with Properties of a Transcriptional Adaptor. *Genes Dev.* **8,** 869-884.
Essner, J. J., Amack, J. D., Nyholm, M. K., Harris, E. B. and Yost, H. J. (2005). Kupffer's Vesicle is a Ciliated Organ of Asymmetry in the Zebrafish Embryo that Initiates Left-Right Development of the Brain, Heart and Gut. *Development* **132,** 1247-1260.
Feldman, B., Gates, M. A., Egan, E. S., Dougan, S. T., Rennebeck, G., Sirotkin, H. I., Schier, A. F. and Talbot, W. S. (1998). Zebrafish Organizer Development and Germ-Layer Formation Require Nodal-Related Signals. *Nature* **395,** 181-185.
Field, H. A., Ober, E. A., Roeser, T. and Stainier, D. Y. (2003). Formation of the Digestive System in Zebrafish. I. Liver Morphogenesis. *Dev. Biol.* **253,** 279-290.
Garnett, A. T., Han, T. M., Gilchrist, M. J., Smith, J. C., Eisen, M. B., Wardle, F. C. and Amacher, S. L. (2009). Identification of Direct T-Box Target Genes in the Developing Zebrafish Mesoderm. *Development* **136,** 749-760.
Gerhart, J. and Keller, R. (1986). Region-Specific Cell Activities in Amphibian Gastrulation. *Annu. Rev. Cell Biol.* **2,** 201-229.
Goering, L. M., Hoshijima, K., Hug, B., Bisgrove, B., Kispert, A. and Grunwald, D. J. (2003). An Interacting Network of T-Box Genes Directs Gene Expression and Fate in the Zebrafish Mesoderm. *Proc. Natl. Acad. Sci. U. S. A.* **100,** 9410-9415.
Griffin, K., Patient, R. and Holder, N. (1995). Analysis of FGF Function in Normal and no Tail Zebrafish Embryos Reveals Separate Mechanisms for Formation of the Trunk and the Tail. *Development* **121,** 2983-2994.
Griffin, K. J., Amacher, S. L., Kimmel, C. B. and Kimelman, D. (1998). Molecular Identification of Spadetail: Regulation of Zebrafish Trunk and Tail Mesoderm Formation by T-Box Genes. *Development* **125,** 3379-3388.

Griffin, K. J. and Kimelman, D. (2002). One-Eyed Pinhead and Spadetail are Essential for Heart and Somite Formation. *Nat. Cell Biol.* **4,** 821-825.
Gritsman, K., Zhang, J., Cheng, S., Heckscher, E., Talbot, W. S. and Schier, A. F. (1999). The EGF-CFC Protein One-Eyed Pinhead is Essential for Nodal Signaling. *Cell* **97,** 121-132.
Halpern, M. E., Ho, R. K., Walker, C. and Kimmel, C. B. (1993). Induction of Muscle Pioneers and Floor Plate is Distinguished by the Zebrafish no Tail Mutation. *Cell* **75,** 99-111.
Harada, Y., Yasuo, H. and Satoh, N. (1995). A Sea Urchin Homologue of the Chordate Brachyury (T) Gene is Expressed in the Secondary Mesenchyme Founder Cells. *Development* **121,** 2747-2754.
Hart, D. O., Raha, T., Lawson, N. D. and Green, M. R. (2007). Initiation of Zebrafish Haematopoiesis by the TATA-Box-Binding Protein-Related Factor Trf3. *Nature* **450,** 1082-1085.
Herrmann, B. G., Labeit, S., Poustka, A., King, T. R. and Lehrach, H. (1990). Cloning of the T Gene Required in Mesoderm Formation in the Mouse. *Nature* **343,** 617-622.
Hinits, Y., Williams, V. C., Sweetman, D., Donn, T. M., Ma, T. P., Moens, C. B. and Hughes, S. M. (2011). Defective Cranial Skeletal Development, Larval Lethality and Haploinsufficiency in Myod Mutant Zebrafish. *Dev. Biol.* **358,** 102-112.
Hitachi, K., Danno, H., Kondow, A., Ohnuma, K., Uchiyama, H., Ishiura, S., Kurisaki, A. and Asashima, M. (2008). Physical Interaction between Tbx6 and Mespb is Indispensable for the Activation of Bowline Expression during Xenopus Somitogenesis. *Biochem. Biophys. Res. Commun.* **372,** 607-612.
Ho, R. K. (1992). Cell Movements and Cell Fate during Zebrafish Gastrulation. *Dev. Suppl.*, 65-73.
Ho, R. K. and Kane, D. A. (1990). Cell-Autonomous Action of Zebrafish Spt-1 Mutation in Specific Mesodermal Precursors. *Nature* **348,** 728-730.
Holley, S. A. (2007). The Genetics and Embryology of Zebrafish Metamerism. *Dev. Dyn.* **236,** 1422-1449.
Horb, M. E. and Thomsen, G. H. (1997). A Vegetally Localized T-Box Transcription Factor in Xenopus Eggs Specifies Mesoderm and Endoderm and is Essential for Embryonic Mesoderm Formation. *Development* **124,** 1689-1698.
Hotta, K., Takahashi, H., Asakura, T., Saitoh, B., Takatori, N., Satou, Y. and Satoh, N. (2000). Characterization of Brachyury-Downstream Notochord Genes in the Ciona Intestinalis Embryo. *Dev. Biol.* **224,** 69-80.
Huang, P., Xiao, A., Zhou, M., Zhu, Z., Lin, S. and Zhang, B. (2011). Heritable Gene Targeting in Zebrafish using Customized TALENs. *Nat. Biotechnol.* **29,** 699-700.
Huang, X., Griffiths, M., Wu, J., Farese, R. V.,Jr and Sheppard, D. (2000). Normal Development, Wound Healing, and Adenovirus Susceptibility in beta5-Deficient Mice. *Mol. Cell. Biol.* **20,** 755-759.
Hug, B., Walter, V. and Grunwald, D. J. (1997). Tbx6, a Brachyury-Related Gene Expressed by Ventral Mesendodermal Precursors in the Zebrafish Embryo. *Dev. Biol.* **183,** 61-73.

Hwang, S. P., Tsou, M. F., Lin, Y. C. and Liu, C. H. (1997). The Zebrafish BMP4 Gene: Sequence Analysis and Expression Pattern during Embryonic Development. *DNA Cell Biol.* **16,** 1003-1011.
Isaacs, H. V., Pownall, M. E. and Slack, J. M. (1994). EFGF Regulates Xbra Expression during Xenopus Gastrulation. *EMBO J.* **13,** 4469-4481.
Jang, S. K., Krausslich, H. G., Nicklin, M. J., Duke, G. M., Palmenberg, A. C. and Wimmer, E. (1988). A Segment of the 5' Nontranslated Region of Encephalomyocarditis Virus RNA Directs Internal Entry of Ribosomes during in Vitro Translation. *J. Virol.* **62,** 2636-2643.
Joseph, E. M. and Cassetta, L. A. (1999). Mespo: A Novel Basic Helix-Loop-Helix Gene Expressed in the Presomitic Mesoderm and Posterior Tailbud of Xenopus Embryos. *Mech. Dev.* **82,** 191-194.
Julich, D., Geisler, R., Holley, S. A. and Tubingen 2000 Screen Consortium. (2005). Integrinalpha5 and delta/notch Signaling have Complementary Spatiotemporal Requirements during Zebrafish Somitogenesis. *Dev. Cell.* **8,** 575-586.
Kanki, J. P. and Ho, R. K. (1997). The Development of the Posterior Body in Zebrafish. *Development* **124,** 881-893.
Kawamura, A., Koshida, S., Hijikata, H., Ohbayashi, A., Kondoh, H. and Takada, S. (2005). Groucho-Associated Transcriptional Repressor ripply1 is Required for Proper Transition from the Presomitic Mesoderm to Somites. *Dev. Cell.* **9,** 735-744.
Kelly, G. M., Greenstein, P., Erezyilmaz, D. F. and Moon, R. T. (1995). Zebrafish wnt8 and wnt8b Share a Common Activity but are Involved in Distinct Developmental Pathways. *Development* **121,** 1787-1799.
Kimmel, C. B., Ballard, W. W., Kimmel, S. R., Ullmann, B. and Schilling, T. F. (1995). Stages of Embryonic Development of the Zebrafish. *Dev. Dyn.* **203,** 253-310.
Kimmel, C. B., Kane, D. A., Walker, C., Warga, R. M. and Rothman, M. B. (1989). A Mutation that Changes Cell Movement and Cell Fate in the Zebrafish Embryo. *Nature* **337,** 358-362.
Kishimoto, Y., Lee, K. H., Zon, L., Hammerschmidt, M. and Schulte-Merker, S. (1997). The Molecular Nature of Zebrafish Swirl: BMP2 Function is Essential during Early Dorsoventral Patterning. *Development* **124,** 4457-4466.
Kishimoto, Y., Lee, K. H., Zon, L., Hammerschmidt, M. and Schulte-Merker, S. (1997). The Molecular Nature of Zebrafish Swirl: BMP2 Function is Essential during Early Dorsoventral Patterning. *Development* **124,** 4457-4466.
Kispert, A. and Herrmann, B. G. (1993). The Brachyury Gene Encodes a Novel DNA Binding Protein. *EMBO J.* **12,** 3211-3220.
Kispert, A., Koschorz, B. and Herrmann, B. G. (1995). The T Protein Encoded by Brachyury is a Tissue-Specific Transcription Factor. *EMBO J.* **14,** 4763-4772.
Kispert, A., Ortner, H., Cooke, J. and Herrmann, B. G. (1995). The Chick Brachyury Gene: Developmental Expression Pattern and Response to Axial Induction by Localized Activin. *Dev. Biol.* **168,** 406-415.

Knezevic, V., De Santo, R. and Mackem, S. (1997). Two Novel Chick T-Box Genes Related to Mouse Brachyury are Expressed in Different, Non-Overlapping Mesodermal Domains during Gastrulation. *Development* **124,** 411-419.
Knezevic, V., De Santo, R. and Mackem, S. (1997). Two Novel Chick T-Box Genes Related to Mouse Brachyury are Expressed in Different, Non-Overlapping Mesodermal Domains during Gastrulation. *Development* **124,** 411-419.
Kragtorp, K. A. and Miller, J. R. (2007). Integrin alpha5 is Required for Somite Rotation and Boundary Formation in Xenopus. *Dev. Dyn.* **236,** 2713-2720.
Lekven, A. C., Thorpe, C. J., Waxman, J. S. and Moon, R. T. (2001). Zebrafish wnt8 Encodes Two wnt8 Proteins on a Bicistronic Transcript and is Required for Mesoderm and Neurectoderm Patterning. *Dev. Cell.* **1,** 103-114.
Li, H. Y., Bourdelas, A., Carron, C., Gomez, C., Boucaut, J. C. and Shi, D. L. (2006). FGF8, Wnt8 and Myf5 are Target Genes of Tbx6 during Anteroposterior Specification in Xenopus Embryo. *Dev. Biol.* **290,** 470-481.
Lustig, K. D., Kroll, K. L., Sun, E. E. and Kirschner, M. W. (1996). Expression Cloning of a Xenopus T-Related Gene (Xombi) Involved in Mesodermal Patterning and Blastopore Lip Formation. *Development* **122,** 4001-4012.
Marcellini, S., Technau, U., Smith, J. C. and Lemaire, P. (2003). Evolution of Brachyury Proteins: Identification of a Novel Regulatory Domain Conserved within Bilateria. *Dev. Biol.* **260,** 352-361.
Maroto, M., Iimura, T., Dale, J. K. and Bessho, Y. (2008). BHLH Proteins and their Role in Somitogenesis. *Adv. Exp. Med. Biol.* **638,** 124-139.
Martin, B. L. and Kimelman, D. (2008). Regulation of Canonical Wnt Signaling by Brachyury is Essential for Posterior Mesoderm Formation. *Dev. Cell.* **15,** 121-133.
Martin, B. L. and Kimelman, D. (2010). Brachyury Establishes the Embryonic Mesodermal Progenitor Niche. *Genes Dev.* **24,** 2778-2783.
Martin, B. L. and Kimelman, D. (2012). Canonical Wnt Signaling Dynamically Controls Multiple Stem Cell Fate Decisions during Vertebrate Body Formation. *Dev. Cell.* **22,** 223-232.
Miller, J. C., Tan, S., Qiao, G., Barlow, K. A., Wang, J., Xia, D. F., Meng, X., Paschon, D. E., Leung, E., Hinkley, S. J. et al. (2011). A TALE Nuclease Architecture for Efficient Genome Editing. *Nat. Biotechnol.* **29,** 143-148.
Miyamoto, S., Hidaka, K., Jin, D. and Morisaki, T. (2009). RNA-Binding Proteins Rbm38 and Rbm24 Regulate Myogenic Differentiation Via p21-Dependent and -Independent Regulatory Pathways. *Genes Cells* **14,** 1241-1252.
Morley, R. H., Lachani, K., Keefe, D., Gilchrist, M. J., Flicek, P., Smith, J. C. and Wardle, F. C. (2009). A Gene Regulatory Network Directed by Zebrafish no Tail Accounts for its Roles in Mesoderm Formation. *Proc. Natl. Acad. Sci. U. S. A.* **106,** 3829-3834.
Mullins, M. C., Hammerschmidt, M., Kane, D. A., Odenthal, J., Brand, M., van Eeden, F. J., Furutani-Seiki, M., Granato, M., Haffter, P., Heisenberg, C. P. et al. (1996). Genes Establishing Dorsoventral Pattern Formation in the Zebrafish Embryo: The Ventral Specifying Genes. *Development* **123,** 81-93.
Naiche, L. A., Harrelson, Z., Kelly, R. G. and Papaioannou, V. E. (2005). T-Box Genes in Vertebrate Development. *Annu. Rev. Genet.* **39,** 219-239.

Nikaido, M., Kawakami, A., Sawada, A., Furutani-Seiki, M., Takeda, H. and Araki, K. (2002). Tbx24, Encoding a T-Box Protein, is Mutated in the Zebrafish Somite-Segmentation Mutant Fused Somites. *Nat. Genet.* **31,** 195-199.
Nowotschin, S., Ferrer-Vaquer, A., Concepcion, D., Papaioannou, V. E. and Hadjantonakis, A. K. (2012). Interaction of Wnt3a, Msgn1 and Tbx6 in Neural Versus Paraxial Mesoderm Lineage Commitment and Paraxial Mesoderm Differentiation in the Mouse Embryo. *Dev. Biol.* **367,** 1-14.
Oginuma, M., Niwa, Y., Chapman, D. L. and Saga, Y. (2008). Mesp2 and Tbx6 Cooperatively Create Periodic Patterns Coupled with the Clock Machinery during Mouse Somitogenesis. *Development* **135,** 2555-2562.
Papaioannou, V. E. and Silver, L. M. (1998). The T-Box Gene Family. *Bioessays* **20,** 9-19.
Pyati, U. J., Webb, A. E. and Kimelman, D. (2005). Transgenic Zebrafish Reveal Stage-Specific Roles for Bmp Signaling in Ventral and Posterior Mesoderm Development. *Development* **132,** 2333-2343.
Rao, Y. (1994). Conversion of a Mesodermalizing Molecule, the Xenopus Brachyury Gene, into a Neuralizing Factor. *Genes Dev.* **8,** 939-947.
Reynolds, L. E., Wyder, L., Lively, J. C., Taverna, D., Robinson, S. D., Huang, X., Sheppard, D., Hynes, R. O. and Hodivala-Dilke, K. M. (2002). Enhanced Pathological Angiogenesis in Mice Lacking beta3 Integrin Or beta3 and beta5 Integrins. *Nat. Med.* **8,** 27-34.
Row, R. H., Maitre, J. L., Martin, B. L., Stockinger, P., Heisenberg, C. P. and Kimelman, D. (2011). Completion of the Epithelial to Mesenchymal Transition in Zebrafish Mesoderm Requires Spadetail. *Dev. Biol.* **354,** 102-110.
Rudnicki, M. A., Schnegelsberg, P. N., Stead, R. H., Braun, T., Arnold, H. H. and Jaenisch, R. (1993). MyoD Or Myf-5 is Required for the Formation of Skeletal Muscle. *Cell* **75,** 1351-1359.
Ruvinsky, I., Silver, L. M. and Ho, R. K. (1998). Characterization of the Zebrafish tbx16 Gene and Evolution of the Vertebrate T-Box Family. *Dev. Genes Evol.* **208,** 94-99.
Ryan, M. D. and Drew, J. (1994). Foot-and-Mouth Disease Virus 2A Oligopeptide Mediated Cleavage of an Artificial Polyprotein. *EMBO J.* **13,** 928-933.
Saka, Y., Tada, M. and Smith, J. C. (2000). A Screen for Targets of the Xenopus T-Box Gene Xbra. *Mech. Dev.* **93,** 27-39.
Sawada, A., Fritz, A., Jiang, Y. J., Yamamoto, A., Yamasu, K., Kuroiwa, A., Saga, Y. and Takeda, H. (2000). Zebrafish Mesp Family Genes, Mesp-a and Mesp-b are Segmentally Expressed in the Presomitic Mesoderm, and Mesp-b Confers the Anterior Identity to the Developing Somites. *Development* **127,** 1691-1702.
Schmid, B., Furthauer, M., Connors, S. A., Trout, J., Thisse, B., Thisse, C. and Mullins, M. C. (2000). Equivalent Genetic Roles for bmp7/snailhouse and bmp2b/swirl in Dorsoventral Pattern Formation. *Development* **127,** 957-967.
Schulte-Merker, S., Ho, R. K., Herrmann, B. G. and Nusslein-Volhard, C. (1992). The Protein Product of the Zebrafish Homologue of the Mouse T Gene is

Expressed in Nuclei of the Germ Ring and the Notochord of the Early Embryo. *Development* **116,** 1021-1032.
Schulte-Merker, S., van Eeden, F. J., Halpern, M. E., Kimmel, C. B. and Nusslein-Volhard, C. (1994). No Tail (Ntl) is the Zebrafish Homologue of the Mouse T (Brachyury) Gene. *Development* **120,** 1009-1015.
Shestopalov, I. A., Pitt, C. L. and Chen, J. K. (2012). Spatiotemporal Resolution of the Ntla Transcriptome in Axial Mesoderm Development. *Nat. Chem. Biol.* **8,** 270-276.
Showell, C., Binder, O. and Conlon, F. L. (2004). T-Box Genes in Early Embryogenesis. *Dev. Dyn.* **229,** 201-218.
Smith, J. C., Price, B. M., Green, J. B., Weigel, D. and Herrmann, B. G. (1991). Expression of a Xenopus Homolog of Brachyury (T) is an Immediate-Early Response to Mesoderm Induction. *Cell* **67,** 79-87.
Souopgui, J., Rust, B., Vanhomwegen, J., Heasman, J., Henningfeld, K. A., Bellefroid, E. and Pieler, T. (2008). The RNA-Binding Protein XSeb4R: A Positive Regulator of VegT mRNA Stability and Translation that is Required for Germ Layer Formation in Xenopus. *Genes Dev.* **22,** 2347-2352.
Spemann, H. and Mangold, H. (2001). Induction of Embryonic Primordia by Implantation of Organizers from a Different Species. 1923. *Int. J. Dev. Biol.* **45,** 13-38.
Stachel, S. E., Grunwald, D. J. and Myers, P. Z. (1993). Lithium Perturbation and Goosecoid Expression Identify a Dorsal Specification Pathway in the Pregastrula Zebrafish. *Development* **117,** 1261-1274.
Stennard, F., Carnac, G. and Gurdon, J. B. (1996). The Xenopus T-Box Gene, Antipodean, Encodes a Vegetally Localised Maternal mRNA and can Trigger Mesoderm Formation. *Development* **122,** 4179-4188.
Stoick-Cooper, C. L., Weidinger, G., Riehle, K. J., Hubbert, C., Major, M. B., Fausto, N. and Moon, R. T. (2007). Distinct Wnt Signaling Pathways have Opposing Roles in Appendage Regeneration. *Development* **134,** 479-489.
Storey, K. G., Crossley, J. M., De Robertis, E. M., Norris, W. E. and Stern, C. D. (1992). Neural Induction and Regionalisation in the Chick Embryo. *Development* **114,** 729-741.
Szeto, D. P. and Kimelman, D. (2004). Combinatorial Gene Regulation by Bmp and Wnt in Zebrafish Posterior Mesoderm Formation. *Development* **131,** 3751-3760.
Szeto, D. P. and Kimelman, D. (2006). The Regulation of Mesodermal Progenitor Cell Commitment to Somitogenesis Subdivides the Zebrafish Body Musculature into Distinct Domains. *Genes Dev.* **20,** 1923-1932.
Tada, M., Casey, E. S., Fairclough, L. and Smith, J. C. (1998). Bix1, a Direct Target of Xenopus T-Box Genes, Causes Formation of Ventral Mesoderm and Endoderm. *Development* **125,** 3997-4006.
Tada, M. and Smith, J. C. (2000). Xwnt11 is a Target of Xenopus Brachyury: Regulation of Gastrulation Movements Via Dishevelled, but Not through the Canonical Wnt Pathway. *Development* **127,** 2227-2238.

Takada, S., Stark, K. L., Shea, M. J., Vassileva, G., McMahon, J. A. and McMahon, A. P. (1994). Wnt-3a Regulates Somite and Tailbud Formation in the Mouse Embryo. *Genes Dev.* **8,** 174-189.
Takada, Y., Ye, X. and Simon, S. (2007). The Integrins. *Genome Biol.* **8,** 215.
Takahashi, H., Hotta, K., Erives, A., Di Gregorio, A., Zeller, R. W., Levine, M. and Satoh, N. (1999). Brachyury Downstream Notochord Differentiation in the Ascidian Embryo. *Genes Dev.* **13,** 1519-1523.
Takahashi, J., Ohbayashi, A., Oginuma, M., Saito, D., Mochizuki, A., Saga, Y. and Takada, S. (2010). Analysis of Ripply1/2-Deficient Mouse Embryos Reveals a Mechanism Underlying the Rostro-Caudal Patterning within a Somite. *Dev. Biol.* **342,** 134-145.
Tam, P. P. and Behringer, R. R. (1997). Mouse Gastrulation: The Formation of a Mammalian Body Plan. *Mech. Dev.* **68,** 3-25.
Taverna, D., Crowley, D., Connolly, M., Bronson, R. T. and Hynes, R. O. (2005). A Direct Test of Potential Roles for beta3 and beta5 Integrins in Growth and Metastasis of Murine Mammary Carcinomas. *Cancer Res.* **65,** 10324-10329.
Taverner, N. V., Kofron, M., Shin, Y., Kabitschke, C., Gilchrist, M. J., Wylie, C., Cho, K. W., Heasman, J. and Smith, J. C. (2005). Microarray-Based Identification of VegT Targets in Xenopus. *Mech. Dev.* **122,** 333-354.
Tazumi, S., Yabe, S., Yokoyama, J., Aihara, Y. and Uchiyama, H. (2008). PMesogenin1 and 2 Function Directly Downstream of Xtbx6 in Xenopus Somitogenesis and Myogenesis. *Dev. Dyn.* **237,** 3749-3761.
Tazumi, S., Yabe, S., Yokoyama, J., Aihara, Y. and Uchiyama, H. (2008). PMesogenin1 and 2 Function Directly Downstream of Xtbx6 in Xenopus Somitogenesis and Myogenesis. *Dev. Dyn.* **237,** 3749-3761.
Theiler, K. and Varnum, D. S. (1985). Development of Rib-Vertebrae: A New Mutation in the House Mouse with Accessory Caudal Duplications. *Anat. Embryol. (Berl)* **173,** 111-116.
Thermes, V., Grabher, C., Ristoratore, F., Bourrat, F., Choulika, A., Wittbrodt, J. and Joly, J. S. (2002). I-SceI Meganuclease Mediates Highly Efficient Transgenesis in Fish. *Mech. Dev.* **118,** 91-98.
Thisse, C., Thisse, B., Schilling, T. F. and Postlethwait, J. H. (1993). Structure of the Zebrafish snail1 Gene and its Expression in Wild-Type, Spadetail and no Tail Mutant Embryos. *Development* **119,** 1203-1215.
Thorpe, C. J., Weidinger, G. and Moon, R. T. (2005). Wnt/beta-Catenin Regulation of the Sp1-Related Transcription Factor sp5l Promotes Tail Development in Zebrafish. *Development* **132,** 1763-1772.
Trichas, G., Begbie, J. and Srinivas, S. (2008). Use of the Viral 2A Peptide for Bicistronic Expression in Transgenic Mice. *BMC Biol.* **6,** 40.
Uchiyama, H., Kobayashi, T., Yamashita, A., Ohno, S. and Yabe, S. (2001). Cloning and Characterization of the T-Box Gene Tbx6 in Xenopus Laevis. *Dev. Growth Differ.* **43,** 657-669.
Wang, J., Li, S., Chen, Y. and Ding, X. (2007). Wnt/beta-Catenin Signaling Controls Mespo Expression to Regulate Segmentation during Xenopus Somitogenesis. *Dev. Biol.* **304,** 836-847.

Watabe-Rudolph, M., Schlautmann, N., Papaioannou, V. E. and Gossler, A. (2002). The Mouse Rib-Vertebrae Mutation is a Hypomorphic Tbx6 Allele. *Mech. Dev.* **119,** 251-256.
Weinberg, E. S., Allende, M. L., Kelly, C. S., Abdelhamid, A., Murakami, T., Andermann, P., Doerre, O. G., Grunwald, D. J. and Riggleman, B. (1996). Developmental Regulation of Zebrafish MyoD in Wild-Type, no Tail and Spadetail Embryos. *Development* **122,** 271-280.
Weinberg, E. S., Allende, M. L., Kelly, C. S., Abdelhamid, A., Murakami, T., Andermann, P., Doerre, O. G., Grunwald, D. J. and Riggleman, B. (1996). Developmental Regulation of Zebrafish MyoD in Wild-Type, no Tail and Spadetail Embryos. *Development* **122,** 271-280.
White, P. H., Farkas, D. R., McFadden, E. E. and Chapman, D. L. (2003). Defective Somite Patterning in Mouse Embryos with Reduced Levels of Tbx6. *Development* **130,** 1681-1690.
Wilkinson, D. G., Bhatt, S. and Herrmann, B. G. (1990). Expression Pattern of the Mouse T Gene and its Role in Mesoderm Formation. *Nature* **343,** 657-659.
Wittler, L., Shin, E. H., Grote, P., Kispert, A., Beckers, A., Gossler, A., Werber, M. and Herrmann, B. G. (2007). Expression of Msgn1 in the Presomitic Mesoderm is Controlled by Synergism of WNT Signalling and Tbx6. *EMBO Rep.* **8,** 784-789.
Yamaguchi, T. P., Takada, S., Yoshikawa, Y., Wu, N. and McMahon, A. P. (1999). T (Brachyury) is a Direct Target of Wnt3a during Paraxial Mesoderm Specification. *Genes Dev.* **13,** 3185-3190.
Yamamoto, A., Amacher, S. L., Kim, S. H., Geissert, D., Kimmel, C. B. and De Robertis, E. M. (1998). Zebrafish Paraxial Protocadherin is a Downstream Target of Spadetail Involved in Morphogenesis of Gastrula Mesoderm. *Development* **125,** 3389-3397.
Yao, T. P., Oh, S. P., Fuchs, M., Zhou, N. D., Ch'ng, L. E., Newsome, D., Bronson, R. T., Li, E., Livingston, D. M. and Eckner, R. (1998). Gene Dosage-Dependent Embryonic Development and Proliferation Defects in Mice Lacking the Transcriptional Integrator p300. *Cell* **93,** 361-372.
Yasuhiko, Y., Kitajima, S., Takahashi, Y., Oginuma, M., Kagiwada, H., Kanno, J. and Saga, Y. (2008). Functional Importance of Evolutionally Conserved Tbx6 Binding Sites in the Presomitic Mesoderm-Specific Enhancer of Mesp2. *Development* **135,** 3511-3519.
Yoo, K. W., Kim, C. H., Park, H. C., Kim, S. H., Kim, H. S., Hong, S. K., Han, S., Rhee, M. and Huh, T. L. (2003). Characterization and Expression of a Presomitic Mesoderm-Specific Mespo Gene in Zebrafish. *Dev. Genes Evol.* **213,** 203-206.
Yoon, J. K., Moon, R. T. and Wold, B. (2000). The bHLH Class Protein pMesogenin1 can Specify Paraxial Mesoderm Phenotypes. *Dev. Biol.* **222,** 376-391.
Yoon, J. K. and Wold, B. (2000). The bHLH Regulator pMesogenin1 is Required for Maturation and Segmentation of Paraxial Mesoderm. *Genes Dev.* **14,** 3204-3214.

Zhang, J., Houston, D. W., King, M. L., Payne, C., Wylie, C. and Heasman, J. (1998). The Role of Maternal VegT in Establishing the Primary Germ Layers in Xenopus Embryos. *Cell* **94,** 515-524.
Zhang, J. and King, M. L. (1996). Xenopus VegT RNA is Localized to the Vegetal Cortex during Oogenesis and Encodes a Novel T-Box Transcription Factor Involved in Mesodermal Patterning. *Development* **122,** 4119-4129.